MONTHLY NOTICES

OF THE

ROYAL ASTRONOMICAL SOCIETY

Volume 123 No. 2 1961

Published and Sold by the

ROYAL ASTRONOMICAL SOCIETY
BURLINGTON HOUSE
LONDON, W.1

Price £1 4*s.* 0*d.* (*US* $3.50)

Subscription for volume £6 (*US* $18)

MONTHLY NOTICES
OF THE
ROYAL ASTRONOMICAL SOCIETY
Vol. 123 No. 2

THE SPECTRAL COMPONENTS OF 150 MAJOR SOLAR RADIO EVENTS (1952–1960)

Judith A. Boorman, D. J. McLean, K. V. Sheridan and J. P. Wild

(Received 1961 April 18)

Summary

A list is given of the spectral components (Types II, III and V bursts, and storms with continuum) of all major solar radio events recorded with the Dapto radio spectrograph (25–210 Mc/s) between August 1952 and September 1960. Where possible the associated flare and ionospheric data are appended.

The list shows that during the period in question the flares associated with major disturbances were twice as numerous in the northern hemisphere of the Sun than in the southern. The list also suggests that the probability of a Type II burst being followed by a continuum storm is much less during the early part of the sunspot cycle than in the later part.

In its most complete form the major solar-flare event is seen on metre-wavelength spectral records to consist of several components (1). The first phase, which usually begins between the start and the maximum of the Hα flare and lasts for a few minutes (see Fig. 1), consists of a group of Type III (fast-drift)

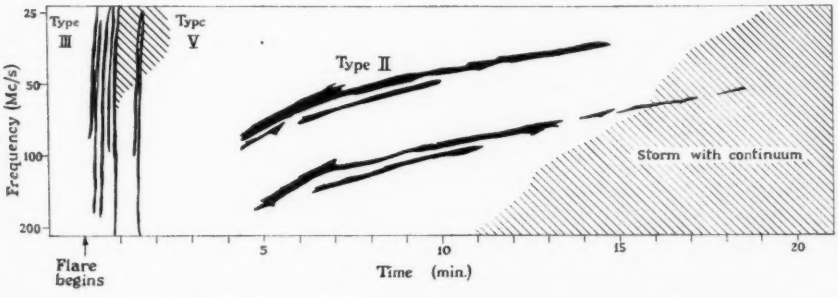

FIG. 1.—*Idealized sketch of spectral record showing the spectral components of a complete major radio event.*

bursts sometimes followed by a brief continuum burst of Type V. After a lull of a further few minutes a second phase begins with the onset of a slow-drift Type II burst which continues for the order of ten minutes. There may then follow a storm of long duration (e.g. hours) consisting of a high level of continuum radiation, sometimes with superposed Type I bursts. In general, one or more of the spectral components may appear without the remainder. Thus by far the commonest type of flare-associated radio disturbance is that containing a first-phase event only. The major events marked by Type II bursts or starts of continuum storms are much rarer, and are of special significance owing to

TABLE I

Major solar radio events recorded with the Dapto radio spectrograph

The list includes all events associated with type II bursts and the beginnings of storms with continuum.

Date		Solar radio event		Storm with continuum	Flare				S.I.D.		Remarks
		Type III	Type II		Time	Imp.	Position		Time	Imp.	
	1952										
Sept.	1	*0337–0339·5G(V)*	0346·5–0355								ref. (3)
Nov.	21/22		*2350–0008*	2355–0130	2343–2350–0027	2 to 3	5–7N	1–2W	2348–0300		ref. (2), (3), (6)
	1953										
May	5	0455–0456·5g(V)									
		0457–0458g	0458–0502						0445–0530		ref. (2), (3)
June	19	0433–0435g									
		0438·5–0440g(V)	0445–0452								
Oct.	14		*0550–0608*								
	1955										
Feb.	24		**0104–0124**								
June	9		**0001–0033**								
	15		0400–0408								
June	21	**2316–2319·5G**	**2330–2355**								
July	5	**0203–0212·5G**	**0215–0224**								
	7	**0200–0204G**	*0206–0213*								
Sept.	10		0509–0520								
	19	0145·5–0148g(V)	0152–0202								
Nov.	15	*0437–0440·5G*	*0441–0505*		0428– –0458	1	26N	9W			
		2205g	*2205–2208*								ref. (5)
	18	*0237–0239G*	*0241–0253*								
	24		*0442–0513*								
	30	*0540·5–0542g(V)*	*0544–0549*								

	1956										
Jan.	16		*0031–0049*								
	19	*0022.5–0024.5g*	**0026–0031**	*0100–0226*	0016–0026–0046	2	22N	26E	0015–0050	2	ref. (5), (6)
Feb.	14		**0554–0620**		0538–0557–0730	2 to 3	20–23N	26–40E	0532–0728	3	ref. (5)
March	8		**0321–0342**								
April	12	0530–0534g	0536–0552		<0530– –0557	1 to 2	16–22N	60–68E	0530–0550	2	
	25/26		*2353–0019*								ref. (5)
	26		0154–0210		<0200–0212–0300	1	14N	8W	0150–0253	2	ref. (5)
May	16		*0007–0039*								
	30		*2331–2351*		2320–2330–2357	1	20S	2E			
July	6		**0245·5–0309**		<0246– –0300	1	20N	47E	0235–0308	2	ref. (5)
Sept.	10		*0134–0141*								
Nov.	12		2309–2323								
	13	0203–0206g	**0207–0220**		<0157–0203–0254	3	28N	50W	0158–0300	2+	
	19		<0219–0225								
	1957										
Jan.	24	*2318–2319·5g*	2327·5–2331								ref. (5)
	28		*2348·5–2354*								
	31	*0358–0403*G	**0407–0424**		0358–0436–>0550	3+	24N	5E	0356–0520	1	
Feb.	28	*0002–0014*G	*0009–0026*	0029–0126	0005–0014–>0057	3	18N	35W	0020–0210	1+	ref. (6)
March	1		**0035–0059**						0040–0150	1−	
	26		**0412–0416**								
April	5		0004–0013								
	8	**0341·5–0344g**(V)	0347–0353		<0342–0342–0359	1 to 2	22–23S	48–51E	0338–0355	1	
	9	0530g	*0532–0544*								
July	17	*0114–0116*G	*0125–0131·5*		0112–0117–0148	1 to 2	11–12N	30–31E			ref. (5)
Aug.	6	**0229–0234G**	*0234–0246*								ref. (5)
		*0423–0430*G	0431–0438								ref. (5)
Sept.	2	*0410–0419*G	0423–0431		<0409–0413–0445	1	13–15N	24–26W	0400–0510	1+	
	11	**0141–0143·5g**(V)	*0150–0200·5*	**0300–0722**	0140–0142–0200	1	13N	90E			ref. (5), (6)
	12	*0709g, 0711–0713g* 0715–0716G	*0712–0721*		0703–0710–0740	1 to 3	8–11N	13–20W PB <1200, >18h, 0·5	0702–0734	3−	

TABLE I (*continued*)

Date	Solar radio event		Storm with continuum	Flare				S.I.D.		Remarks
	Type III	Type II		Time	Imp.	Position		Time	Imp.	
1957										
Sept. 19			**0427–0730**	<0350–0412–0555	2 to 3+	20–24N	1–6E	0359–0453	3	ref. (6)
24	*0201–0206*G	*0212–0226*		<0224–0227–0307	—	15N	91E			
		0504–0507		0507–0513–0522	1	15N	90E			Flare assoc. doubtful
Oct. 9		**0402–0422**		0340–0357–>0500	1 to 3	37–40S	11–16W			
23	2203–2206g	2204–2205								
	*2224–2229*G	2226–2227		<2222– –2236	1	18S	79W			
24		2310–2315								
		2341–2358								
Nov. 4		*2240–2242*								
6		*0424·5–0434*								
13	**0457·5–0503**G	**0502–0505**		0457–0458–0511	1	25S	27E	0458–0513	1	ref. (5)
20		*0050·5–0052*						0040–0138	2	
22		**0410·5–0427**		0404–0409–0446	2	30–32N	26–29W	0406–0439	3–	Meudon IV: 0406, ref. (5)
25		0416–0430								
		0504–0532 II?		<0457– –>0509	1	29N	71W			
26		*2301–2330* II?		2251–2256–2310	1	17–18S	1–8W			
29	*0059·5–0101·5*g	*0059–0103*		0045–0213–>0600	3+	41N	63E			
Dec. 6		*0400–0419*		0347–0353–0443	1 to 2	14–17N	44–47E	0348–0414	2	ref. (5)
18		0236–0304 II?		<0241–0245–>0314	2	14S	10E			
19		**0803–0825**		<0757–0801–0958	1 to 2	17–22N	10–17E	0757–0820	3	Type II occurs in continuum storm. ref. (5)
20	**0544–0546·5**G	**0546·5–0552**		<0543–0545–0606	1	15–17N	1E–2W	0545–0611	2	

	1958										
Jan.	2	**0542–0547**G	0457 II?		0541–0551–0622	1 to 2	14–18S	26–29E	0545–0614	1	
	15	*0333–0335*g	*0335–0355*								ref. (**5**)
	16	*0415*g	0418–0530 II?								
		*2300–2307*G	2313–2316		2255–2307–2347	1 to 2	15–16S	46–48E			
Feb.	26	**0550–0551**g(V)	*0602–0611·5*		0527–0552–0632	1 to 2	17–20S	59–64W	0540–0636	2+	Meudon IV: 0551
March	11	0029·5–0036G	*0032–0046*		<0030–0034–0042	1	11N	2E	0048–0320	3	
	12		**0043–0048**		<0024– –>0233	2	8N	2E	0052–0439	3+	
					<0027– –>0128	1	10–12N	4W			
			0100–0103·5								
	25	2318–2320g	*2320–2332·5*								
		*2322·5–2323·5*G									
	26		0007·5–0032 II?								
		0034·5–0036g	0035–0047·5		<0036–0036–>0040	1	21N	50W	0029–0035	2	
			0110–0127 II?		No observations						
April	8		0304–0311		0301–0309–0329	1	17S	44W	0306–0415	1+	ref. (**5**)
June	26		**0304–0320**	0319–0515	<0300– –>0320	2	10N	49E	0247–0412	2+	ref. (**4**), (**6**)
July	7	**0027–0029**g(V)	**0032·5–0048**	0042–0050	0022–0103–0324	1 to 3+	24–28N	7E–9W	0025–0230	3	ref. (**4**), (**6**)
									PB 0130, $>78^h$, >15		
		0059–0101g	**0101–0117**	**0108–0320**							ref. (**6**)
	12		*2330–2335*		2317–2330–>2330	1	26N	78W			
	20	**0242–0244**G	0251·5–0254		No observations				0244–0315	1	
	25		0609·5–0630 II?		<0548– –>0745	2	8N	80E			
	29		**0304–0319**	**0320–0500**	<0303–0303–0359	3	14S	43W	0240–0440	3+	ref. (**6**)
									PB 0405, $>4^h$, 0·7		
			0325 II?								
Aug.	4		*0439–0453* II?		0421–0432–0610	2 to 3	28–30N	27–37W	0422–0558	3	
	20	**0040–0045**G	**0046–0105**		0042–0046–0128	2 to 3	15–16N	16–18E	0042–0115	2+	
	21	*0332·5–0335*g(V)	0338–0340 II?		0324–0334–0336	1	4N	67E			
	23		**0256–0257** II?								
	26	0020–0022g	**0021–0045**	**0030–0430**	0005–0027–0124	3	20N	54W	0010–0410	3+	ref. (**6**)
									PB 0100, $>57^h$, >10		
Oct.	2	2146g	**2149–2157**		2143–2150–2201	1	8S	37W			
	21/22		**2328–2400**	**2342–0400**	2321–2333–>0006	2	2–4S	20–23W	2328–0040	3+	ref. (**6**), (**7**)
	24		0520–0533		No observations						

TABLE I (*continued*)

Date		Solar radio event		Storm with continuum	Flare			S.I.D.		Remarks
		Type III	Type II		Time	Imp.	Position	Time	Imp.	
	1958									
Nov.	27/28	*2355–2356*G	*2358–0001*		<2350–2356–0013	1	15–23N 15–36W	2358–0008	1−	
Dec.	10	**0220**g(V)	*0224–0231*		0221–0221–0306	2	00 20–23E	0220–0237	1+	
	18	0432·5–0434g	*0438–0451*		No observations			0435–0445	1−	ref. (7)
	19	0521–0525g(V)	0527–0532							
	1959									
Jan.	7		*0245–0247*	*0246–0443*	0218– –0305	1	12–14S 3–10W			
Feb.	3		*0054–0106*		0040–0044–0107	2	12N 8E	0038–0100	1+	
	9	0204–0207g	**0208–0245**	0215–0317	<0058–0157–0246	2	13N 90E			
	18	0501–0506G	*0508–0523*		No observations			0500–0525	2+	
March	13		*0441–0457*							
May	13	**0512–0515**g(V)	**0516–0525**	0525–0630	0458–0514–0550	1 to 2	19–24N 19–27E	0511–0547	2	
	18		0407–0412		No observations			0404–0454	2	
June	5		0546–0550		<0545– –0600	1−	14S 12E			
	10		*0247–0308*							
	22	*0507–0508*g	0503–0512							
July	5		2338–2349		2330–2345–2350	1	8N 24W			
	7		0343·5–0345							
	14	**0338–0339**g	**0338–0412**	**0401–0535**	0319–0342–0900	1 to 3+	12–20N 0–10E	0328–0628	3+	
		0340–0349g(V)		0535–0610	–0349–			PB <0700, >51^h, >15		
	17		0602–0606		0520–0626–0656	1	16N 40W			
Aug.	17	*0330–0332*G	*0334–0341*		0328–0335–0346	1	14–15N 15–16W	0330–0400	2	
	28		*0039–0127*	0055–0330	0027–0040–0128	1 to 2	7–13N 69–74E	0028–0248	2+	
Sept.	3	**0422–0423**G	**0424·5–0438**		0421–0423–0439	2	23–27N 85–86W	0422–0442	3	
Nov.	11		*0657–0714*							
	18		0043–0044		<0008– –0200	2	18N 19E			
	30	**0248**g	**0251–0358**	0312–0350	0247–0250–0356	2	8N 16E	0249–0320	3−	
Dec.	8	**0116–0120**G	**0121–0126**		<0120– 0145	1	12N 38W	0118–0200	1+	
	10	*0515–0518·5*G	**0521–0529**		0512–0518–>0537	2	15N 70W	0518–0545	1+	
	11	0406·5–0409g	**0412–0418**					0407–0430	1	
	18	**0634·5–0638**G(V)	*0640–0647*	0653–0723	<0636–0638–>0700	1	7S 53W	0637–0657	1+	
	21	**0043·5–0051**G(V)	*0055–0120*	0120–0250	<0045–0055–0104	1	3S 53W			

	1960										
Feb.	18	**0059–0107**G(V)	0170–0118						0103–0254	3+	
	29		0153·5–0156		0140– –>0200	2	32S	56W			
March	30		*0325–0337* II?	**0325–>0740**					PB 17xx, >29h		
April	5	**0156–0200**G		**0207–0300**	<0215–0245–0308	2 to 3	12N	60–62W	0140–0417	3+	
									PB 10xx, >24h		
	28	**0117g**	**0120–0146**	0145–0230	<0130–0137–>0145	3	5S	34E	0120–0300	3+	
	29	{	*0214–0225*	0200–0305 } **0350–>0645** }	0140– –>0549	2	10–12N	19–22W	0205–0355	2+	
									0355–0500	2+	
May	6		0312–0315								
	10		2349–2350 II?								
	13	**0517–0525**G	**0523–0538**	0530–>0609	{ <0522– –>0545	2	13S	} 85E	0512–0853	3+	Flare assoc. ambiguous
					{ <0522–0550–0735	1 to 3+	29–30N	} 64–68W			
June	10		0435–0438 II?								
	15	**0248–0254·5**G(V)	*0300–0316*		{ 0248–0301–0349	1	18N	13W }	0250–0325	1	Flare assoc. ambiguous
					{ 0251–0254–0339		22N	53W }			
	20	**0126–0130**G(V)	*0130–0146*		0126–0129–0205	2	13–17S	59–60W	0128–0156	1+	
	23	**0331–0333**G(V)	0335–0339		0329–0332–0344	1	12N	23W			
	27		**0004–0008·5**	0013–0050	0002–0023–>0057	2 to 3	7–9S	34–35E	0003–0110	2–	
		*0420–0421*g	**0422–0443**	0425–0539	0418–0429–0615	1	19–23N	18–19W	0417–0453	1+	
		0450–0452G	0453–0454·5	0425–0539					0453–0521	1+	
		0500–0503G(V)	**0503–0505**	0425–0539							
	29		*0149·5–0158*	0143–0230	0125–0144–>0220	1	23N	56W	0138–0346	2	
July	14		**0517–0523** II?								
	26		**0332·5–0340**						0325–0352	1+	
		0348g	0351–0404								
Aug.	11	**0248–0257**G(V)	**0257·5–0314**	0307–>0615	0247–0304–0315	2	21N	33E	0225–0335	2	
Sept.	2	0242g	*0244–0249*		<0250–0250–>0305	2	14S	54W			
			0545–0559								
	26	**0537–0541**G	*0543–0604*	>0554–>0611							

their relations with other solar geomagnetic and cosmic-ray effects. It is the purpose of the present communication to list the spectral components of all such major events recorded with the Dapto (N.S.W.) radio spectrograph between 1952 and 1960, and to give also data on their related optical flares and ionospheric effects. This listing is intended primarily for the use of workers in allied fields, but a few comments on statistical features of the table are appended.

The following remarks explain the use of the table:

Dates and times are in U.T. Total times of observation are not given but may be found in the *Quarterly Bulletin of Solar Activity*.

The radio events refer to the frequency range 40–210 Mc/s up to 1958 November, and 25–210 Mc/s thenceforth. They are described with the aid of the notation used in the *Quarterly Bulletin*, viz. g and G signify groups of Type III bursts containing fewer than and more than 10 bursts respectively, and V signifies that the Type III event includes a Type V continuum event. A subjective indication of intensity or importance is denoted by three different faces of type: roman, *italics* and **bold** in ascending order.

Entries in the column "Storm with continuum" are often referred to as Type IV events; however they should not necessarily be taken to indicate the presence of an extended, outward-moving source implied by Boischot's original definition of Type IV, since the recognition of this phenomenon requires additional (directional) information; nor need they necessarily be related to events in the centimetre-wave spectrum, which have also been called Type IV. It is not yet known whether the storms with high continuum (with or without storm bursts) that begin after flares differ intrinsically from the ordinary (Type I) storms.

Flare data have been taken from the *Quarterly Bulletin*, and reports issued by C.R.P.L. (National Bureau of Standards, Boulder, Colorado), the Fraunhoffer Institute (Freiburg-im-Bresgau) and the National Standards Laboratory, C.S.I.R.O. (Sydney).

When it is definitely known that flare observations cited were not in progress during an event, a note to this effect is inserted in the Flare column; however, the complete absence of an entry in the Flare column could mean either that no observations were in progress or that no flare was observed.

The S.I.D.'s listed have been taken from the C.R.P.L. reports. In the same column are occasionally listed the starting time, duration and strength of polar blackouts, the letters P.B. being used to distinguish them from S.I.D.'s. The data on polar blackouts are those of Reid and Leinbach (**8**), with additional recent information from Arnoldy, Hoffman and Winckler (**9**).

The heliographic distribution of flares associated with the events of Table I is shown in Fig. 2. It is seen that Type II-associated flares are distributed in longitude across the whole disk; the gradual falling off towards each limb could be due wholly or partly to the fact that flares are more difficult to see near the limb than near the centre. The storm-associated flares are also widely distributed, but 20 out of the 23 fall between longitudes 0 and $\pm 60°$.

The distribution in latitude of flares associated with Type II bursts and with storms both show a marked excess (about 2:1) of events North of the Equator. An examination of data published by Thompson and Maxwell (**10**) reveals a similar trend (18 northerly to 9 southerly) in the case of storm-associated flares

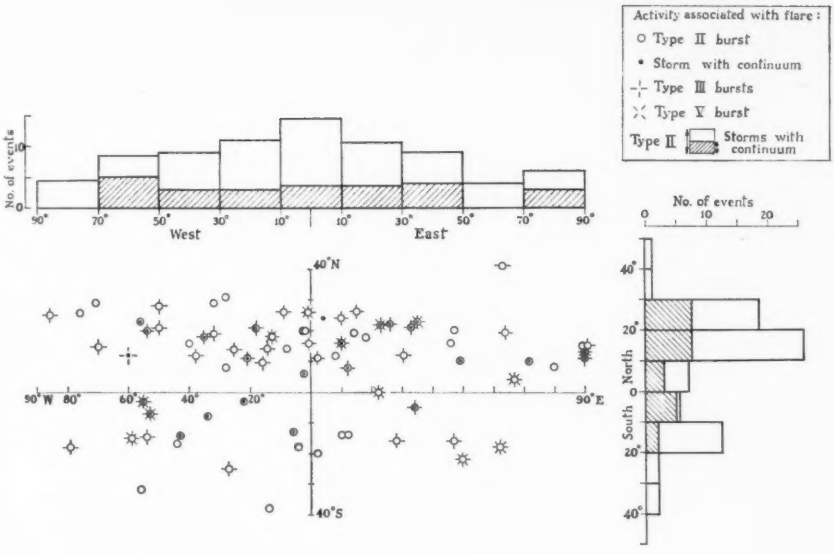

FIG. 2.—*The heliographic distribution of flares associated with the major radio events, and histograms showing their east–west and north–south distribution.*

recorded at Fort Davies, Texas, during different daily hours of observation within a 27-month period centred on the year 1958. Corresponding data for the Type II-associated flares (**11**) (recorded between 1956 October and 1957 September) also show a slight, though scarcely significant, northerly increase.

Inspection of Table I clearly shows the general increase of activity following the minimum of solar activity in 1954. It is interesting to note that during the first part of the sunspot cycle (1954–1958·5) storms with continuum were detected on the spectral records on only four occasions, while 75 Type II bursts were recorded; between 1958·5 and 1960, on the other hand, there appeared 25 storms to 66 Type II bursts. This result indicates that the continuum storm may be a feature of the late phase of the sunspot cycle, perhaps requiring a well-developed corona for its generation.

The observations and analysis of Table I have involved the work of different members of this Laboratory at different times; of the numerous people who have contributed, the authors wish particularly to acknowledge the major contributions of Mr J. D. Murray, Dr J. A. Roberts and Mr J. Joisce.

C.S.I.R.O.,
Radiophysics Laboratory,
Sydney, Australia:
1961 *March* 3.

References

(1) J. P. Wild, " Solar Radio Spectroscopy ". Varenna Lectures of 1959, *Nuovo Cimento* (in press).
(2) J. P. Wild, J. D. Murray and W. C. Rowe, *Aust. J. Phys.*, **7**, 439, 1954.
(3) J. P. Wild, *Transactions of the I.A.U.*, **9**, 661, 1957.
(4) J. P. Wild, K. V. Sheridan and G. H. Trent, *Paris Symposium on Radio Astronomy* (ed. R. N. Bracewell), p. 176, (Stanford University Press, 1959).
(5) J. A. Roberts, *Aust. J. Phys.*, **12**, 327, 1959.
(6) D. J. McLean, *Aust. J. Phys.*, **12**, 404, 1959.
(7) K. V. Sheridan, G. H. Trent, and J. P. Wild, *Observatory*, **78**, 51, 1959.
(8) G. C. Reid and H. Leinbach, *J. Geophys. Res.*, **64**, 1801, 1959.
(9) R. L. Arnoldy, R. A. Hoffman and J. R. Winckler, *J. Geophys. Res.* (in press).
(10) A. R. Thompson and A. Maxwell, *Nature*, **185**, 89, 1960.
(11) A. Maxwell, A. R. Thompson and G. Garmire, *Planet Space Sci.*, **1**, 325, 1959.

A NOTE ON THE UNUSUAL VARIATIONS OF COSMIC RAY INTENSITY DURING THE PERIOD 1960 NOVEMBER 10 TO 16

T. Mathews, T. Thambyahpillai and W. R. Webber

(Communicated by H. Bondi)

(Received 1961 June 7)

Summary

An unusual sequence of cosmic ray variations, observed in London in connection with the high level of solar and geophysical activity prevailing during the period 1960 November 10–16, is described. The results are compared with cosmic ray observations made elsewhere and with other relevant geophysical phenomena. Some of the features encountered are unique in the type of event considered, and the implications of these results are briefly discussed.

---

1. *Introduction.*—The cosmic ray intensity observed deep in the Earth's atmosphere was subject to a series of unusual changes during the period 1960 November 10–16. Additional cosmic radiation accelerated at the Sun to energies high enough to be detectable at sea level was observed twice during this period, even though increases of this kind are relatively rare. Moreover, at least two Forbush decreases exhibiting a high degree of anisotropy occurred on November 12 and 13. In addition to these cosmic ray observations, the associated series of solar and geophysical phenomena were observed by a wide range of experimental techniques. This circumstance, taken together with the remarkable superposition of a variety of effects which took place during this period, provides a valuable opportunity of deriving a large amount of information about the solar, interplanetary, and geophysical processes which were operating at that time. It is intended in this note to report the cosmic ray intensity variations observed with the different types of detectors located at Imperial College, and to make a preliminary attempt at integrating these results with similar observations made elsewhere as well as with the associated solar and geophysical phenomena.

2. *Solar and geophysical data.*—During the week under consideration an exceptionally active region (McMath plage region 5925), associated with a complex sunspot group was passing across the visible disk of the Sun at a latitude of 26° to 29° N, with central meridian passage on November 12*. Flares of importance 3 or 3+ occurred in this region on the 10th, 12th, and 15th, while one of class 2+ was seen on the 14th. The flares of class 3+ of November 12 and 15 were responsible for the additional cosmic radiation detected by sea-level neutron monitors at high latitude on these dates (see Section 3). A flare which

* We are indebted to Professor M. A. Ellison who provided us with detailed records of the flares mentioned.

occurred on the 11th was missed by the visual observation network but was detected by its radio emission.

In the case of the flare on November 10, maximum light output was reached at $10^h 21^m$ and the associated S.I.D. showed that the ultra-violet or X-radiation produced was of moderate intensity. The radio emission from the flare, recorded over a wide band of frequencies, was of moderate intensity ($\sim 3 \times 10^{-17}$ w.m^2 (c/s) min at 200 Mc/s and 12×10^{-17} w.m^2 (c/s) min at 3000 Mc/s).

At about $03^h 15^m$ on November 11 a flare of major importance probably occurred but no reports of visual observations of this event are available. However, strong radio emission of over 7×10^{-17} w.m^2 (c/s) min at 200 Mc/s was reported as reaching peak intensity at $03^h 15^m$. The radio emission was particularly strong at frequencies below 1000 Mc/s and, since strong emission below 500 Mc/s appears to be a distinctive feature of flares which subsequently produce geomagnetic storms (Sinno and Hakura 1958), it appears likely that a plasma cloud ejected at the time of this flare was responsible for the severe magnetic storm with a sudden commencement (S.C.) at $13^h 48^m$ on November 12. The severity of the S.I.D. which occurred between $03^h 17^m$ and $05^h 00^m$ showed that the flare was also a strong source of ultra-violet or X-radiation.

A flare of major importance (3+) occurred again in this active region (27° N, 2° W) at $13^h 21^m$ on November 12 and the visible light from it rapidly reached a maximum between $13^h 28^m$ and $13^h 31^m$ (flash point). The emission then decayed to a rather small value till $14^h 20^m$ when a second weak outburst occurred. By $16^h 00^m$ the visible light had reached a low intensity even though the flare is listed as observable until $19^m 22^h$. The radio emission from the flare followed a very similar pattern with the observations at 3000 Mc/s showing a broad maximum around $13^h 28^m$ to $13^h 50^m$ and subsequent decay with a small secondary peak at $14^h 20^m$. The intensity maximum of 10^{-17} w.m^2 (c/s) reached at this frequency is one of the highest recorded during the current solar cycle. This feature appears to be significant in view of the acceleration of particles to cosmic ray energies (several GeV*) which accompanied the flare. At frequencies below 1000 Mc/s the emission was not particularly strong, but it is worthy of note that the radiation was strongly (35 per cent) polarized during the later stages of the event. Radio bursts of Types II and IV were recorded at Sydney in association with this flare. The ionospheric disturbance and the sudden enhancement of atmospherics (S.E.A.) which accompanied the solar flare were especially strong. It is probable that the plasma cloud from this flare was responsible for the magnetic storm with a S.C. at $10^h 23^m$ on November 13.

Activity recommenced in the plage region 5925 early on November 14 when there occurred a 2+ flare which reached its peak light intensity at $03^h 04^m$. Moderate radio emission and strong S.I.D. were associated with this flare. The solar stream which produced the magnetic storm with a S.C. at $13^h 04^m$ on the 15th probably originated in this flare.

The final great burst of activity from this plage region occurred on November 15, when a flare of class 3+ was observed at the heliographic coordinates 26° N, 35° W. The emission of optical radiation began at $02^h 07^m$, reached a maximum at $02^h 21^m$, and subsequently decayed to very faint intensity by $04^h 27^m$. The second increase of intensity recorded by neutron monitors during the week under review was associated with this flare. The burst of radio emission which occurred

* 1 GeV ≡ 10^9 electron volts.

during the event rose to a maximum at $02^h\,17^m$ and was strong, especially at the higher frequencies. Strong S.I.D. were also recorded at about this time.

The first magnetic storm to occur during the period under consideration was a particularly strong one which began with a S.C. at $13^h\,48^m$ on November 12. There can be little doubt that this storm, the S.C. of which, by a coincidence, occurred only 20 minutes after the optical and radio maxima of the great flare which generated cosmic radiation, has added much to the complexity of the observed phenomena. As explained earlier, the plasma cloud which arrived at the Earth around $13^h\,48^m$ was in all probability produced by the visually unobserved flare at $03^h\,15^m$ on the 11th and, on this basis, the time lag between the flare and S.C. is 34·5 hr. If, on the other hand, the cloud is ascribed to the flare of the 10th, the time delay would be 51·5 hr. The progress of this magnetic storm can be followed by reference to Fig. 1 and Fig. 4, in which the changes of the horizontal intensity of the Earth's field observed at the equatorial station Colombo are plotted.

About $3\frac{1}{4}$ hours after the S.C., at $17^h\,00^m$, the intensity of the horizontal magnetic field at equatorial stations had decreased below the values prevailing before the S.C., showing that the main phase of the storm had set in. The decrease proceeded continuously until about $20^h\,00^m$, by which time the decrease amounted to over 120γ. After $20^h\,00^m$ there was a small recovery till $04^h\,00^m$ on November 13, subsequent to which time the decrease proceeded uninterrupted until the minimum of over 300γ below normal was attained around $09^h\,00^m$. The magnitude of the decrease classifies the storm as an extremely severe one. Recovery of the equatorial horizontal field from this storm appears to set in after $09^h\,00^m$.

During this period of recovery, the S.C. of a second magnetic storm occurred at $10^h\,23^m$ on the 13th, indicating that the plasma cloud from the strong flare of the 12th had arrived in the vicinity of the Earth taking a time of about 21 hours to traverse the Sun-to-Earth distance. The effect of this storm on the horizontal intensity at the equator was rather weak and produced only a small trough in the recovery curve of the earlier major storm. This magnetic storm, however, was associated with a pronounced Forbush decrease in the cosmic ray intensity accompanied by a marked anisotropy, as will be seen in Section 4 of this paper. The value of H at the equator continued to rise throughout the rest of the day and levelled off during the 14th to a roughly constant value 50 to 100γ below the level obtaining before the S.C. on the 12th. The intensity continued to be depressed during the 14th and the first half of the 15th until $13^h\,04^m$ when the S.C. of a magnetic storm due to the class 2+ flare of the previous day occurred. The delay between flare and S.C. in this case is 34 hours.

3. *Observations of the solar injections of cosmic radiation.*—We shall first consider the increases observed by the standard neutron monitor at London but, as already mentioned, the occurrence of a magnetic storm a short while after the flare on the 12th which accelerated the cosmic rays adds to the complexity of the observed phenomena and it is evident that the data from any one station can provide only a part of the complete picture of the operative factors, and caution should be exercised in the interpretation of the observed features. For this reason we shall compare our results with those from a number of stations in Europe which provide a useful latitude coverage over a limited range of longitudes before proceeding to discuss the possible origins of the variations (see Fig. 1).

About 30 minutes after optical and radio maxima of the major flare of the 12th, a significant increase of intensity was detected by the neutron monitor at London indicating the arrival of solar particles at the Earth. From $14^h\,00^m$ onwards the intensity showed a slow growth, which took a rather long time in reaching

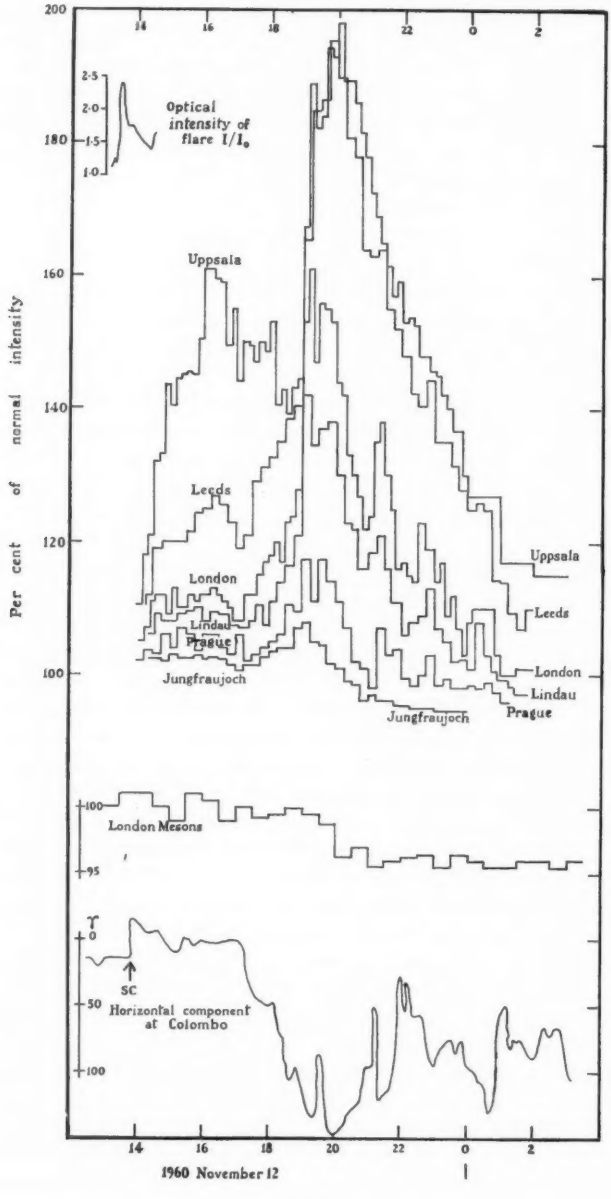

FIG. 1

a broad maximum of about 13 per cent above the pre-flare level around $16^h\,30^m$. The intensity then started a decline which continued until $17^h\,15^m$ when a further increase of a roughly linear character commenced. It will be seen from Fig. 1 that the rapid diminution in H at Colombo also started at about this time. The slow increase continued until $19^h\,00^m$, by which time a value of 28 per cent above normal was being recorded. At $19^h\,00^m \pm 1^m$ a sudden and sharp increase of intensity occurred with a maximum intensity of 1·6 times normal at $19^h03^m \pm 1^m$. This sudden rise occurred approximately 30 minutes before the beginning of a Forbush decrease recorded by the meson telescope at sea level in London. Between $19^h\,00^m$ and $20^h\,15^m$, the neutron intensity showed a double hump structure as can be seen in Fig. 1. The final decline of the solar cosmic rays observed at London began at $20^h\,00^m$ and continued in a roughly exponential decay on which were superposed a number of peaks that were about 75 minutes apart. This series of pulses in the flux of solar cosmic rays is of a highly unusual character and is of exceptional interest. It may be noted that the peaks correspond roughly in time to a series of pulsating decreases which occurred in the equatorial H. By $05^h\,00^m$ on November 13 the intensity of the solar cosmic rays had fallen below the minimum observable level at London. At no time during the observation of solar particles by the neutron monitor was a significant increase detected by the meson telescope at sea level. The production of solar cosmic rays, then, was confined to the low energy end of the spectrum (below 5 GeV) during this event.

We have included the increases observed by the neutron monitors at Uppsala, Leeds, Lindau, Praha, and Jungfraujoch in Fig. 1 for comparison with the London data. The results from Amsterdam are almost identical with those from London and are not shown here. The intensities are expressed as percentages of the mean intensity during the first half of the 12th. Whilst the broad pattern of variations described earlier, consisting of an increase due to solar cosmic rays superposed on a Forbush decrease, is evident at all these stations, the following dissimilarities cannot be ignored. During the initial phase of the increase between $14^h\,00^m$ and $16^h\,00^m$ the maximum was reached earlier at lower latitudes than at higher ones. Also, Uppsala was observing an increase about twice as large as the one at Leeds. Between $17^h\,00^m$ and $19^h\,00^m$ the slow growth of the intensity of solar cosmic rays was most pronounced at London, Amsterdam, and Lindau. The intensity at Uppsala was actually decreasing during this period, and because of this Leeds, which has a higher geomagnetic threshold rigidity than Uppsala at normal times, was observing nearly the same intensity as Uppsala just before $19^h\,00^m$. The double hump between $19^h\,00^m$ and $20^h\,00^m$ in the intensity curve occurred at most stations, but the initial increase at $19^h\,00^m$ was not so rapid at Uppsala and Leeds as at London. Finally, the pulses on the decay portion of the curves after $20^h\,00^m$ were also most marked at London, Amsterdam, and Lindau, whilst they were not perceptible at Uppsala and Leeds. Moreover, the increases measured by the monitors at Uppsala and Leeds were still approximately equal during this decay phase.

It is known that the response of a neutron monitor at sea level to the primary radiation falls off rather rapidly at primary rigidities less than 1 GeV*, and in

* The rigidity is here defined as pc/Ze where p is the momentum and Z the atomic number of the particle. pc is expressed in GeV so that the rigidity is in units of 10^9 volts.

order to study the behaviour of the flux of solar particles at the low energy end it is necessary to examine the cosmic noise absorption (C.N.A.) measured at high geomagnetic latitudes. The results from the stations Longyearbean ($\bar{\lambda}=74°{\cdot}2$)*, Kiruna ($\bar{\lambda}=65°{\cdot}7$) and Trondheim† ($\bar{\lambda}=62°{\cdot}5$) relating to the event of November 12 are shown in Fig. 2 where the equivalent daylight C.N.A. is plotted against time, the values obtained during the night being increased by a factor of 3·3 in order to convert them to the equivalent daylight values. It is

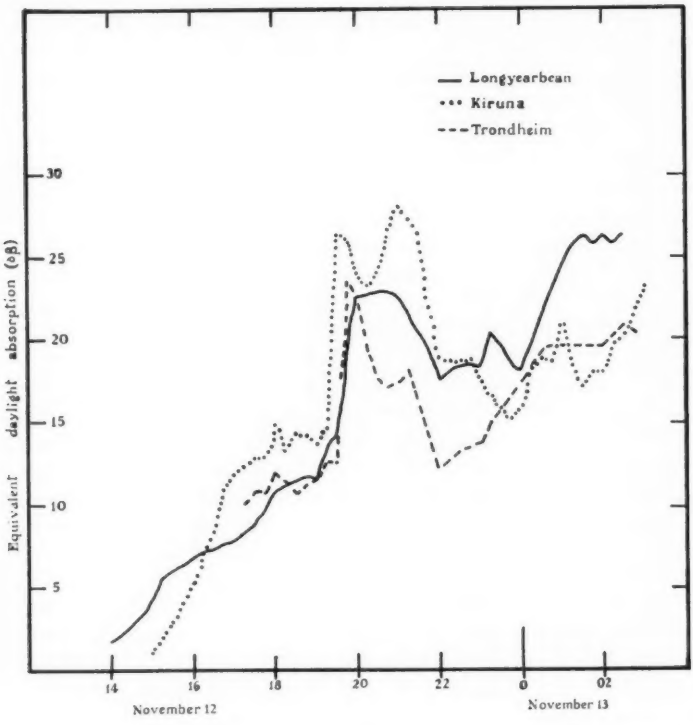

FIG. 2

worth pointing out that the C.N.A. is sensitive to the incidence of cosmic rays of low energy as well as to auroral particles of similar energies in the upper atmosphere, and this should be taken into account when attempting to interpret the results.

It will be seen from the diagram that the solar particles of low energy first arrived at the Earth at about $14^h\,30^m$, that is to say, some 40 minutes later than the arrival time of the higher energy flux detected by neutron monitors at near-by stations. The growth of intensity of these low energy particles was also much slower than that of the higher energy flux, the maximum intensity being reached

* $\bar{\lambda}$ is the effective geomagnetic latitude (see Quenby and Webber 1959).

† We are indebted to Dr K. W. Eriksen for the data from Longyearbean and Trondheim and to Dr B. Hultquist for those from Kiruna Geophysical Observatory.

only after $04^h\,00^m$ on the 13th, whilst the corresponding maximum of neutron intensity occurred around 16·00 on the 12th. Indeed, the entire character of the C.N.A. variations is radically different from that seen by the neutron monitors and it is evident that we are now dealing with flare particles in a different and much lower energy range, as is shown by the much longer time taken by the particles to diffuse through the inner solar system. It is also clear from Fig. 2 that the C.N.A. variations at the three stations, spread over a wide range of latitudes, were very similar. Attention should also be drawn to the sharp increases of C.N.A. which occurred over the interval $19^h\,00^m$ to $21^h\,00^m$ and which were apparently related to the sudden increase observed by neutron monitors around $19^h\,00^m$. The magnitude of these increases in the primary flux as detected by C.N.A. and as observed by neutron monitors both appear to be roughly equal to a factor of 3.

A consideration of the results outlined above as well as those from other stations distributed on a world-wide basis, including polar stations, permits us to establish the following broad features in relation to this event of November 12.

The first solar particles to arrive at the Earth appeared between $13^h\,50^m$ and $14^h\,00^m$. Although impact zones in the normal sense were not identifiable during the initial phase of the increase, very marked longitudinal anisotropies in the incident flux were present during the period $14^h\,00^m$ to $18^h\,00^m$. The rise in intensity was steepest and the maximum increase was largest and earliest at stations which, when geomagnetic deflection is allowed for, were scanning those portions of the sky that lie between 0° and 120° due west of the Sun–Earth line. In the case of stations viewing the remaining part of the sky, the growth was slower and the maximum intensities of solar particles recorded were only about half as large as those in the first group of stations. The stations in Europe were at this time recording solar particles arriving from directions away from the Sun and were therefore recording the lower intensities from these directions. The ratio of the intensities measured at Uppsala and London as well as the ratio of Leeds to London were increasing during the first two hours of the flare increase, and this shows that the lower energy part of the solar particles was building up more slowly than the higher energy portions in these directions.

By $16^h\,00^m$ to $17^h\,00^m$, however, the flux of solar particles appears to have become sufficiently isotropic to enable a spectrum determination to be made, and the differential rigidity spectrum of the extra radiation from the Sun at this time is of the form $dN/dp = (p_0/p)^n$ (p in units of rigidity) where p_0 is a constant and $n = 7{\cdot}2$ on the average, in the rigidity range 1 to 4·5 GeV. The curve of solar particle intensity plotted against threshold rigidity for this event is, however, markedly different from that for 1956 February 23, in that the curve for the November 12 event flattens off more sharply at lower rigidities even though the spectrum appears to be steeper at the higher rigidities. The equivalent value of n in the recent event varies from ~ 5 to 1 GeV to ~ 8 at 4·5 GeV. This could reflect a flattening of the flare spectrum itself. We argue that this flattening cannot be ascribed entirely to the fact that the low energy particles had not arrived in comparable abundance at that time, but was due rather to a systematic lowering of the geomagnetic threshold rigidities appropriate to each station. Such a lowering of thresholds appears to be necessary to reconcile the sharp differences between the intensities of low energy radiation implied by neutron monitor and C.N.A. measurements. A consistent explanation for the flattened

latitude curve and the differences in intensities of the low energy particles as implied by the two methods of detection can be obtained by assuming that the geomagnetic thresholds had been lowered by a filamentary ring current of 5×10^6 amp having a radius 8 to 10 times the Earth's radius. Such a ring current would also lower the equatorial horizontal field by 50γ. It should be noted that this ring current is postulated as being relative to the conditions which prevailed on 1956 February 23 and is to be envisaged as a quiet time current which existed before the onset of the main phase of the magnetic storm.

During the period $17^h 00^m$ to $19^h 00^m$ the intensity of the solar flux as recorded at high latitudes appears to decrease continuously. The intensity of the secondary radiation measured in the geomagnetic latitude range 45° to 55°, however, was increasing steadily during the period. This behaviour is clearly seen in Fig. 1 and is borne out by the data from other parts of the world. This is precisely the character of the changes to be expected if there was, during this interval, a systematic and progressive further reduction in the geomagnetic thresholds at all stations. It can be seen from Fig. 1 that a remarkable correlation exists between this reduction and the decrease of H at equatorial stations during the main phase of the magnetic storm. The lowering of threshold rigidities appears as a progressive shift to higher rigidities of the knee of the curve depicting solar particle intensity against the normal threshold rigidity (e.g. the curve is now almost completely flat below 1·8 GeV). It is obvious that the lowered thresholds produce an increase in the primary flux entering the atmosphere at all stations, but this increase is reflected in an increase in neutron monitor intensity at middle latitudes only because of the very weak response of the high latitude monitors to the additional flux.

Around $19^h 00^m$ there occurred a sharp increase of the neutron intensity recorded at all stations, including those at high latitudes. The time of commencement varied from station to station by as much as 10 minutes, and the times taken to reach maximum intensity were also widely different. It is evident from the foregoing discussion that this increase cannot be attributed to a sudden further lowering of the geomagnetic thresholds which would introduce additional low energy radiation from a constant intensity of solar particles present outside the Earth's magnetic field. Instead, there is little doubt that a sudden increase occurred in the flux of solar particles arriving in the vicinity of the Earth at this time (outside the geomagnetic field) and that it was related to a changing geometry of the trapping region in the interplanetary magnetic field. It could, of course, be connected also with the modulating mechanism which produced the Forbush decrease commencing at $19^h 30^m$. The lack of isotropy prevailing at this time prevents us from making an accurate determination of the energy spectrum of this additional radiation, but, broadly speaking, the absence of any correspondingly sudden changes in the Uppsala to London and Leeds to London ratios indicates that the increase was not accompanied by any marked change in the energy spectrum. The absence of change in these ratios also lends weight to the view that this increase was not of geomagnetic origin.

Between $19^h 00^m$ and $20^h 00^m$ the recorded intensities at many stations showed marked fluctuations, with a particularly sharp trough occurring at $19^h 30^m$, thus producing the double hump appearance already mentioned. The dissimilarities between stations are rather pronounced, the first hump being a particularly variable feature. We believe that this interval represents a transition

from a region of low intensities to another where the intensities were three times as great, this transition being due to the outward motion of the interplanetary trapping field past the Earth. The transition to high intensity was irregular and the particle flux became very anisotropic during this time. It is worth noting that a strong positive pulse of $\sim 100\gamma$ occurred at $19^h 30^m$ in the horizontal (magnetic) intensity at equatorial stations and the possibility is not excluded, therefore, that the trough in neutron intensity occurring at this time, as well as certain other anisotropic features during this time, were due to some geomagnetic effect causing a sharp increase in the threshold rigidities.

By $20^h 00^m$, however, at most stations maximum intensity was reached together with the establishment of a high degree of isotropy in the flux of solar protons arriving at the Earth. At about this time the horizontal field intensity at equatorial stations was also passing through a shallow minimum of about 120γ below normal, and it seems likely that the maximum lowering of geomagnetic thresholds also occurred about this time. The Uppsala to London ratio had by now been reduced to 1·6 : 1 (as against 4·6 : 1 at $16^h 00^m$) and Leeds was observing nearly the same increase as Uppsala. In fact, by considering the data from a world-wide network of stations, it appears that all stations which had thresholds below 2·0 GeV at normal times were registering very nearly the same intensity. It is estimated that a simple filamentary ring current of radius 6 to 8 Earth radii and of strength 10^7 amp would produce the necessary lowering of geomagnetic thresholds which could explain the above results. Such a current would also reduce the equatorial H by 100γ below that prevailing between $16^h 00^m$ and $17^h 00^m$. This estimate is evidently in fair agreement with the observations of H at Colombo.

During the decay phase which set in after $20^h 00^m$ the solar particles were arriving uniformly from all directions, as can be seen by the close agreement between the increases observed by the world-wide network of stations. Derivation of a mathematical form for the decay of the radiation is complicated by further changes in magnetic thresholds, but it can nevertheless be stated that the highest energy particles disappeared most quickly thus producing an increasingly steep spectrum of the solar flux at the Earth. The exponent n of the differential spectrum was $8{\cdot}5 \pm 0{\cdot}3$ in the range 1 to 4 GeV by $02^h 00^m$ on the 13th.

Additional evidence for lowered geomagnetic thresholds at various stations during this event is provided by the C.N.A. measurements. Considering, for example, the intensities at $18^h 00^m$, we note that if the threshold at Uppsala at this time was the normal value of 1·2 GeV as determined by the Earth's internal field, the additional flux of flare particles at the top of the atmosphere could be deduced, using specific yield functions, to be about 100 times the normal galactic flux above this energy. If we now extrapolate the spectrum (with exponent $n = 7{\cdot}2$) derived from cosmic ray observations in the range 1 to 4 GeV down to lower energies, we can predict that the C.N.A. at Trondheim with a normal threshold of 0·7 GeV should be 4 dB corresponding to an intensity of flare particles 1000 times the normal galactic flux. As a matter of fact the observed absorption is 12 dB, indicating that the estimated flux is too low by a factor of 10 or more. Indeed, the estimated value of 4 dB is probably already too high because the lower energy radiation, as measured by the C.N.A., was still increasing at this time.

If, however, we assume that the threshold at Uppsala was 0·7 GeV the corresponding flux of solar particles at the top of the atmosphere is 1000 times the galactic flux and we would now expect to observe an absorption of 12 dB at stations having a threshold of 0·5 GeV or less. It appears, then, that the cosmic ray and cosmic noise absorption measurements can be reconciled only if we assume a systematic lowering of the geomagnetic thresholds appropriate to each station. Taking this in conjunction with the cosmic ray evidence it is apparent that both before and particularly after the main phase each observatory was admitting particles having energies very much lower than could conceivably have been allowed on the basis of thresholds determined solely by the internal magnetic field of the Earth.

Mention should also be made of the pulses of neutron intensity which were superposed on the exponential decay of the radiation after $20^h\,00^m$ on the 12th. These pulses were the strongest around the latitude of London but were not observed at geomagnetic latitudes above 55°. They occurred at the same universal time at all stations which were in a suitable position to observe them and were centred at $21^h\,10^m$, $22^h\,40^m$ and $00^h\,30^m$ U.T. As the latitude dependence of the magnitude of these sharp increases is closely similar to that encountered earlier for the increases during the period $17^h\,00^m$ to $19^h\,00^m$, when a lowering of geomagnetic thresholds occurred, and because of the correspondence in time between these pulses of solar cosmic rays and the pulsating decreases observed in equatorial H, it seems very likely that these enhancements of intensity were caused by sudden and short-lived decreases in the geomagnetic thresholds which recurred at intervals of about $1\frac{1}{2}$ hours.

In contrast to the great complexity of the flare outburst of November 12, the second flare-associated increase of neutron intensity which followed the 3+ flare of $02^h\,21^m$ on the 15th showed all the characteristics that have come to be regarded as typical of such events.

At London, the neutron intensity rose gradually from $02^h\,40^m$ onwards, reaching a maximum of about 15 per cent above the pre-flare level by about $03^h\,30^m$ and thereafter decaying away in a nearly exponential manner. These results, together with those from other stations in Europe, are shown in Fig. 2 were it can be seen that similar features were observed at other stations as well. However, these stations were not lying within impact zones for this event. The rapid and large increases characteristic of impact zones were seen by stations receiving primary particles arriving from asymptotic directions lying between 40° and 100° to the west of the Earth–Sun line. The oscillations reported by Steljes, Carmichael and McCracken (1961) were observed during the transition from this initial phase to the isotropic phase. The oscillations, however, appear to have been even more highly localized than the impact zones themselves.

Almost complete isotropy of the incoming particle radiation had set in between $04^h\,30^m$ and $05^h\,00^m$ and about this time the exponential decay of the flare flux also commenced. A characteristic time t_0 for the decay could be deduced, which varied systematically from station to station (for example, $t_0 = 4{\cdot}0$ hr at Uppsala, $t_0 = 3{\cdot}5$ hr at London, $t_0 = 1{\cdot}8$ hr at Jungfraujoch). The characteristic time was, in fact, rigidity dependent with a form $t_0(p) = 4{\cdot}5p^{-1/2}$, where t_0 is in hours and p in GeV. The rigidity spectrum at $05^h\,00^m$ had the same exponent as that at $17^h\,00^m$ to $18^h\,00^m$ during the earlier increase. Even the flattening-off of the solar particle intensity versus normal threshold curve below about 1·5 GeV,

observed early in the November 12 event, was reproduced. This last fact is easily understandable because the Earth's magnetic field had not recovered completely from the storms of the 12th and 13th and it is likely that the geomagnetic thresholds were still below normal.

The increase of C.N.A. remained below 2 dB until $06^h\,00^m$, at which time the intensities recorded by neutron monitors had already been decaying from their maxima for about an hour. The intensities of low energy particles implied by the C.N.A. measurements indicate that the $p^{-7\cdot2}$ spectrum of the solar particles, as measured at rigidities above 1 GeV, must have flattened out below 0·8 GeV. The flux of low energy particles in fact continued to grow throughout the major part of the 15th and produced a maximum daylight equivalent C.N.A. of about 50 dB by $20^h\,00^m$, at which time the neutron monitors at high latitudes were showing increases of only a few per cent above the galactic flux. The solar particle flux as implied by neutron monitor measurements and the C.N.A. measurements are consistent provided we assume lowered thresholds are still operative at this time. We estimate that the flux at this time had reached an intensity of $\sim 7 \times 10^4$ per $cm^2\,sec^{-1}$ above an energy of about 10 MeV. The value of the maximum C.N.A. suggests that the flare of the 15th was much more copious in its production of low energy particles than the earlier one, when the maximum absorption was about 30 dB corresponding to an intensity $\sim 2{\cdot}5 \times 10^4/cm^2\,sec^{-1}$.

4. *The Forbush decreases.*—In addition to providing these spectacular examples of the acceleration of particles to cosmic ray energies during solar flares, the high level of solar activity prevailing during this eventful week was also responsible for the production of a series of Forbush decreases which followed one another in rapid succession. At high latitudes, these decreases were best observed by meson detectors which were too insensitive to detect the large influx of solar particles which overlapped the Forbush decreases on both occasions. The detectors at London consisted of standard cubical telescopes operated at sea level and two semi-cubical scintillator telescopes having a high counting rate (50 000/hr) operated underground at a depth of 60 metres water equivalent (m.w.e.)*. The data from these recorders and the neutron monitor are plotted in Fig. 4, which also shows the changes of the horizontal magnetic field at Colombo.

It can be seen from Figs. 1 and 4 that the first decrease of the series commenced at $19^h\,30^m \pm 15^m$, nearly 6 hours after the S.C. and about $2\frac{1}{2}$ hours after the beginning of the main phase of the magnetic storm accompanying the decrease. It would appear that the commencement and the initial stages of this Forbush event, within the limits of experimental accuracy, were simultaneous on a world-wide scale. A maximum depression of about 4 per cent was reached within an hour or two of the commencement by the counter telescope at London, and thereafter a slow recovery to normal started. The underground monitor also followed a pattern of variations similar to that of the telescope at sea level, but the maximum decrease was $1{\cdot}2 \pm 0{\cdot}3$ per cent. The rapidity with which the decrease took place, particularly in the high energy radiation measured by the underground telescope, is remarkable, and this determines the strength of the screening magnetic field that is required to move past the Earth as being of the order of 100γ if we assume a mean rigidity of 200 GeV for the primary particles

* The absorbing material over the recorders has the same effect as a water absorber of 60 m thickness.

which are monitored at a depth of 60 m.w.e. Comparison of our results with those from other stations shows that the recovery from the first decrease was not associated with any marked anisotropies.

This first decrease cannot be readily identified in the intensities registered by neutron monitors at latitudes over 50° because of the prevailing flare-associated increases, but it is possible to deduce that the decreases in these monitors must

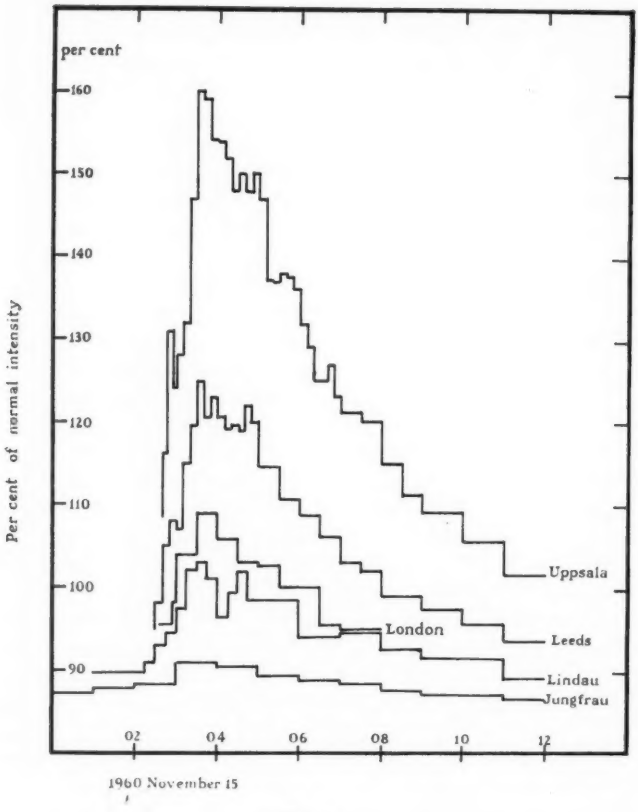

FIG. 3

have been about 6 to 8 per cent. The flux of solar particles had decayed to less than a few per cent even at high latitudes by $12^h 00^m$ on the 13th, and between this time and $02^h 00^m$ on the 15th the intensity variations recorded by the neutron monitor and the cubical telescope at London were roughly parallel.

A short while after $10^h 30^m$ on the 13th, a second Forbush decrease occurred which depressed the intensities further in all three recorders at London. Unlike the first decrease, the second one began at about the same time as the S.C. of the weak magnetic storm which was probably caused by the arrival of the plasma cloud from the flare of the 12th. The time taken to reach the minimum between $21^h 00^m$ and $23^h 00^m$ was much longer for this event, and during the course of the decrease exceptionally strong anisotropies were developing. The solar

particles that were still arriving at high latitudes from the event on the 12th were completely removed at the onset of this event although no corresponding depletion of the low energy particles as measured by the C.N.A. was noted at this time.

The total decrease resulting from the two Forbush events amounted in London to 13 per cent in the neutron intensity, 8·5 per cent in the meson intensity at sea level, and 1·4 per cent in the meson intensity at a depth of 60 m.w.e. The ratio

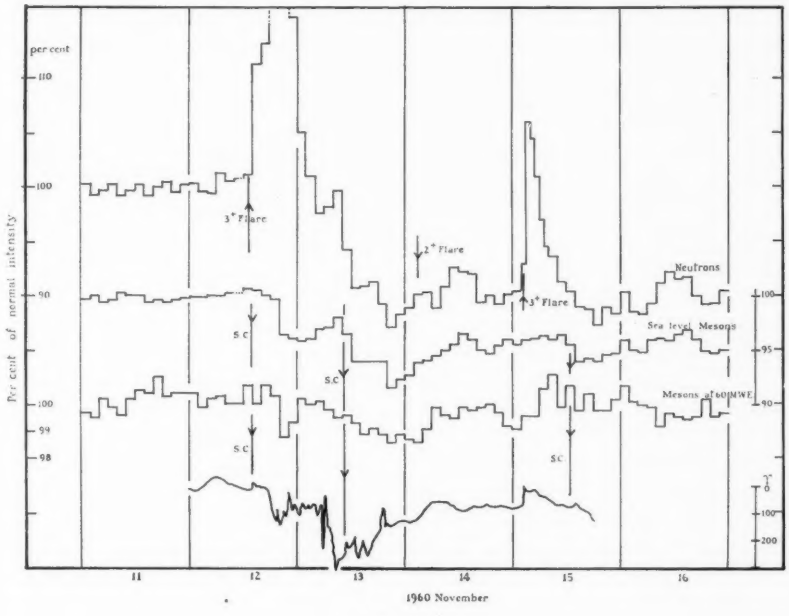

FIG. 4

of $0{\cdot}15 \pm 0{\cdot}03$ for the decrease measured underground to that in meson intensity at sea level would imply, on the basis of specific yield functions available at present, that the fractional modulation of the primary intensity during this event could not have been steeper than a power of -1 in rigidity (or energy) over the range 20 to 200 GeV. In fact the average modulation over this range fits the results closely when represented by a function of the form

$$\frac{dP}{dJ} = \frac{P_0}{P}\left(\frac{dJ_0}{dP}\right)$$

where dJ_0/dP is the unmodulated spectrum and P_0 is a constant.

During the early hours of the 14th the recovery of the meson intensity had commenced and the period of recovery was attended by continued strong anisotropies. Large anisotropies were also observed by the underground detector. There is some evidence that the axis of the anisotropy was such that the greatest decrease occurred at a local time of $03^{h}\,00^{m}$, and this direction of anisotropy was maintained until the anisotropy disappeared on the 15th.

These features are identical for the very high energy cosmic rays observed by the underground detector as well as the lower energy particles observed by neutron monitors at sea level.

It is of interest that the direction from which solar particles arrived in direct paths from the Sun in this second flare outburst was roughly perpendicular to the axis of anisotropy of the Forbush decrease which was still in progress at this time.

A more detailed analysis of various aspects of these Forbush decreases, including a comparison with models suggested as explanations of these events, is at present under way.

5. *Conclusions.*—The remarkable sequence of events described above gives promise of much valuable information on the conditions existing in interplanetary space and in the outer regions of the Earth's magnetic field at this time. Meanwhile, it is convenient to summarize some aspects of the flare increases which have become clearly evident for the first time in the course of this event and which can provide quantitative information on the factors controlling the propagation of solar cosmic rays between the Sun and the Earth.

(i) The important effects on the Earth's magnetic field (Webber 1961) and possible modifications in its structure were amply demonstrated by such results as the apparent flattening of the flare energy spectra at low energies and the apparent intensity variations which did not necessarily reflect the conditions existing outside the influence of the Earth's field.

(ii) The first event in particular showed that trapping regions with well-defined boundaries may exist in the inner solar system which may be filled to much higher intensities with solar particles than the surroundings. There is quite probably a relationship between these trapping regions and the mechanism producing Forbush decreases. There is also the possibility that the trapping regions may be linked directly to the flare regions.

(iii) The intensity–time characteristics of both the initial and the decay stages of these events, as well as the degree of anisotropy, which was ~ 1 per cent during the decay phases of both events, indicate that scattering and diffusion are important aspects of the interplanetary magnetic field between the Sun and the Earth as well as outside the Earth's orbit.

(iv) The preferential arrival of solar particles from directions lying well to the west of the Sun was encountered at the beginning of both events, as also during the event of 1960 May 4 (McCracken and Palmeira 1960), and this suggests the action of a deflecting influence which changes the apparent position of the "source". This preferential direction may be closely related to anisotropies existing in the galactic radiation at these times.

(v) The flux of solar particles at low energies may reach a level 10^5 times the normal cosmic ray flux, and the corresponding energy density about 1000 times normal or 1000×10^{-12} erg/cm^3.

Acknowledgments.—It is a pleasure to acknowledge our debt to Professor H. Elliot for the benefit of many valuable discussions. We are greatly indebted to Professor M. A. Ellison of Dunsink Observatory for the solar data, and to Drs K. W. Eriksen and B. Hultquist for the results of C.N.A. measurements. We gratefully acknowledge the geomagnetic data from equatorial stations sent by Dr V. Appapillai from Colombo and Captain R. A. Earle of the Geophysics Division, U.S. Department of Commerce. Special thanks are due to all the investigators who made cosmic ray observations and communicated their results, and in particular to the groups at Amsterdam, Berne, Buenos Aires, Durham,

Hobart, Leeds, Lincoln, Lindau, M.I.T., Munich, New York, Ontario, Ottawa, Paris, Praha, Swarthmore, Uppsala, and Yakutsk. We wish to thank Miss A. Benton and Mr F. Romero for assistance in the preparation of this paper.

Imperial College of Science and Technology,
London, S.W.7:
1961 *June* 6.

References

McCracken, K. G., and Palmeira, R. A. R., 1960, *J. Geophys. Res.*, **65**, 2673.
Pomerantz, M. A., Duggal, S. P., and Nagashima, K., 1961, *Phys. Rev. Lett.*, **6**, 123.
Quenby, J. J., and Webber, W. R., 1959, *Phil. Mag.*, **4**, 90.
Sinno, K., and Hakura, Y., 1958, *Rep. Ion. Res. in Japan*, **12**, 285.
Steljes, J. F., Carmichael, H., and McCracken, K. G., 1961, *J. Geophys. Res.* (to be published).
Webber, W. R., *Prog. in C.R. Physics*, Vol. **6**, 1961.

A RADIO SURVEY OF THE GALACTIC PLANE AT A FREQUENCY OF 408 MC/S

I. The Discrete Sources

M. I. Large, D. S. Mathewson and C. G. T. Haslam*

(Communicated by the Director, Nuffield Radio Astronomy Laboratories)

(Received 1961 June 8)

Summary

Part of the galactic plane has been surveyed at 408 Mc/s using the 250 ft radio telescope at Jodrell Bank. The results are compared with the Sydney 85 Mc/s survey and the Leiden 1390 Mc/s survey in order to group the discrete sources of radio emisson according to their spectral index. Of fifty-one sources, thirty-six are found to have a spectral index consistent with the assumption that they radiate thermally, and fifteen, including the source at the galactic centre, have a non-thermal spectral index. Most of the sources lie within 1/4° of the new galactic plane, and are thought to be at distances of several kiloparsecs. Some of the thermal sources are a few degrees from the galactic plane, and probably less than one kiloparsec from the Sun. The continuum background emission from the galactic disk is discussed in a second paper.

---

1. *Introduction.*—The radio emission from the Galaxy has been divided into three major components. First, the corona (Baldwin 1955), which has a very extended distribution and is responsible for the greater part of the emission at metre wavelengths. Second, a disk component (Mills 1959), which is closely confined to the galactic plane, and is roughly co-extensive with the visible parts of the Milky Way. Third, a population of discrete sources of radio emission (Hanbury Brown and Hazard 1953; Mills 1959) which lie close to the ridge line of the disk. A large number of these discrete sources are thermal, having a spectrum characteristic of a hot gas. Some of these sources have been identified with emission nebulae (Westerhout 1958). The spectrum of the remainder suggests that the radio emission is produced by a non-thermal mechanism. The three known supernova remnants in the Galaxy are radio sources of this kind, and the suggestion has been made that all non-thermal galactic sources are supernova remnants (Mills 1959; Hanbury Brown 1954).

In this paper the results of a 408 Mc/s survey of part of the galactic plane are presented. The survey is used in conjunction with the Sydney 85 Mc/s survey (Hill, Slee and Mills 1958) and the Leiden 1390 Mc/s survey (Westerhout 1958) to investigate the spectrum and distribution of the discrete sources in the area common to the three surveys. The continuum background emission from the galactic disk will be discussed in a second paper.

* Now at C.S.I.R.O., Sydney.

2. *Observations.*—In May 1959 the region of the sky bounded by $b^{II} = \pm 6°$ and $l^{II} = 350°$ to $56°$ was surveyed at 408 Mc/s using the 250 ft radio telescope at Jodrell Bank (Lovell 1957)*. The equipment was substantially the same as that used in previous surveys (e.g. Large, Mathewson and Haslam 1959). The aerial beam had a width to half power points of 40×54 minutes of arc. The beam solid angle as defined by Seeger, Westerhout and van de Hulst (1956) was measured to be 0·70 square degrees. The receiver was stabilized by a Dicke system; the overall noise figure was 6 dB and bandwidth 4 Mc/s. A daily calibration was made by observing the Cygnus A (19N4A) radio source, taking the flux density of that source to be 4210×10^{-26} w.m.$^{-2}$(c/s)$^{-1}$ (Seeger, Westerhout and Conway 1957). The region was surveyed mainly by driving the telescope in right ascension at 1 deg/min at constant declination. Fig. 1 is typical of these scans, which were made at 20 minutes of arc intervals. A few scans along the galactic plane were made by driving the telescope in galactic longitude, at constant latitude. An example is shown in Fig. 2.

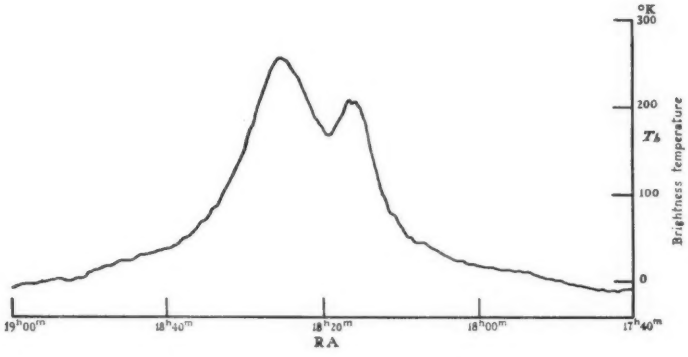

FIG. 1.—*A typical scan in right ascension at constant declination,* $\delta = -11° 50'$.

Fig. 3 (*a*) shows the 408 Mc/s radio isophotes drawn in units of 43 °K brightness temperature, measured above a selected reference region (at $\alpha = 19^h 20^m$, $\delta = 0°$). The brightness temperature is calculated from the chart deflection by the method described in a previous paper (Mathewson, Large and Haslam 1960).

The position of the beam has been computed from the azimuth and elevation dial readings of the telescope. Corrections have been added for refraction, and for the deviation of the radio axis from the nominal axis of the paraboloid. These corrections were determined experimentally by observing strong radio sources at various elevations. The probable error of position over the whole survey is ± 5 minutes of arc. The error in the quoted position of weak or extended sources may be greater than this value.

3. *The list of discrete sources.*—Fig. 2 shows a 408 Mc/s radio profile obtained by scanning the telescope along the path close to the galactic plane. The discrete sources are clearly seen above the background. In measuring the sources a

* The symbols b^{II} and l^{II} are used to indicate the new galactic latitude and longitude (*Trans. I.A.U.*, 1958).

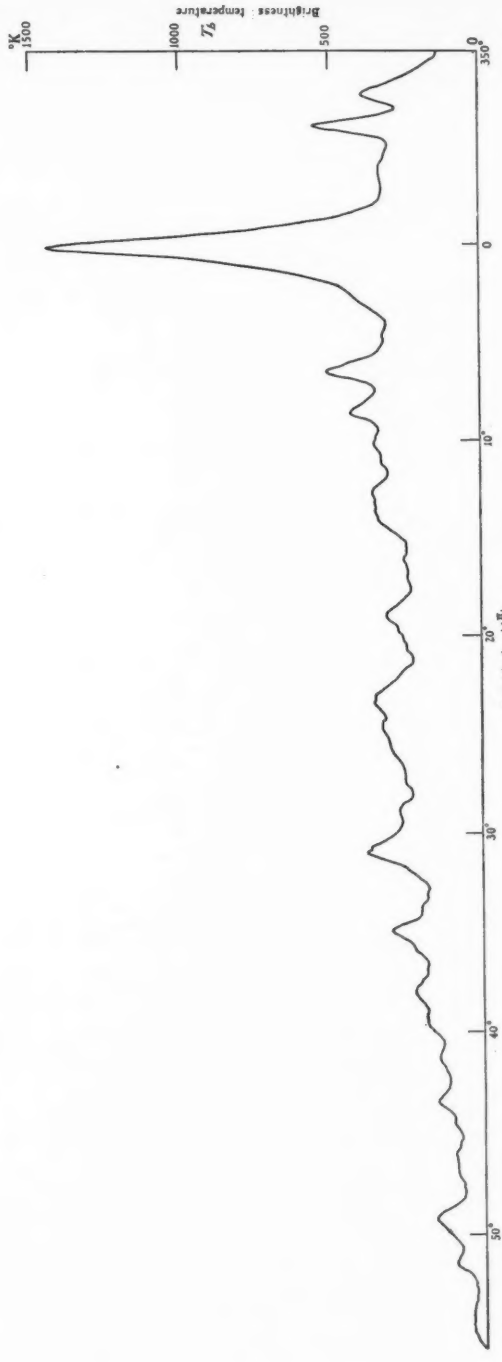

FIG. 2.—*A scan along the galactic ridge, close to the line* $b^{II}=0°$.

Table I

A list of 51 sources in the galactic plane, showing positions, intensities and spectral indices.

Abbreviations used: W, Westerhout (1958); WB, Wilson and Bolton (1960); MSH, Mills, Slee and Hill (1958 and 1960); 3C, Cambridge third survey, Edge *et al.* (1959); l^{II}, b^{II}, l^{I}, b^{I}, α, δ: new and old galactic coordinates, right ascension and declination; in abs., in absorption; T_B brightness temperature; $\alpha(408/1390)$, flux density spectral index deduced from ratio of T_B at 408 Mc/s and 1390 Mc/s; $\alpha(85/408)$, flux density spectral index deduced from ratio of T_B at 85 Mc/s and 1390 Mc/s; em. neb., emission nebula; non-th., non-thermal spectrum; th., thermal spectrum.

Source					Position						Flux	Brightness temperature T_B			Spect. index		
									(1950·0)								
No.	W	WB	MSH	3C and I.A.U.	l^{II}	b^{II}	l^{I}	b^{I}	α	δ	w.m.$^{-2}$(c/s)$^{-1}$	85 Mc/s	408 Mc/s	1390 Mc/s	$\alpha\left(\frac{408}{1390}\right)$	$\alpha\left(\frac{85}{408}\right)$	Notes
					°	°	°	°	h m	°		°K	°K	°K			
1		39	17–34?		351·5	+0·5	319·2	−0·8	17 18·4	−35·8	110×10^{-26}	0±1000	100	8	0·0	th.	em. neb.
2	22	40			353·3	+0·8	321·0	−0·5	17 22·1	−34·1	500	(in abs)	420	44	+0·1	th.	em. neb.
3			17–37		*353·8*	*0·0*	*321·5*	*−1·3*	*17 26·6*	*−34·2*	30±20	1500	30±20	< 3		−0·5	non-th.
4			17–38		*355·3*	*+0·6*	*323·0*	*−0·8*	*17 28·3*	*−32·6*	0	1500	0	0		?	non-th.
5	23				355·6	+0·1	323·3	−1·3	17 31·1	−32·6	50	0	30	3	+0·1	th.	em. neb.
6					358·0	0·0	325·7	−1·4	17 37·6	−30·6	40		35	3	0·0		th.
7	27?	44			358·7	−5·0	326·4	−6·4	17 59·4	−32·6			50				th?
8	25				358·9	−1·8	326·6	−3·2	17 47·1	−30·8	35	0	30	3	+0·1	th.	em. neb.
9	24	42	17–213	17S2A	0·0	0·0	327·7	−1·4	17 42·4	−28·9							Sgr. A
10					3·0	0·0	330·7	−1·4	17 49·5	−26·4	35		30	3	+0·1		th.
11	29	46			6·0	−1·25	333·7	−2·7	18 1·0	−24·4	200	−2000 (in abs)	190	17	0·0	th.	em. neb.
12	28	45	17–216		6·6	−0·2	334·3	−1·7	17 58·3	−23·4	450	15,000	330	22	−0·2	−0·4	non-th. (12)
13	30	47	18–21		8·7	0·0	336·4	−1·5	18 2·1	−21·5	180	3500	130	12	0·0	−0·1	th. $T_e>25{,}000$°K (13)
14	31	49	18–23?		10·3	0·0	338·0	−1·4	18 5·4	−20·0	65	0	60	6	+0·1	th.	th. (14)
15	36?				10·7	−4·0	338·4	−5·5	18 21·3	−21·6		500	40	3	0·0	tn.	th.
16					11·2	−0·1	338·9	−1·6	18 7·7	−19·3	30	0	30±20	4±2	+0·2	th.	th.
17					*11·7*	*+0·2*	*339·4*	*−1·3*	*18 7·6*	*−18·7*	<20	750	<20			non-th.	non-th.
18	33				12·9	0·0	340·6	−1·5	18 10·8	−17·7		0	100	9	0·0	th.	th.
19			18–13		13·4	+0·2	341·1	−1·3	18 11·2	−17·3	<40	3000	<40	0		−0·7	non-th.
20	33				14·0	+0·1	341·7	−1·4	18 12·6	−16·8			100	9	0·0	th.	th.
21	38	52		18S1A	15·2	−0·6	342·9	−2·1	18 17·6	−16·1	250	0	230	48	+0·7	th.	em. neb (21)
22	37	51			17·0	+0·8	344·7	−0·7	18 15·9	−13·8	130	−1,000 (in abs)	120	13	+0·2	th.	em. neb.
23			18–17		*17·6*	*−0·3*	*345·3*	*−1·8*	*18 21·4*	*−13·8*	20	1,000	20			non-th.	non-th.
24	35	50			18·5	+1·8	346·2	+0·3	18 15·3	−12·0	150	−1,000 (in abs)	120	13	+0·2	th.	em. neb. $T_e<7000$°K (24)
25	39	53	18–18		19·0	−0·1	346·7	−1·6	18 23·2	−12·5	65	2,000	60	6	+0·1	−0·2	Th. $T_e\geqslant10{,}000$°K (25)

26			18–19		20·2	+0·1	347·9	−1·4	18	25·0	−11·3	<20	1,000	<20			non-th.	non-th.
27	26				20·4	+5·1	348·1	+3·6	18	7·3	− 8·8	>30		25	3	+0·2		th.
28			18–*113*		22·0	−0·4	349·7	−1·9	18	29·9	−10·0	100	4,500	90	5	−0·4	−0·5	non-th.
29	41	56	18–*08*		23·3	−0·2	351·0	−1·7	18	31·7	− 8·7	150	3,500	140	12	0·0	0·0	th. $T_e \gg 10{,}000$°K (29)
30	42	57		3C–385?	24·7	0·0	352·4	−1·5	18	33·6	− 7·4	90	0	80	8	+0·1	th.	th.
31			18–09	3C–387?	27·2	0·0	354·9	−1·5	18	38·3	− 5·2	20	1,000	20			−0·5	non-th.
32			18–*010*		28·6	0·0	356·3	−1·5	18	40·9	− 3·9	60	2,000	40	3	−0·2	−0·5	non-th.
33	40	55			28·7	+3·3	356·4	+1·8	18	29·3	− 2·3			45	4	0·0		em. neb.
34			18–*011*		*30·6*	*+0·8*	*358·3*	*−0·7*	*18*	*41·8*	*− 1·8*	0	500	0	0		non-th.	non-th.
35	43	59			30·9	0·0	358·6	−1·4	18	45·0	− 1·9	200	0	150	24	+0·5	th.	th. (35) small diameter.
36			18–*012*	3C–391	*31·9*	*+0·2*	*359·6*	*−1·3*	*18*	*46·3*	*− 0·9*	0	500	0			non-th.	non-th.
37	44	60	18+*011*	3C–392	34·8	−0·4	2·5	−1·8	18	53·6	+ 1·4	230	9,000	210	13	−0·3	−0·4	non-th.
38	47	64			37·7	0·0	5·4	−1·4	18	57·7	+ 4·2	70	0	45	5	+0·2	th.	th.
39		65		3C–396	39·2	−0·1	6·9	−1·5	19	1·0	+ 5·5	50	0	40	3	0·0	th.	th.
40	50	69	19+*01*		39·7	−1·9	7·4	−3·3	19	8·1	+ 5·1		2,000	70	3	−0·5	−0·2	non-th.
41	45	61			41·0	+2·6	8·7	+1·2	18	54·5	+ 8·3		0	40	3	−0·1	th.	th.
42		67		3C–397	41·1	−0·2	8·8	−1·5	19	4·5	+ 7·1	20	0	20	2	+0·1	th.	th.
43	46	62			42·7	+3·1	10·3	+1·7	18	55·8	+10·0		in abs	20±10	4±2	+0·7	th.	th. $T_e < 6000$°K (43)
44	49	68		3C–398	43·3	0·0	11·0	−1·4	19	8·2	+ 9·2	70	0	60	6	+0·1	th.	th.
45		70			45·7	−0·2	13·4	−1·5	19	13·4	+11·2	20		20	2	+0·1		th.
46					46·9	−0·1	14·6	−1·4	19	15·3	+12·3	20		20	2	+0·1		th.
47	51	73		3C–400?	49·1	−0·2	16·8	−1·5	19	20·0	+14·1	250		230	27	+0·2		th.
48					49·5	+0·5	17·2	−0·8	19	18·2	+14·8	40		30	3	+0·1		th.
49		74			51·2	+0·1	18·9	−1·2	19	23·0	+16·1	50		40	3	0·0		th.
50					52·6	−0·4	20·3	−1·7	19	27·6	+17·1	20		20				th.
51	52				53·4	+0·2	21·1	−1·0	19	27·1	+18·1	20		20	2	+0·1		th.

Notes on Sources

12. Bright emission nebula, M.20 near to a non-thermal source.

13. Extended source classed as non-thermal by Wilson and Bolton. Alternatively a thermal region of high electron temperature. Possibly identified with an H II region (Sharpless' (1959) catalogue no. 43) which is 1°·5 in diameter and 0°·3 from this source.

14. Wilson and Bolton class as non-thermal. They wrongly identify it with the Hill Slee and Mills' source at $1' = 336°.4$ (i.e. no 18 −2*1*).

21. Identified by Westerhout as the Omega Emission Nebula. The spectral index of +0·7 between 1390 Mc/s and 408 Mc/s implies a source with an optical depth of 2·3 at 408 Mc/s. Hence the diameter is calculated to be 8′, the emission measure 10^6 cm^{-6} pc., and electron density 500 cm^{-3}. See text, Section 4 (iv).

24. Seen in absorption at 85 Mc/s against a 9000°K background. This implies a low electron temperature for an H II region. Sharpless' (1959) catalogue no. 54.

35. The optical depth of this source is 2·1 at 408 Mc/s. If the electron temperature is 10^4 °K, the diameter is calculated to be 5′ and the emission measure 10^6 cm^{-6} pc. It appears to be situated in a more extended optically thin region. The closest visible H II region, Sharpless no. 66, is 8′ diameter and 0°·5 from the radio position. See text, Section 4 (iv).

43. Apparently seen in absorption at 85 Mc/s, against a 5,000 °K background. This implies a low electron temperature for an H II region. Possibly 3C–394 with lobe shift south.

smooth curve has been drawn through the most marked minima of such profiles to represent the background component. A similar procedure has been applied to the 85 Mc/s and 1390 Mc/s surveys to obtain a consistent definition of a source, and in order to compare the source flux densities at the three frequencies.

Table I is a list of all the discrete sources recognized within the limits of the 408 Mc/s survey. They have been given reference numbers in order of increasing longitude. Subsequent columns of the table indicate, where appropriate, the source number assigned by Westerhout (1958), by Wilson and Bolton (1960), by Mills, Slee and Hill (1958 and 1960), by the third Cambridge survey (Edge *et al.* 1959) and by the I.A.U.

Most of the sources appearing on Hill, Slee and Mills' 85 Mc/s survey and on Westerhout's 1390 Mc/s survey have been detected at 408 Mc/s, and the table lists the position measured from the 408 Mc/s results. Occasionally, when a source is barely detected at 408 Mc/s, the position has been measured from Hill, Slee and Mills' survey. The positions of these sources appear in italics in the table. The positions of the sources at each frequency are marked on the key map (Fig. 3 (*b*)). It will be seen that the positional agreement of the 408 Mc/s survey with *either* the 85 Mc/s *or* the 1390 Mc/s is good but that frequently sources do not appear on all three surveys. The next columns of the table show 408 Mc/s flux density and the measured brightness temperature (T_s) of each source at each frequency. In the case of the 1390 Mc/s results, the temperature quoted has been obtained by convolving the published 1390 Mc/s survey (made with a 35 minutes of arc beam) with a 32 minutes of arc gaussian function to render the effective resolution equal to that of the other two surveys. The ratios of these three brightness temperatures may then be used to obtain a spectral index of brightness temperature for a source, and thence a spectral index of flux density, which is tabulated. A study of these spectral indices (in Section 4) has led to a division of the thermal sources into four groups with different spectral properties, and has also distinguished clearly the non-thermal sources.

4. *The continuum spectrum of the discrete sources.*—The spectral index of flux density for a thermal radio source may range from $+2$ for optically opaque regions to $-0{\cdot}1$ for optically thin regions. In the sky, thermal sources are frequently associated with emission nebulae (H II regions) where the ionization of the hydrogen is maintained by the intense ultra-violet radiation of O and B stars. In such nebulae, the electron temperature is thought to be usually about 10^4 °K (Aller 1956). If other mechanisms of ionization are present, such as collisional excitation, then the electron temperature can be much higher than this (for example in NGC 6992, 6995 it is about 4×10^4 °K (Oosterbrook 1958)). Since a thermal source absorbs incident radiation, the apparent brightness temperature (T_s) depends on the background brightness temperature T_b, and is given by

$$T_s=(T_e-T_b)(1-e^{-\tau})$$

where T_e is the electron temperature of the gas, and τ is its optical depth (Mills, Little and Sheridan 1956). This shows that if T_b is comparable with T_e then the excess temperature of the thermal source is small, and indeed it appears in absorption (as a negative source) if T_b is greater than T_e. Non-thermal sources are assumed not to absorb radiation, and thus to appear in emission against any background temperature. The spectral index of galactic non-thermal sources is observed to range between 0 and -1 (Whitfield 1959).

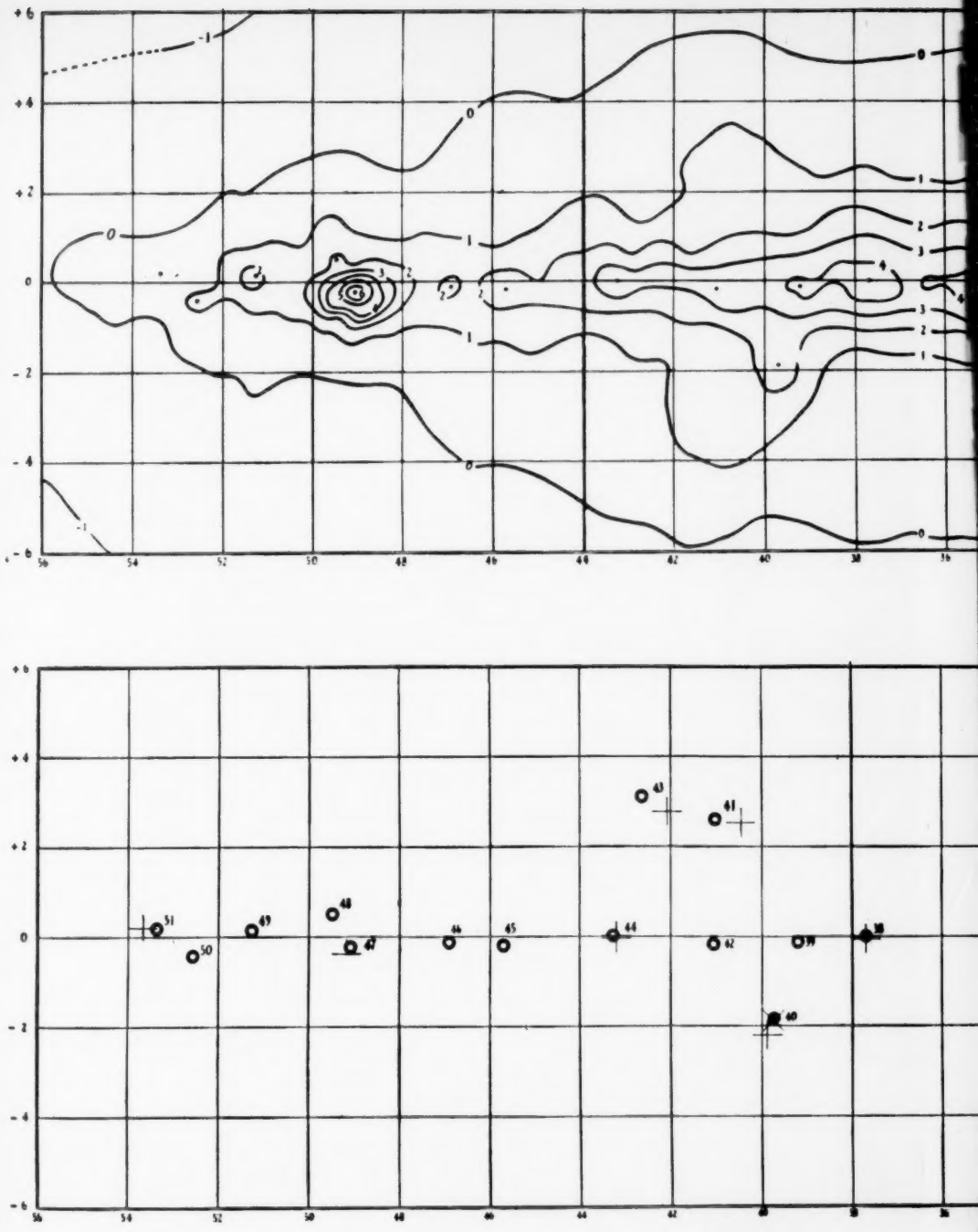

FIG. 3.—408 *Mc/s isophotes (a), and key diagram (b). The intensity unit is 43 °K brightness temperature. The tabulated sourc*

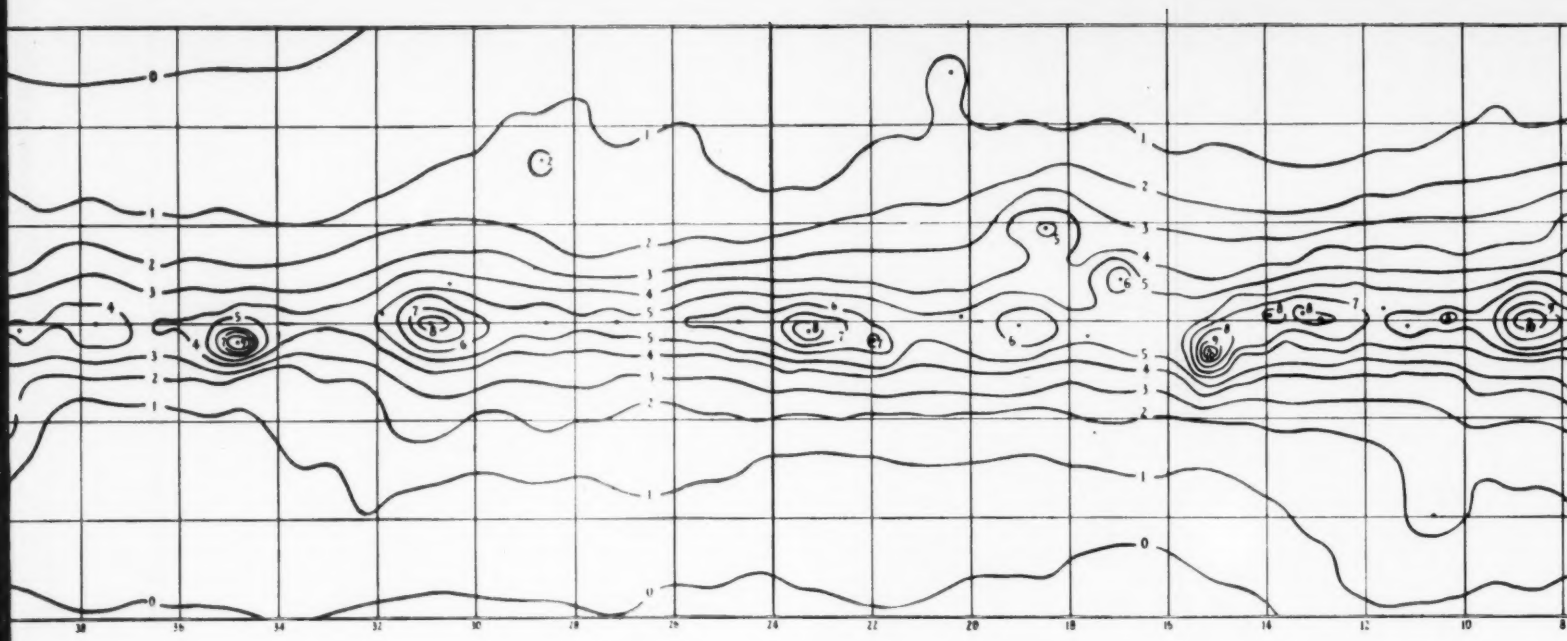

(a)

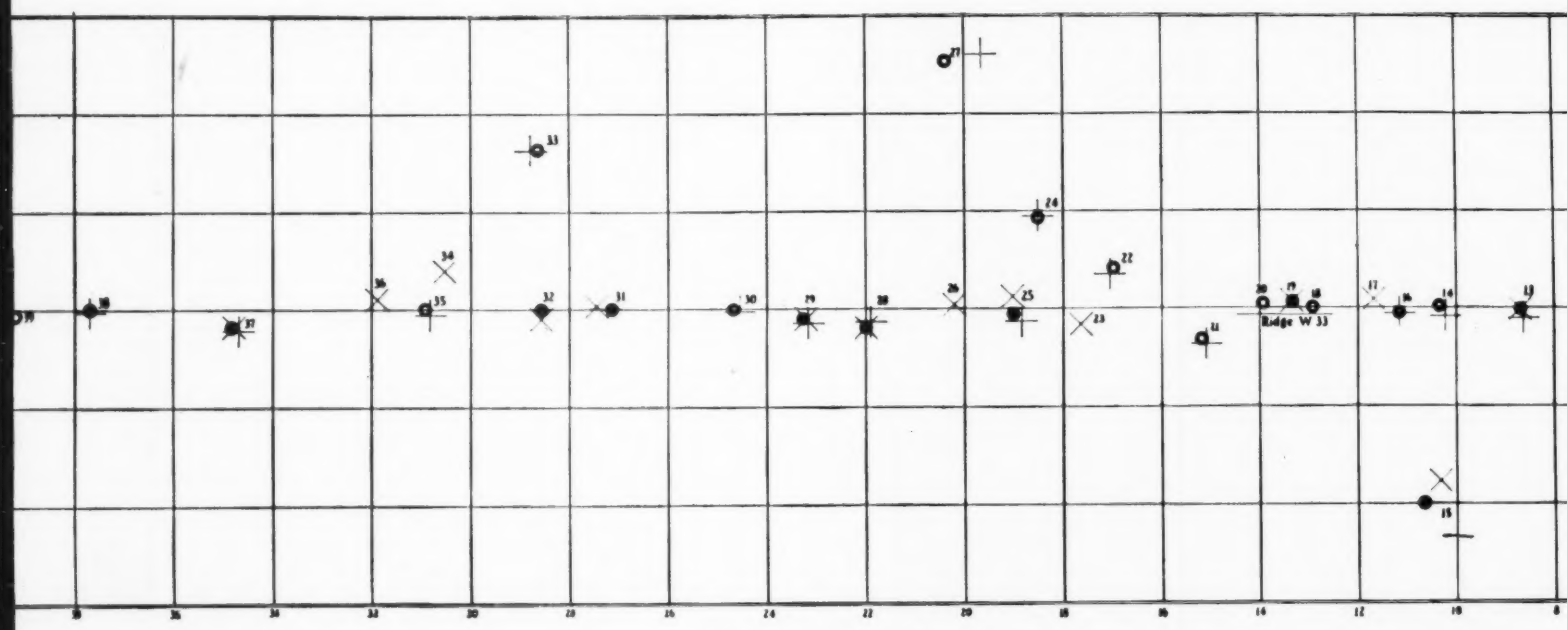

Galactic longitude (l^{II}) degrees

(b)

re. The tabulated source positions are marked with dots on the isophotes. On the key diagram, the 408 Mc/s sources are marked with circles. Open circles indicate thermal sources and clos
non-thermal are indicated by closed circles. Hill, Slee and Mills' positions are indicated by × signs and Westerhout's positions by + signs.

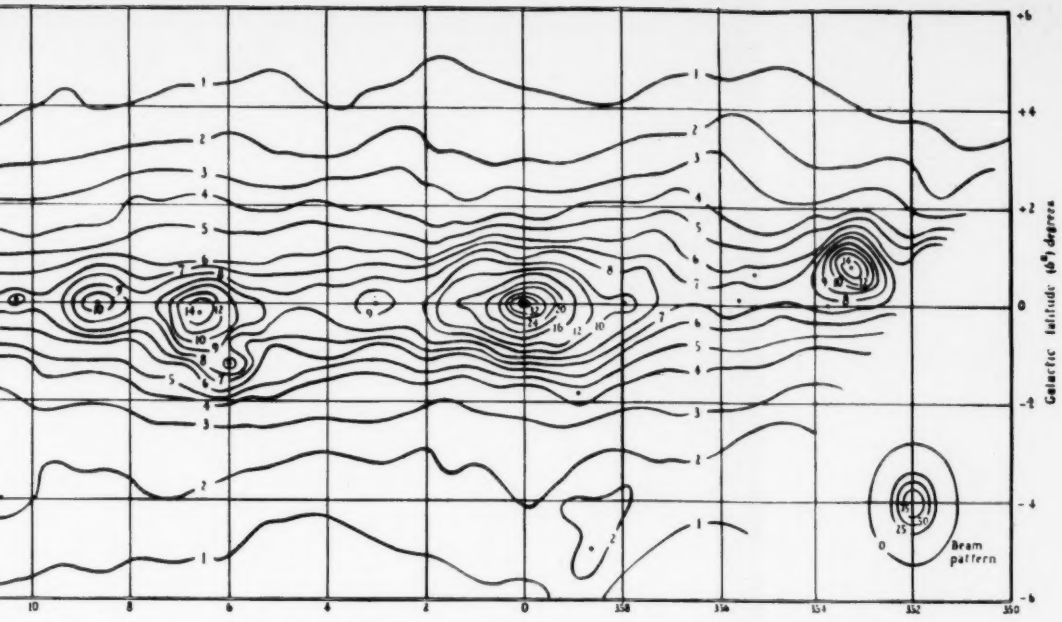

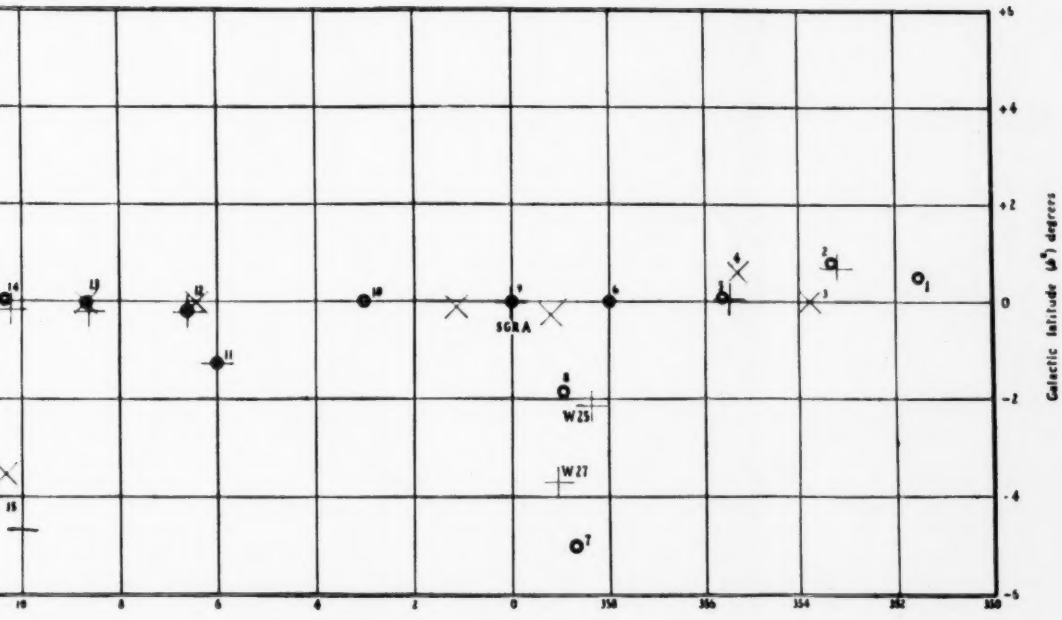

sources and closed circles indicate non-thermal sources. The three sources discussed in Section 4 (iii) which may be thermal or

Fourteen sources in Table I have spectral indices lying between $-0{\cdot}2$ and $-0{\cdot}7$, and are therefore classed as non-thermal (the source 17S2A at the galactic centre is considered separately). Some of the sources are detected at 85 Mc/s only, or at 85 Mc/s and 408 Mc/s only. This seems to be because at the higher frequencies weak non-thermal sources are not easily distinguished from the thermal emission of the Galaxy. Where measurements were possible on the three frequencies it is seen from Table I that consistent values of spectral index were obtained. None of these non-thermal sources has been optically identified.

The remaining thirty-six discrete sources in Table I have spectral indices between $-0{\cdot}1$ and $+2{\cdot}0$ and are consequently classed as thermal. It is very likely that most of these sources are H II regions, and a number of them have been so identified by various authors.

Differences of spectral index observed in the present work are discussed by splitting the thermal sources into four groups, as follows:

(i) Twenty-nine of the sources have spectral indices close to zero as measured between 1390 Mc/s and 408 Mc/s, and appear weakly in emission or absorption at 85 Mc/s, according to whether the background temperature at that frequency is greater or less than 10^4 °K. Many of them are not detected at 85 Mc/s. They are probably all H II regions with typical electron temperatures of 10^4 °K.

(ii) Two of the thermal sources (Nos. 24 and 43) appear in absorption against an 85 Mc/s background of less than 10^4 °K, and thus appear to be H II regions of abnormally low electron temperatures (less than 7000 °K). A similar result was reported by Mills, Little and Sheridan (1956) for the source No. 2 (W22), but the revision of Mills' (1958) temperature scale renders this result invalid, and there is no evidence that the electron temperature of W22 differs appreciably from 10^4 °K.

(iii) Three sources (Nos. 13, 25, 29) have spectral indices close to zero, and yet appear strongly in emission against a high 85 Mc/s background temperature. They are *either* non-thermal sources with very flat spectra indeed, *or* thermal optically thin regions with abnormally high electron temperatures, say 2×10^4 °K. It is generally thought that H II regions do not have electron temperatures as high as this, but such high temperatures can be achieved by collisional excitation mechanisms. Observations at a much lower frequency than 85 Mc/s would be needed to determine the nature of these objects. They do not coincide with any obvious emission nebulae.

(iv) Two sources (Nos. 21, 35) have spectral indices apparently greater than zero, indicating a source optically opaque at 408 Mc/s. By assuming the true electron temperature to be 10^4 °K, and calculating the optical thickness from the spectral index, it is possible to calculate the brightness temperature of the source. This is compared with the apparent brightness temperature to find the dilution factor in the aerial beam and hence the source diameter. In the case of source No. 35 (W43) this diameter was found to be 5 minutes of arc, in reasonable agreement with an interferometer measurement (Wilson and Bolton 1960).

5. *The distribution of the discrete sources in latitude.*—The distribution in galactic latitude of the sources listed is illustrated in Fig. 4, in which the number of sources lying in each $\frac{1}{2}°$ range of latitude is plotted. One histogram includes the sources for which the spectral index lies in the range $+2$ to $-0{\cdot}1$, and the

other histogram the sources for which the spectral index lies between $-0{\cdot}1$ and $-1{\cdot}0$. In the following discussion, the sources in the first group are called thermal, and those in the second group non-thermal. It is seen from this diagram that the majority of the sources lie within $1/4°$ of the galactic plane. Only one non-thermal source lies more than $1°$ from the plane. A number of thermal sources are found several degrees from the plane.

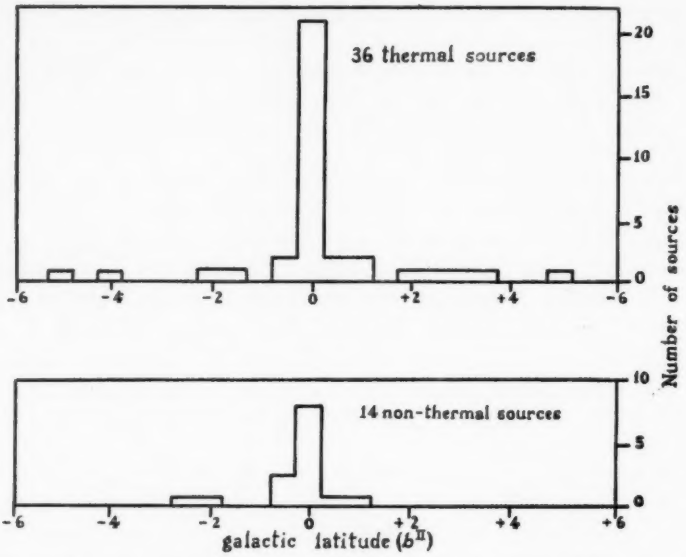

FIG. 4.—*The upper histogram shows the number of sources with spectral index greater than or equal to* $-0{\cdot}1$ *falling in each* $\frac{1}{2}°$ *range of galactic latitude. These are the sources assumed to be thermal in the text. In the lower histograms the sources of spectral index less than* $-0{\cdot}1$ *are plotted. These are the non-thermal sources.*

5. (*a*) *The thermal sources.*—The distribution of the thermal sources may be described by means of a model distribution in which approximately one third of the sources are evenly distributed in latitude up to $\pm 5°$ from the galactic plane, and the remaining two thirds have a gaussian distribution with standard deviation $0°{\cdot}35$, symmetrical about the galactic plane. The galactic plane which is used in this description of the latitude distribution of the sources is that given by $b^{II} = 0$, which is determined by the large scale distribution of neutral hydrogen in the Galaxy (Gum, Kerr and Westerhout 1960). The observation that most of the thermal sources lie very close to this plane suggests that they too are a large scale feature of the Galaxy. The neutral hydrogen in the Galaxy lies in a disk about 200 pc thick at the half density points. The observations of Van Tulder (1942) and Schmidt (1959) have shown that, in the vicinity of the Sun, O and B stars (which maintain the ionization in H II regions) are slightly more concentrated to the galactic plane, the distribution being about 150 pc thick. High frequency radio observations of the thermal emission indicate that the disk of ionized hydrogen is about 200 pc thick, appearing in the sky as a band of radiation $1°{\cdot}6$ wide (Westerhout 1958). It is therefore surprising to find that a majority of the

discrete thermal sources in Table I lie within 1/4° of the galactic plane. Two factors may account for this extremely narrow distribution of the thermal sources in latitude. It is possible that there is an observational bias because weak sources are less readily detected when they lie on the gradients away from the galactic plane. Also, a number of the sources classed as thermal may in fact be non-thermal sources of extremely flat spectra. We conclude that the majority of these thermal sources are individual H II regions or fine structure in the more continuous thermal emission of the Galaxy, and at distances of a few kpc.

5. (*b*) *The non-thermal sources.*—The non-thermal sources fit a model distribution which is gaussian with standard deviation 0°·65. Since there are comparatively few non-thermal sources (i.e. 14) this figure is strongly influenced by individual sources, and if for example the source at $b^{II} = -1°{\cdot}9$ is omitted the standard deviation is nearly halved. In interpreting the distribution of the non-thermal sources we use arguments similar to those used for the thermal sources. The symmetry of the distribution about $b^{II}=0$ is an indication that the sources are within the Galaxy, and the narrowness of the distribution can only mean that they are at distances of several kiloparsecs. They are also comparatively rare objects. The mean distance from the galactic plane of six radio sources thought to be supernova remnants (Cassiopeia A, Crab Nebula, Cygnus Loop, IC443, Tycho Brahe's and Kepler's Supernovae) is about 120 pc, i.e. they are strongly concentrated to the galactic plane. Thus the distribution of the fourteen non-thermal sources is consistent with the suggestion that they are distant supernovae.

It is not worth while to proceed to a more detailed calculation until more information on the range and space density of type I and type II supernovae is available, but it is interesting to note that our non-thermal sources have a distribution very different from that of ordinary novae in the Galaxy, for the mean z-distance of 80 observed novae (Payne-Gaposchkin 1957) is over 500 pc. Such a value cannot be taken as typical of the z-distance of the galactic non-thermal sources because it would imply a distribution in latitude far wider than that which is observed.

6. *The source at the galactic centre.*—The present 408 Mc/s observations of Sagittarius A seem to be consistent with earlier higher resolution studies at 1420 Mc/s (Davies and Jennison 1960) and 8000 Mc/s (Drake 1959), which show that there are several small diameter sources within $\frac{1}{2}°$ of the galactic centre. One of these sources (at $l^{II}=0°{\cdot}18$, $b^{II}=0°{\cdot}07$) Drake claims is non-thermal. Detailed examination of the 408 Mc/s isophotes at this position shows no trace of a point source, and this makes it unlikely that Drake's source has a non-thermal spectrum.

Acknowledgments.—We thank Professor Sir Bernard Lovell for making available the facilities at Jodrell Bank, and Professor R. Hanbury Brown, whose continuing interest in the work is very much appreciated. D. S. Mathewson gratefully acknowledges his Leverhulme Research Fellowship.

Nuffield Radio Astronomy Laboratories,
Jodrell Bank,
Macclesfield,
Cheshire:
1961 *June.*

References

Aller, L. H., 1956, *Gaseous Nebulae*, Chapman and Hall.
Baldwin, J. E., 1955, *M.N.*, **115**, 690.
Davies, R. D., and Jennison, R. C., 1960, *Observatory*, **80**, 74.
Drake, F. D., 1959, Annual Report. Nat. Radio Astronomy Observ., U.S.A.
Edge, D. O., *et al.*, 1959, *Mem. R. A. S.*, **68**, pt. II.
Gum, C. S., Kerr, F. J., and Westerhout, G., 1960, *M.N.*, **121**, 132.
Hanbury Brown, R. and Hazard, C., 1953, *M.N.*, **113**, 109.
Hanbury Brown, R., 1954, *Observatory*, **74**, 185.
Hill, E. R., Slee, O. B., and Mills, B. Y., 1958, *Aust. J. Phys.*, **11**, 530.
Large, M. I., Mathewson, D. S., and Haslam, C. G. T., 1959, *Nature*, **183**, 1250.
Lovell, A. C. B., 1957, *Nature*, **180**, 60.
Mathewson, D. S., Large, M. I., and Haslam, C. G. T., 1960, *M.N.*, **120**, 242.
Mills, B. Y., Little, A. G., and Sheridan, K. V., 1956, *Aust. J. Phys.*, **9**, 218.
Mills, B. Y., Hill, E. R., and Slee, O. B., 1958, *Observatory*, **78**, 116.
Mills, B. Y., Slee, O. B., and Hill, E. R., 1958, *Aust. J. Phys.*, **11**, 360.
Mills, B. Y., Slee, O. B., and Hill, E. R., 1960, *Aust. J. Phys.*, **13**, 676.
Mills, B. Y., 1959, Paris Symposium on Radio Astronomy, Stanford Press.
Osterbrook, D. E., 1958, *P.A.S.P.*, **70**, 180.
Payne-Gaposchkin, C., 1957, *The Galactic Novae*, Amsterdam.
Schmidt, M., 1959, *Ap. J.*, **129**, 243.
Seeger, C. L., Westerhout, G., and van de Hulst, H. C., 1956, *B.A.N.*, **13**, 89.
Seeger, C. L., Westerhout, G., and Conway, R. G., 1957, *Ap. J.*, **126**, 585.
Sharpless, S., 1959, *Ap. J. Suppl.*, **4**, 257.
Trans. I.A.U., 1958, **10**, 509.
Tulder, J. J. M. van., 1942, *B.A.N.*, **9**, 315.
Westerhout, G., 1958, *B.A.N.*, **14**, 215.
Whitfield, G. R., 1959, Paris Symposium on Radio Astronomy, Stanford Press.
Wilson, R. W., and Bolton, J. G., 1960, *P.A.S.P.*, **72**, 331.

A RADIO SURVEY OF THE GALACTIC PLANE AT A FREQUENCY OF 408 MC/S

II. The Continuum Emission from the Galactic Disk

M. I. Large, D. S. Mathewson and C. G. T. Haslam*

(Communicated by the Director, Nuffield Radio Astronomy Laboratories)

(Received 1961 June 8)

Summary

The 408 Mc/s Jodrell Bank survey of the galactic plane has been used in conjunction with the Sydney (85 Mc/s) survey and the Leiden (1390 Mc/s) survey to delineate the distribution of thermal and non-thermal radio emission from the Milky Way. The results of this analysis are presented in the form of both isophotes and profiles at constant galactic latitudes. They extend and confirm a similar analysis carried out by Westerhout. Some features of the distributions could indicate a spiral structure of the Galaxy, but it is found that there are difficulties in fitting Mill's spiral model to the parts of the Milky Way seen from the northern hemisphere.

---

1. *Introduction.*—In the preceding paper (Large, Mathewson and Haslam 1961), which will be referred to as Paper I, the results of a survey of part of the galactic plane at 408 Mc/s using the 250 ft radio telescope at Jodrell Bank were described. In that paper the isophotes were presented, together with a discussion of the discrete source component of the galactic radio emission. A study has now been made of the more extended emission from the galactic disk, the 408 Mc/s results being compared in detail with the Sydney 85 Mc/s survey (Hill, Slee and Mills 1958) and the Leiden 1390 Mc/s survey (Westerhout 1958). The variation of spectral index with galactic latitude in regions close to the galactic plane has been used by Westerhout (1958) as evidence for a concentration of ionized hydrogen radiating thermally. Mills (1959) identifies certain " steps " in the metre-wave radiation from the Galaxy with points where the line-of-sight is tangential to the spiral arms. The purpose of this paper is to present the results of a new spectral analysis of the galactic radiation, and to interpret these results in the light of the conclusions of Mills and Westerhout.

2. *Theory.*—An inspection of surveys of the galactic plane on various frequencies shows that the brightness temperature varies less rapidly with frequency at points within 1° of the galactic plane than at points at higher latitudes. It is known that in other parts of the Galaxy the spectral index is remarkably constant (for example, see Costain 1960) as it also appears to be in

* Now at C.S.I.R.O. Sydney.

the Andromeda nebula (Baldwin and Costain 1961). Shain's survey at 19·7 Mc/s (1957) shows a minimum in the galactic radiation in the position of the galactic plane, which is thought to be caused by ionized hydrogen emitting thermally and appearing in absorption against the very bright background temperature. Accordingly, we make the assumption that the variation of spectral index over the galactic plane is due to a variation in the proportion of the emission that is produced by thermal processes. While this is a reasonable assumption it is important to bear in mind the possibility (stressed by Mills (1959)) that some or all of the variation may represent a real variation in the spectrum of the non-thermal emission.

Westerhout (1958) has shown that if certain other assumptions are made, then the apparent brightness temperature, T, of a mixture of thermal and non-thermal sources is given by

$$T=(T_e+T_n/\tau)\,(1-e^{-\tau}), \tag{1}$$

where T_e is the electron temperature of the thermal material, τ is its optical depth, and T_n is the brightness temperature of the non-thermal emission (supposing thermal material to be absent). Westerhout applied this expression to his own survey and to the 85 Mc/s Sydney survey to separate the thermal and non-thermal contributions to the 1390 Mc/s brightness temperatures. A similar analysis has been carried out incorporating the 408 Mc/s results (Section 4). The assumptions on which this analysis is based are briefly discussed:

(i) The variation of spectral index across the galactic plane is due principally to the emission from ionized hydrogen.

(ii) The electron temperature of the ionized hydrogen is constant and equal to 10^4 °K. Unless the electron temperature is grossly different from this value, it scarcely affects the analysis.

(iii) The sources of thermal and non-thermal emission are well mixed in the line-of-sight. This condition is important only when $\tau \sim 1$, and thus applies only to the 85 Mc/s results near the central regions of the Galaxy.

(iv) The non-thermal sources do not appreciably absorb incident radiation.

(v) The spectral index of the non-thermal radiation is unvarying with frequency between 1390 Mc/s and 85 Mc/s.

In applying equation (1) to the results of the surveys at 85 Mc/s, 408 Mc/s and 1390 Mc/s, the optical depth τ has been taken to be inversely proportional to the square of the frequency, and the non-thermal brightness temperature to have a spectral index α, thus:

$$\left.\begin{aligned}\tau &\propto f^{-2}\\ T_n &\propto f^{-\alpha}\end{aligned}\right\}. \tag{2}$$

In principle, the results of surveys at three frequencies could be used to deduce distribution of three quantities, such as τ and T_n at one frequency, and the value of α. The details of the analysis are described in the following sections.

3. *Calibrations.*—The method of observation, and details of the receiver will be found in Paper I. For the present purpose we are particularly concerned with the accuracy of the temperature scales of the three surveys used in the analysis, with the determination of the true zero level of brightness temperature and with the contribution from extragalactic radiation.

The spectral analysis of the discrete sources (Paper I) provides good evidence that the temperature scales of the three surveys are in the correct ratio; for the spectral index of many of these sources was found to be close to zero, an appropriate value for the optically thin H II regions with which these sources were identified. Furthermore, the non-thermal discrete sources had spectral indices which were consistent as measured between 85 Mc/s and 408 Mc/s and 408 Mc/s and 1390 Mc/s.

Since the flux densities of the discrete sources were measured by using nearby regions in the galactic plane as reference points, further information is required to determine the absolute brightness temperatures. Westerhout (1958) estimates that the true brightness temperatures at 1390 Mc/s are obtained by adding 1·5 °K to the temperatures indicated by his published isophotes, over the greater part of his survey. He obtained this figure by using the 900 Mc/s survey of Denisse *et al.* (1957) and assuming a suitable spectral index. The brightness temperatures at 408 Mc/s were measured relative to the temperature of a reference region (at $\alpha = 19^h\ 20^m$, $\delta = 0°$); therefore it is necessary to determine the true brightness temperature of this point. In the analysis which follows, this temperature (T_{RR}) of the reference region is taken to be

$$T_{RR} = 80 \pm 15\ °\mathrm{K}$$

at 408 Mc/s. It was determined by first measuring the reference region temperature relative to cold parts of the sky at high galactic latitudes, and estimating the temperature at these points by using the Sydney 85 Mc/s survey. The result was confirmed by repeating in detail the method used by Westerhout in establishing the true temperatures in his survey. No zero level correction is applied to the 85 Mc/s results.

Westerhout has pointed out that the 85 Mc/s brightness temperatures are more consistent with his and other surveys if the temperatures at 85 Mc/s are multiplied by a factor of 1·32. No such correction has been applied in the present analysis. Indeed the 408 Mc/s results seem to be more consistent with the published 85 Mc/s temperature scale.

No attempt has been made to correct any of the results for the contribution to the brightness temperature made by integrated extragalactic radiation.

4. *Method of analysis.*—On the isophotes of radio brightness temperature at 85 Mc/s, 408 Mc/s and 1390 Mc/s a grid of points was constructed by drawing the lines of constant new galactic latitude and longitude at 2° intervals. At each point a "background temperature" was read from the isophote diagrams. The contribution from any discrete source was not included, and any local irregularities in the isophotes were allowed for by a "smoothing" of the isophotes in the vicinity of the point. The results were tabulated, zero level corrections of 1·5 °K and 80 °K being added to the 1390 Mc/s and 408 Mc/s figures respectively. These temperatures are taken to represent the distribution of radiation from the large-scale features of the Galaxy. They are presented in Fig. 1 in the form of smooth profiles at constant galactic latitude.

These results have been used to determine the thermal and non-thermal contributions to the brightness temperature at 408 Mc/s by applying the theory described in Section 2. In order to fit the data to equations (1) and (2) a table was computed (using the Manchester Mercury Computer) giving the brightness temperatures at the three frequencies as a function of the spectral

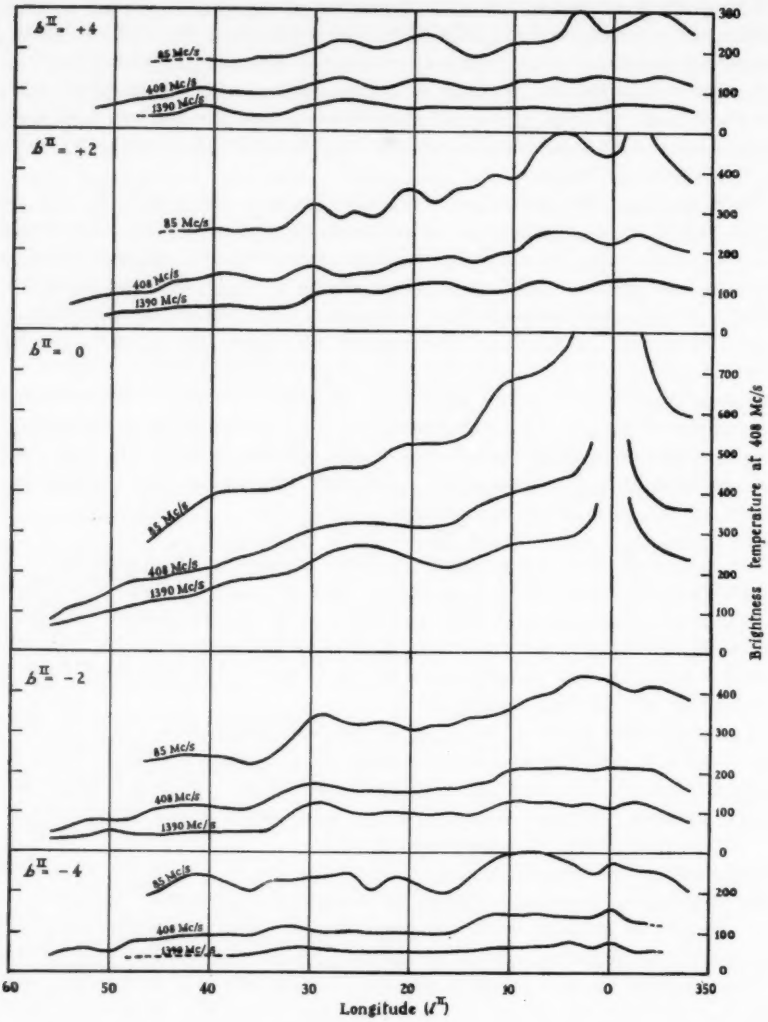

FIG. 1.—*Profiles showing the longitude distribution of galactic radio emission at* 85 *Mc/s,* 408 *Mc/s* and 1390 *Mc/s at five latitudes. The profiles are derived from the Sydney, Jodrell Bank and Leiden surveys in the manner described in the text. The vertical scale is the brightness temperature at* 408 *Mc/s. The temperature scale at* 85 *Mc/s is obtained by multiplying these numbers by* 25, *and at* 1390 *Mc/s by dividing by* 12·5.

index, α, of the non-thermal component. Using the table and the three brightness temperatures at a point, it was possible to determine the spectral index to the nearest tenth of a unit, and the thermal and non-thermal contributions to the 408 Mc/s temperature to an accuracy of a few degrees. The value of α varied from point to point, but it was soon found that the variations in α were not significant in view of the experimental errors. At most points, a value

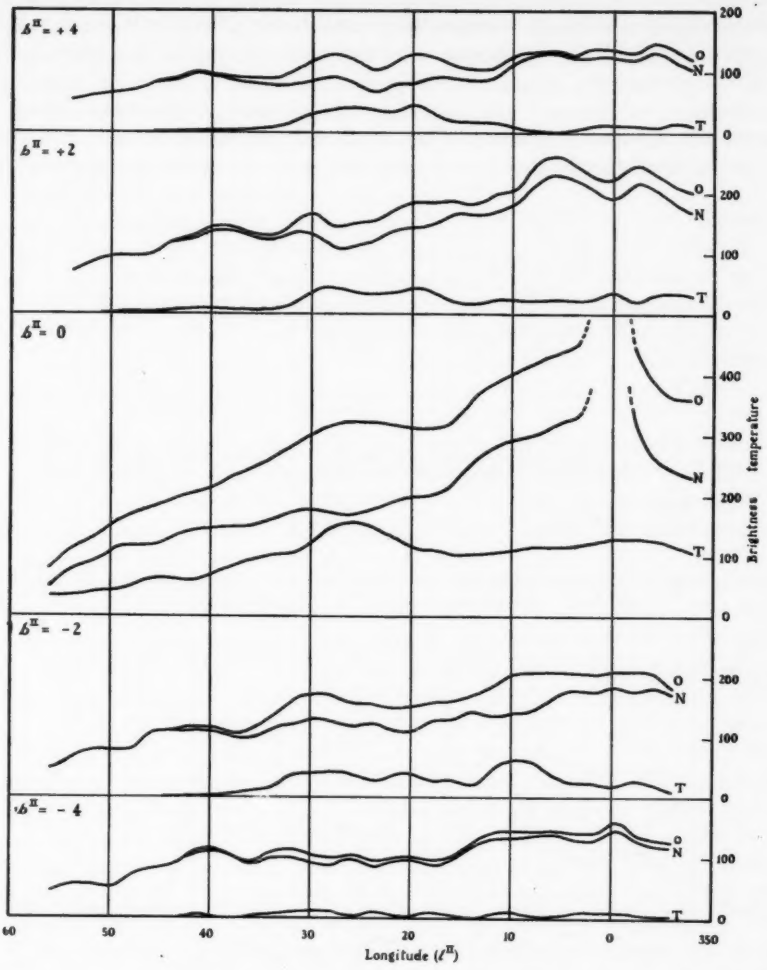

FIG. 2.—*Profiles showing the longitude distribution of radio radiation at 408 Mc/s at five latitudes (labelled* O*) and its separation into thermal and non-thermal components (labelled* T *and* N *respectively).*

of α of 2·6 gave the best fit to the measured brightness temperatures. This value was then used at every point of the 2° grid, and the fit to equation (1) was within the experimental error for nearly all the points. The results of the analysis are shown in the form of profiles at constant latitudes of the thermal and non-thermal emission at 408 Mc/s (Fig. 2) and in the form of isophotes in Fig. 3.

The observations at 408 Mc/s (and at 1390 Mc/s) are confined to galactic longitudes north of the galactic centre. In an attempt to extend the spectral index measurements to southern galactic longitudes, we have used the 600 Mc/s survey of Piddington and Trent (1956). The resolution of this survey is less

than that of the surveys we have considered so far, and there is reason to believe that the temperature scale is inconsistent with other surveys. We find that the 600 Mc/s survey is in agreement with the other results in the northern sky if the brightness temperature scale is multiplied by a factor of 0·75. The contributions of thermal and non-thermal emission at 600 Mc/s along the line $b^{II}=0$ were determined by fitting equation (1) to the 85 Mc/s and 600 Mc/s results in both the northern and southern sky. In order to carry out this

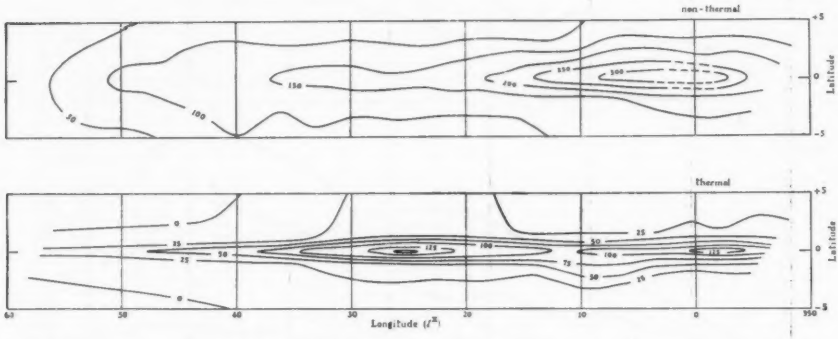

FIG. 3.—*Isophotes showing the distribution of thermal and non-thermal radiation in the Galaxy at 408 Mc/s. The intensity unit is 1°K of brightness temperature.*

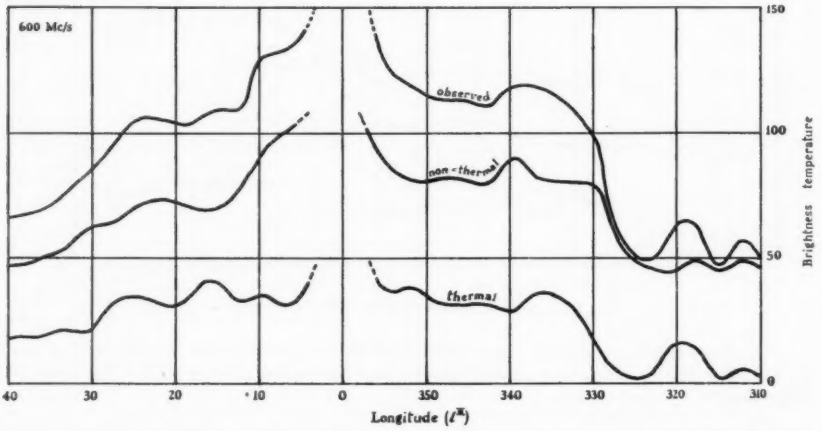

FIG. 4.—*The upper curve is a profile of the radio emission from the Galaxy (at $b^{II}=0$) derived from the 600 Mc/s survey of Piddington and Trent (1956). The brightness temperatures have been mutliplied by 0·75. The middle and lower curves show the division of this radiation into non-thermal components.*

analysis, the 85 Mc/s map was convolved with a 3° gaussian function to make its resolution equal to that of the 600 Mc/s survey. The result is shown in the form of a profile in Fig. 4. The detailed results shown in Figs. 2, 3 and 4 depend on the assumptions listed in Section 2, and to some extent on a subjective judgment in reading the isophote diagrams and fitting the temperatures

to equations (1) and (2). However we are confident that the broad features of the results are correct. In the following discussions we assume that the thermal and non-thermal brightness temperatures are distributed as shown in the diagrams.

5. *The spiral arms of the Galaxy*

In this section we review the large-scale structure revealed in the thermal and non-thermal radiation from the Galaxy, and consider the possibility that it reflects the spiral structure.

5*a*. *The distribution of the thermal emission.*—If the source of thermal emission in the Galaxy were concentrated into a spiral or circular arm structure, its presence would be revealed in the distribution of thermal radiation in galactic longitude. The thermal emission would be at a maximum in those directions where the line-of-sight passes through the greatest depth of material, i.e. in directions which are tangential to the arms of the Galaxy. This corresponds to a special case (isotropic emission, $n=0$) in the idealized model of the Galaxy proposed by Hanbury Brown and Hazard (1960).

The distribution of thermal radiation shown in Fig. 3 indicates broad maxima in the emission at $l^{II}=25°$ and $l^{II}=0°$, with a steady decrease in intensity for longitudes greater than 25°. Westerhout's (1958) analysis led to a somewhat similar result as regards the maximum at $l^{II}=25°$, but in the direction of the galactic centre he did not find a second maximum.

We have analysed the 600 Mc/s survey of Piddington and Trent (1956) in conjunction with the other three surveys (see Section 4) in order to investigate the distribution of thermal radiation south of the galactic centre. Although the beam size of the 600 Mc/s survey was 3°, the peak in the thermal emission at $l^{II}=+25°$ is clearly indicated in the result (Fig. 4) and a symmetrical feature appears at about $l^{II}=-25°$ (i.e. 335°). The striking fall in the radio intensity at 600 Mc/s at this longitude is seen to be partly thermal and partly non-thermal. Thus what evidence there is supports the suggestion that at $l^{II}=+25°$ the line-of-sight is tangential to an approximately circular arm of radius 3·5 kpc. This was suggested by Westerhout (1958), who deduced a radial distribution of ionized hydrogen in the Galaxy. Mills (1959) points out that the data are inadequate to prove the existence of this 3·5 kpc arm, and that the apparent structure could equally well be explained in terms of local irregularities.

It is significant that apart from the maximum at $l^{II}=25°$, a slight rise towards the galactic centre and the well-known thermal emission region of Cygnus X (at $l^{II}=80°$) there is no indication of any other large-scale structure in the thermal emission from the galactic disk between $l^{II}=0$ and $l^{II}=90°$. In fitting a spiral arm model to these features, arms would be placed in radii of 3·5 kpc and 8 kpc in the northern sky. There is no indication of thermal emission from an arm of an intermediate radius.

The isophotes of Fig. 3 show vividly the concentration of the thermal emission to the galactic plane, the mean width to half-intensity points being 1°·5. This width is consistent with the theory that the source of the emission is a disk of ionized hydrogen concentrated to the plane of the Galaxy and having a thickness to half-density points of 200 pc.

Between longitudes $l^{II}=20°$ and $l^{II}=35°$, the thermal emission appears to extend weakly towards positive galactic latitudes. This is the region where a continuation of the north polar spur of the Galaxy would intersect the galactic

plane (see Hanbury Brown, Davies and Hazard 1960). Thus there is some indication that the base of the spur has a thermal spectrum. A recent survey in Cambridge (Costain 1960) seems to indicate that at higher latitudes the spectrum of the spur is if anything more steeply non-thermal than the rest of the galactic corona.

5*b*. *The distribution of the non-thermal radiation.*—In a recent paper, Hanbury Brown and Hazard (1960) have calculated the distribution of radio brightness which would be observed from the position of the Sun for spiral (and circular) arm models of our galactic system. The emission is taken to be anisotropic, the intensity depending on $(\cos\theta)^n$ where n lies between 0 and +2 and θ is the angle

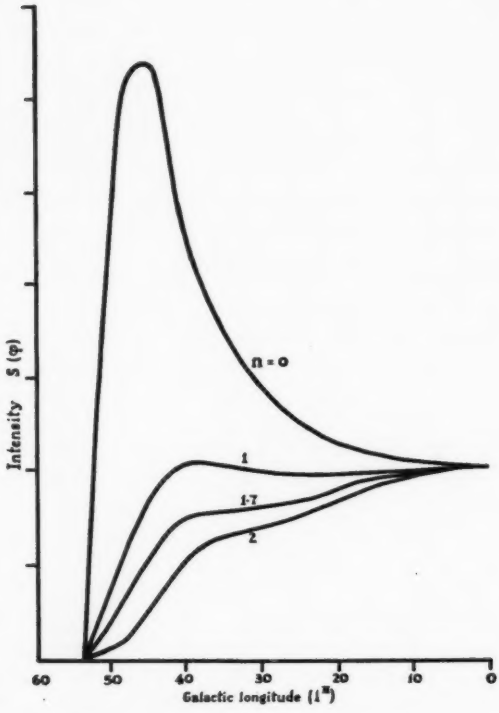

FIG. 5.—*This diagram is reproduced from Hanbury Brown and Hazard's recent paper* (1960). *It shows the expected distribution in longitude of galactic radio emission from a circular arm of radius 6 kpc, the emissivity in a direction θ to the radius being proportional to* $\cos^n\theta$. *Curves are drawn for* $n=0$, 1, 1·7, 2.

between the line-of-sight and the tangent to the spiral arm. Fig. 5, which is reproduced from their paper, shows the longitude distribution of radio emission expected from an arm of 6 kpc radius for various values of n. If, as is widely believed, the non-thermal emission of the galaxy is synchrotron emission, then n would be about 1·7. This supposes perfect alignment of the magnetic field along the spiral arms. If random deviations occur, rather more pronounced "steps" would be produced in the longitude distribution.

Mills (1959) fits the Sydney 85 Mc/s observations of the continuum emission to a spiral arm model of the Galaxy, in which the spirals obey an equation of the form

$$R = 0{\cdot}22R_0 \exp\left\{0{\cdot}12\theta + \begin{matrix}0\\ \text{or}\\ \pi\end{matrix}\right\}.$$

The parameters being chosen to give the best fit to marked "steps" in the longitude distribution of the 85 Mc/s radiation In the southern sky ($270° < l^{II} < 360°$) the steps are well marked, and are such as might be expected in a spiral model of the Galaxy in which the magnetic field deviated randomly by about 20° from perfect alignment with the spiral arms. In the northern sky ($0° < l^{II} < 90°$) these steps are less well marked.

The longitude distribution of radio emission in the northern sky is clearly shown in Fig. 1, in which profiles at constant latitudes are drawn for the three surveys used in the analysis. A critical examination of these figures shows that the distribution is complex even when contributions from easily recognized point sources have been removed. Since the profiles close to the galactic plane include both the thermal and non-thermal components, it might be thought that the profiles at constant latitude, one or two degrees from the galactic plane, would show the structure of the non-thermal radiation more clearly. Inspection of these profiles at $\pm 2°$ and $\pm 4°$ latitude (also Fig. 1) indicates no simple pattern in the emission. A striking step pattern is observed in the 408 Mc/s and 1390 Mc/s profiles at $b^{II} = -2°$ (with steps at $l^{II} = 10°$, 30°). These steps do not agree well with the steps found by Mills (at $l^{II} = 14°$, 24°, 40°), nor are they confirmed by the profile of $b^{II} = +2°$. We conclude therefore that an examination of profiles of the northern Milky Way does not lead to a clear recognition of "steps" in the longitude distribution, and that most of the features might be due to irregularities in the emission.

The separation of the galactic emission into thermal and non-thermal components is illustrated in Figs. 2 and 3, and it is natural to look for evidence of a spiral structure in these diagrams. The isophotes of non-thermal emission in Fig. 3 are drawn from the profiles of Fig. 2 with, inevitably, a certain "smoothing" of the data. We believe that all the significant large scale features of the radiation are preserved in this isophote diagram. We draw attention to two features of the longitude distribution of the non-thermal radiation. This first is a marked discontinuity at approximately $l^{II} = 14°$ (the position of one of Mills's steps). The second feature is a region in which the brightness temperature remains constant with increasing longitude between $l^{II} = 20°$ and $l^{II} = 40°$, and then decreases rapidly, reaching a low value at $l^{II} = 60°$, the limit of the present survey. Beyond this limit and as far as $l^{II} = 90°$, the non-thermal radiation from the Galaxy seems to be weak, although a full survey at 408 Mc/s has not been made. The radiation from the Cygnus X region has been shown to be almost entirely thermal (Mathewson, Large, and Haslam 1960).

These two features of the non-thermal emission might be fitted to a spiral model of the Galaxy of the kind discussed by Hanbury Brown and Hazard if 'n' is taken to lie between 1 and 2 and the direction of the magnetic field does not deviate randomly from the mean direction by angles which greatly exceed 20°.

There would be two spiral (or circular) arms of radii 2 kpc and 6 kpc, the line-of-sight being tangential to the arms at $l^{II}=15°$ and $l^{II}=50°$. The positions of these arms are significantly different from those fitted to the thermal emission.

6. *Conclusions.*—It will be clear from the foregoing remarks that any attempt to fit the continuum observations to a spiral model of the Galaxy is at present speculative. Our understanding of the emission will be much improved when the thermal (i.e. high frequency) component has been surveyed from the southern hemisphere with reasonably good resolution. Until such a survey has been made and until we have definite information on the position and direction of the galactic magnetic field we believe that identification of steps in the galactic radio emission with spiral arm structure is unlikely to prove correct.

The present work has drawn attention to certain large scale features of the Galaxy seen from the northern hemisphere. These are the two thermal maxima observed at $l^{II}=25°$ and $l^{II}=80°$, and the broad "steps" in the non-thermal emission at $l^{II}=15°$ and $l^{II}=50°$. These features are well marked and can be interpreted in terms of a spiral model of the Galaxy, only if one postulates an independent distribution for the thermal and non-thermal emission.

Acknowledgments.—We thank Professor Sir Bernard Lovell for making available the facilities at Jodrell Bank, and Professor R. Hanbury Brown, whose continuing interest in the work is very much appreciated. D. S. Mathewson wishes to acknowledge the receipt of his Leverhulme Research Fellowship.

Nuffield Radio Astronomy Laboratories,
Jodrell Bank,
Macclesfield,
Cheshire:
1961 *June.*

References

Baldwin, J. E., and Costain, C. H., 1961, *M.N.*, **121**, 413.
Costain, C. H., 1960, *M.N.*, **120**, 248.
Denisse, J. F., *et al.*, 1957, *Comptes Rendus*, **244**, 3030.
Hanbury Brown, R., Davies, R. D., and Hazard, C., 1960, *The Observatory*, **80**, 191.
Hanbury Brown, R., and Hazard, C., 1960, *The Observatory*, **80**, 137.
Hill, E. R., Slee, O. B., and Mills, B. Y., 1958, *Aust. J. Phys.*, **11**, 530.
Large, M. I., Mathewson, D. S., and Haslam, C. G. T., 1961, *M.N.*, **123**, 113.
Mathewson, D. S., Large, M. I., and Haslam, C. G. T., 1960, *M.N.*, **120**, 242.
Mills, B. Y., 1959, Paris Symposium on Radio Astronomy, Stanford Press.
Piddington, J. H., and Trent, G. H., 1956, *Aust. J. Phys.*, **9**, 481.
Shain, C. A., 1957, *Aust. J. Phys.*, **10**, 195.
Westerhout, G., 1958, *B.A.N.*, **14**, 215.

ON THE COUNTING OF RADIO SOURCES IN THE STEADY-STATE COSMOLOGY

F. Hoyle and J. V. Narlikar

(Received 1961 June 13)

Summary

The problem of the number count of radio sources as a function of the incident flux is shown to depend on two crucial features: (i) the size and behaviour of condensations (ii) the dependence on age of the probability of a galaxy being a radio source. Provided the probability rises by a factor $\sim 10^2$ for galaxies with ages from H^{-1} to about $2{\cdot}5H^{-1}$, and provided the primary condensations of the steady-state theory possess initial dimensions of order 30 megaparsecs, the radio source count can rise more steeply than is the case for sources uniformly distributed in Euclidean space. Each primary condensation contains of the order of 10^5 galaxies, which in the main expand apart from each other as the universe expands.

It is shown that a luminosity function can be chosen for the radio sources giving results consistent with observation, not only for the source count, but also with the data on angular diameters and with experience in the problem of optical identifications.

---

1. *The $\log N - \log P$ curve.*—Six years ago, Ryle announced in his Halley lecture (**16**) that counts of the number $N(P)$ of radio sources brighter than P did not behave in the manner to be expected of uniformly distributed objects in Euclidean space.

From the point of view of the theoretician, the situation over the last six years has seemed uncertain, since different observers have been in disagreement over the real value of the slope of the $\log N - \log P$ curve. In a comparison over a common portion of the sky, the slope obtained at Cambridge (**1**) was $-2{\cdot}5$ at 81·5 Mc/s and $-2{\cdot}7$ at 159 Mc/s, whereas Mills, Slee and Hill (**2**) obtained $-1{\cdot}8$. Very recently, the Cambridge observers have announced the result of a new survey, yielding about $-1{\cdot}8$ for the slope, and this they regard as superseding their former estimates. Another recent survey, at 960 Mc/s, by Kellermann and Harris (**3**) gives $-2{\cdot}0$.

Although the concordance between the recent Cambridge work and that of MSH suggests that the slope probably is steeper than the Euclidean value of $-1{\cdot}5$ (a view expressed by Bolton in his survey given at the U.R.S.I. General Assembly, London, 1960 September), it must be noted that Mills has remarked on the likely existence of a systematic progressive error in his judgment of the values of P. In a "noise-limited" instrument, such as the Mills Cross, the observer tends to overestimate P more and more as the limit of detectability is reached. Mills has suggested that this effect could reduce the slope to $-1{\cdot}65$,

or even to $-1{\cdot}5$ (4)*. On the other hand, the Cambridge instrument is not noise-limited, and no such systematic effect should be present. The concordance between the Sydney and the Cambridge work may therefore be coincidental.

In the present paper we propose to accept the Cambridge claim that the slope is steeper than $-1{\cdot}5$ for values of P less than 3×10^{-25} watt $m^{-2}(c/s)^{-1}$. We do not propose, however, to attach importance to the precise value of $-1{\cdot}8$. In fact, our best result for the slope will turn out close to $-1{\cdot}6$. We do not regard the difference between this value and the recent Cambridge result as a significant discrepancy.

At $P>3\times10^{-25}$ w.$m^{-2}(c/s)^{-1}$ the slope may well be less steep. Indeed, Mills (4) gives a slope no greater than $-1{\cdot}3$ at high flux values. Certainly it does not seem necessary for the theory to provide a slope steeper than the Euclidean value at large P. (The values of P mentioned above refer to a frequency of 160 Mc/s. This frequency will be taken as standard throughout the paper.)

2. *The general problem.*—Before the steady-state cosmology was proposed, ambiguities made the predictions of theory uncertain: three choices were available for the world curvature, and a double infinity of parametric values was also available for adjustment (the parameters being the cosmical constant and a constant of integration). Steady-state cosmology does not suffer from these ambiguities. There is no uncertainty concerning the line element, except for the numerical value of Hubble's constant. Once this has been fixed from observation, purely geometrical questions can be settled explicitly.

A further feature adds a still greater degree of definiteness. Because the time axis is open, into the past as well as the future, and because the line element is stationary (but not of course static), all observable properties must reproduce themselves, otherwise the continuing expansion would weaken and ultimately destroy the property in question. For example, galaxies must continue to condense, otherwise the spatial density of galaxies would tend to zero. Dynamo action must preserve any intergalactic magnetic field that may exist; and so on.

These advantages seem to have encouraged an erroneous optimism that the theory is capable of handling explicitly a physical property whose nature is not specified—for example, that the theory will predict the slope of the $\log N-\log P$ curve for radio sources without it being necessary to specify in any precise way the properties of radio sources. In a recent criticism of the steady-state theory Ryle and his colleagues (15) obtained a $\log N-\log P$ curve without apparently needing to use any of the physical properties of radio sources. Manifestly, there is a paradox in this, for one cannot count objects without some close specification of what are the objects to be counted. The paradox is actually resolved by the circumstance that the mathematical analysis necessary to arrive at the $\log N-\log P$ curve used by the Cambridge radio-astronomers itself imposes physical properties on the radio sources. If it should turn out that the properties thus imposed are indeed satisfied by the radio sources, then the claim that observation contradicts the steady-state theory may well be correct.

In the following sections we shall construct a counter-example, showing that properties can be imposed on the radio sources that lead to a $\log N-\log P$ in

* We are indebted to Drs Allen, Palmer and Rowson for the information that the effect reported by Mills has been investigated also at Jodrell Bank. The effect is found to be present, and of quantitatively the order stated by Mills.

satisfactory agreement with the observations. It will be necessary to use a definite picture of the mode of formation of galaxies. Before beginning the cosmological discussion it will be useful to review briefly the astrophysical features of this picture. It is perhaps relevant to add that the essential features of the following section are not new (cf. (**5, 6**)). We shall therefore be using an astrophysical picture that arose quite independently of the present radio source problem, not a picture invented specifically for explaining the radio observations.

3. *Condensations in the steady-state theory.*—It has been realized for some years that the formation of galaxies, and of clusters of galaxies, implies the existence of a distance scale apparently quite independent of the cosmological distance scale. In the steady-state cosmology, for example, the constants appearing in the cosmological equations are c, H, and G; and from these cH^{-1} is a length. But this is the so-called "radius of the observable Universe", about 3000 mpc ($H = 100\,\mathrm{km\,s^{-1}\,(mpc)^{-1}}$), very much larger than ~ 3 mpc given by the galaxies and their clusters.

To obtain a distance scale appropriate to the galaxies and their clusters, it was suggested (**5**) that condensation may occur from an intergalactic gas at high temperature. Write V for the velocity of sound in the gas, then VH^{-1} is a length. To obtain ~ 3 mpc, with $H = 100\,\mathrm{km\,s^{-1}\,(mpc)^{-1}}$, V must be $\sim 300\,\mathrm{km\,sec^{-1}}$. It appeared immediately significant that this latter value is just of the order of the internal motions found in the galaxies, and also of the order of their peculiar motions.

It was further suggested (**5**) that condensation is promoted by cooling in the hot gas—locally-cooled regions being compressed by surrounding hotter gas. The idea that pressure gradients are necessary for producing condensation has been supported by an investigation of Harwit (**7**), who has shown that in the steady-state model condensation cannot take place through the operation of purely gravitational forces. This is clearly connected with the remarks of the previous paragraph—if condensation through gravitational forces could take place, a distance scale for the condensation process involving only cosmological constants would be expected to turn up in the theory, and this we know to be impossible. A similar argument applies to other systems of cosmology; since the appropriate scale for the condensations cannot be built from the cosmological constants c, G, λ, it is improbable that condensation can take place under purely gravitational forces. This argument is strongly supported by an investigation of Lifshitz (**8**). In other systems of cosmology it is difficult, however, to ascribe a high kinetic temperature to the intergalactic medium *at the onset of condensation of the galaxies* (a temperature of 10^7 °K is required at the expansion stage where the density falls below $10^{-25}\,\mathrm{g\,cm^{-3}}$).

Investigation of radiation by free-free electron-proton collisions showed that cooling can take place in a time scale of the required order, viz. the reproduction time of the steady-state theory, $\frac{1}{3}H^{-1}$, provided the gas density is not lower than $\sim 10^{-27}\,\mathrm{g\,cm^{-3}}$. Initially, the cooling is slow, the energy of contraction being mostly dissipated by radiation. A large measure of dissipation implies that a bound, stable structure will very likely be formed. However, after contraction to about $\frac{1}{3}$ of the initial dimension—i.e. to about 1 mpc, the density rising meanwhile to $\sim 10^{-26}\,\mathrm{g\,cm^{-3}}$—the cooling accelerates rapidly, and thereafter only a comparatively small fraction of the energy of contraction is dissipated

as radiation. The energy of contraction then appears as dynamical energy, implying a fragmentation into sub-units, the sub-units being individual galaxies.

Cooling within an intergalactic medium of temperature $\sim 10^7$ °K and density 10^{-27} g cm^{-3} therefore fitted the broad requirements of a theory of the formation of galaxies and of clusters. It gave the dimensions, time-scales, and fragmentation properties correctly. Moreover, rapid cooling by hydrogen ceases at about 10^4 °K. The requirement that the hydrostatic pressure within and without a highly cooled zone be essentially the same, thus yielded a density $\sim 10^{-24}$ g cm^{-3} inside a highly cooled zone, and this is precisely the order of the densities that must have occurred in the galaxies *before* flattening to a disk structure took place in many cases. If, further, we ask: what mass of gas, at density $\sim 10^{-24}$ g cm^{-3}, can control dynamical motions of order 200–300 km sec^{-1}, the answer is about $10^{11} M\odot$. This was an additional cogent result—the theory immediately determined the general order of the masses of the main class of galaxy (smaller galaxies were thought to be splinters from the dynamical disruption of lesser masses). Finally, the hydrostatic pressure in question, $\sim 10^{-12}$ dyne cm^{-2}, is a value that still affects the structure of our own galaxy in a remarkable degree.

So far, the former theory appeared to be on a sound basis—the results obtained were sufficiently numerous to be reckoned a satisfactory return for the single important hypothesis of a high kinetic temperature (the assumption of a gas density $\sim 10^{-27}$ g cm^{-3} cannot be regarded as a serious assumption, since this is just the general order of the mean densities actually found observationally to be present in many clusters of galaxies). To bring these considerations into closer relation with the steady-state cosmology it was found necessary to introduce further ideas, however, and these were more removed from the astronomical and astrophysical evidence. Accordingly, it is of great interest to find these further ideas turning out to be of particular relevance to the subject of the present paper. It does not seem likely that without these ideas the radio source counts could be explained within the framework of the steady-state theory.

The mean intergalactic density appearing in the steady-state theory is of order 10^{-29} to 3×10^{-29} g cm^{-3}, the exact value depending on H and on the particular mathematical formulation of the theory. Hence 10^{-27} g cm^{-3} cannot be used everywhere in space but only in regions that are already partially condensed. The question thus arose as to how such regions became partially condensed.

It was suggested that condensation occurs in two stages, a primary stage from 10^{-29} g cm^{-3} to 10^{-27} g cm^{-3}, and a secondary stage from $\sim 10^{-27}$ g cm^{-3} to $\sim 10^{-24}$ g cm^{-3}, the secondary stage being controlled by radiative cooling in the manner described above. Pressure gradients also play an important role in promoting primary condensation, the basic concept being one of equal hydrostatic pressure, the separate stages following the lines of the following table:

	Density (g cm^{-3})	Temperature (°K)	Distance scale (mpc)	Mass ($M\odot$)
Before primary condensation	10^{-29}	10^9	30	10^{16}
After primary condensation	10^{-27}	10^7	3	10^{15}
After secondary condensation	10^{-24}	10^4	0·1	10^{11}

The differences of mass in the last column take account of the effects of fragmentation during condensation. Since the distance scales are not accurate within a factor ~ 2, the masses should not be taken as accurate within ~ 10, except in the last line of the table, where the mass is determined from the criterion of stability given above, not simply from multiplying volume by density.

A primary temperature of $\sim 10^9$ °K implies an energy of $\sim 2 \times 10^{17}$ erg per gram of hydrogen. It was noticed that this is just the amount of energy to be expected if the newly created matter of the steady-state theory consists of neutrons, allowance being made for the energy lost by neutrinos in the neutron decay. The existence of a high kinetic temperature could thus be explained in terms of the form of the newly created material.

The main question that now arose was: how does primary condensation take place? Not by radiative cooling; it was shown (**5**) that even under rather favourable conditions not more than about 5 per cent of the thermal energy can be dissipated by ordinary radiative processes. A possibility considered by Gold and Hoyle (**9**) was that, since the intergalactic material on the present picture possesses widely different temperatures in different places, "heat engines" may operate without the necessary dissipation needing to be even as high as 5 per cent. Such an engine could convert thermal energy almost entirely into the dynamical energy of mass motions of the gas. The precise nature of the heat engine was not specified, however, by Gold and Hoyle. It was thought that where the thermodynamic possibility exists for the operation of heat engines of great efficiency such engines are almost certain to arise. The situation has a logical analogy to the case of convection, where one considers the phenomenon to exist even though the detailed properties of the convective cells are not precisely specified.

If the fraction of energy dissipated in primary condensation is small, thermal energy being converted largely into the dynamical motions of a number of condensed units (which subsequently undergo secondary condensation) then the units are most unlikely to stay bound together as an aggregate. Rather do we expect primary condensation to result in a number of clusters of galaxies in motion with respect to each other at speeds of the order of the speed of sound in a gas of kinetic temperature 10^9 °K, viz. ~ 3000 km sec^{-1}. That is to say, we expect primary condensation to result in a number of comparatively dense blobs of gas ($\sim 10^{-27}$ g cm^{-3}) moving with speeds ~ 3000 km sec^{-1} with respect to each other. The largest of these blobs possess radii ~ 3 mpc, while the whole group of blobs possesses a radius ~ 30 mpc. For each blob of radius ~ 3 mpc there may well be many smaller blobs.

Although the blobs possess kinetic energy large enough to expand the group, there is no reason why the initial motions should all be directed radially outward. Inward motions can occur, and may well be more common than outward ones, particularly if the system has experienced compression from the surrounding hot gas. But inward motions can serve only to delay, and not to prevent, the eventual expansion of the group—inward motions eventually become outward motions. The situation is similar to an element of hot gas without bounding walls. Even without collisions between the constituent particles, the element soon begins to expand, and eventually all the particles move outward. In a similar way, the blobs of our group expand apart from each other, assisted in the cosmological case by the expansion of the Universe.

We may sum up the features of the picture as follows:

(i) A primary condensation consists of an appreciable number of blobs of gas with density $\sim 10^{-27}\,\mathrm{g\,cm^{-3}}$.

(ii) *All galaxies forming within the blobs of a particular primary condensation are age-correlated.*

(iii) The blobs move initially with criss-crossing motions, their velocities with respect to each other being $\sim 3000\,\mathrm{km\,sec^{-1}}$.

(iv) After the initial criss-crossing, the blobs expand apart from each other.

(v) The whole age-correlated region has an initial radius $\cong 30$ mpc, and may contain from $\sim 10^5$ galaxies.

(vi) The largest of the blobs may contain upwards of 10^3 galaxies, but small blobs are probably much more common than large ones.

The need for criss-crossing motions, followed by expansion, was noted in (**5**), where it was pointed out that an intergalactic magnetic field cannot be maintained unless some such phenomenon exists.

We have now reached the stage where it is necessary to consider the relation of primary condensations one to another. This will be conveniently treated in the following section. It remains in this section only to point out that in special cases blobs with a primary condensation may possess small relative velocities, and may come close enough to enable them to resist the general expansion of the Universe. It is of interest in this connection that both Shane and Wirtanen (**10**) and Abell (**11**) find cases where clusters of galaxies form groups of dimensions ~ 20 mpc, a value satisfactorily close to the radii of our primary groups.

(Although Abell gives a value ~ 20 mpc, this refers to $H \cong 180\,\mathrm{km\,s^{-1}\,(mpc)^{-1}}$. For the distance scale of the present paper, $H = 100\,\mathrm{km\,s^{-1}\,(mpc)^{-1}}$, Abell's value should be increased to ~ 40 mpc.)

4. *The discrete model.*—The existence of a condensation distance scale introduces a discrete element into the steady-state theory. In accordance with the discussion of the previous section, this distance scale will be taken as that associated with the primary condensations.

To preserve the steady-state characteristic it is necessary that every feature of the Universe shall repeat itself in a time interval $\sim \frac{1}{3}H^{-1}$. The distribution of primary condensations existing at any moment is maintained, in spite of their expansion apart from each other, by the formation of new condensations. The interval $\frac{1}{3}H^{-1}$ may be spoken of as the "length of a generation".

The discreteness referred to above is inherent in the theory. For the sake of simplicity, we shall introduce a second discreteness representing a convenient approximation, recognizing however that this second discreteness would not enter into a strict theory. We shall regard the inherently discrete primary condensations as arising at particular moments of time, the moments being separated by interval $\frac{1}{3}H^{-1}$. Suppose that time t is one of these moments. Then at time t a system of primary condensations comes discretely into being. Between t and $t+\frac{1}{3}H^{-1}$ no further primary condensations arise, the system of condensations born at time t simply expand apart from each other in accordance with the de Sitter expansion factor $R(t) = \exp(Ht)$. But at time $t+\frac{1}{3}H^{-1}$ a new system of primary condensations again comes into being, the individual condensations and their mean spacing apart being exactly the same as was the case for the system born at time t. And so on for subsequent generations.

And we shall introduce the further artificial discreteness that the lattice formed by the primary condensations of each generation always has the same structure. For simplicity, we take the lattice to be cubic, and we also take the primary condensations to be spheres having centres at the lattice points of the cubic structure. After an initial delay we expect each primary condensation to join in the general expansion—once the delay caused by the criss-crossing motions discussed in the previous section is over, expansion of the lattice units keeps step with the expansion of the lattice itself. That is to say, the radius of a lattice unit maintains a constant ratio to the lattice distance. We take the ratio to be $\frac{1}{3}$. This requires the lattice units of each generation to be well separated, since the choice of this ratio requires the distance separating two neighbouring condensations A and B to be made up in the following way: $\frac{1}{3}$ in A, $\frac{1}{3}$ in neither A nor B, $\frac{1}{3}$ in B.

Our choice of this particular ratio has been guided by the consideration that if the lattice units were initially almost touching each other, and if a time $\sim\frac{1}{3}H^{-1}$ be allowed for the delay in the expansion of the lattice units, then the ratio must be $\frac{1}{2}e^{-1/3}$, which is close to $\frac{1}{3}$.

Write a_1 for the radius of each lattice unit and l_1 for the lattice spacing at the beginning of uniform expansion. Then, from what has been said, $a_1 \sim 30$ mpc, $l_1 \sim 90$ mpc. The precise numerical values of a_1, l_1 will not affect the following work in any important respect—their values could be changed by a factor of at least 2 without appreciable consequences. On the other hand, the ratio a_1/l_1 does turn out to be important. A decrease in this ratio would make the number count problem simpler, although a marked decrease would probably raise a different difficulty in that non-isotropic effects would then arise in marked degree. The latter question will be taken up later in the paper.

It is convenient to describe the lattice characterized by (a_1, l_1) as the "first generation" lattice. This will be the "youngest" lattice that an observer will expect to find. The observer will also detect older lattices. Those older by $(n-1)/3H$, $n=2, 3, \ldots$ will possess lattice units and lattice spacing characterized by (a_n, l_n) given by

$$(a_n, l_n) = e^{n-1/3}(a_1, l_1). \qquad (1)$$

We shall refer to (a_n, l_n) as the "nth generation lattice". Allowing for the initial delay period of $\frac{1}{3}H^{-1}$, the age of the nth generation is just $\frac{1}{3}nH^{-1}$.

The galaxies to be found in the lattice units of a particular generation will not possess ages as long as that of the lattice in question, since an interval of time must elapse before the galaxies and the stars within them are formed. We tentatively set this interval as $\sim\frac{2}{3}H^{-1}$. Then galaxies containing stars appear in the second generation. Galaxies possessing stars of age $\sim H^{-1}$ appear, however, only in the 5th generation. The 5th generation lattice has $a_5 \sim 100$ mpc, $l_5 \sim 300$ mpc, although once again, we note that these numerical values could easily be in error by a factor ~ 2.

Since the majority of definitive identifications of radio sources are with giant E galaxies, and since the stars of E galaxies give a late colour index, and are almost certainly at least of age H^{-1} (**12**), it appears that radio sources occur mainly in old lattices, in generations later than the 5th. We therefore see that the discreteness inherent in steady-state cosmology must enter the radio source problem on a scale at least as great as $l_5 \sim 300$ mpc. For the most part in what

follows we shall be able to employ simple averages derived from the usual continuous form of the steady-state theory. The present discrete picture is not then needed. At certain stages of the argument, however, the discreteness of the condensation picture is required, indeed at one crucial point. It is important to notice that this crucial aspect is concerned with the inherent discreteness of the condensation picture, not with the artificial discreteness of the sequence of regular lattices.

Several further points will be used at later stages. The probability that an observer at random lies inside a lattice unit belonging to the nth generation is given by

$$f = \frac{4\pi}{3}\left(\frac{a_n}{l_n}\right)^3 = \frac{4\pi}{3}\left(\frac{a_1}{l_1}\right)^3 \cong \frac{1}{6{\cdot}4} \tag{2}$$

the ratio $\frac{1}{3}$ being used for a_1/l_1. The probability is therefore the same for all generations.

Although f is appreciably less than unity, the observer must lie in lattice units belonging to an infinite sub-set of $n = 1, 2, \ldots$. But since the space density of galaxies weakens with increasing n as $\exp(-n)$ the main contribution to the density of galaxies at the observer's position comes from the smallest value of n in the sub-set.

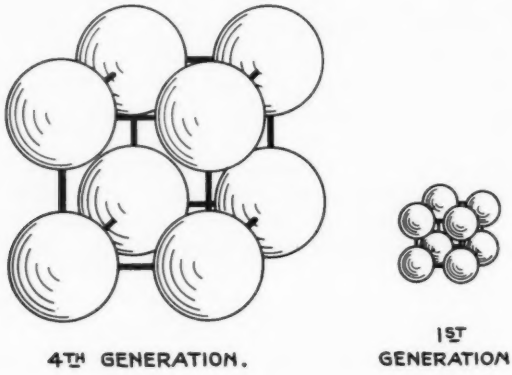

FIG. 1

The oldest stars in our Galaxy appear to have ages of order $1{\cdot}5 \times 10^{10}$ years $\cong 4H^{-1}/3$. This implies that we ourselves are inside a sixth generation lattice unit. We may also lie inside a younger lattice unit, and we must certainly lie inside older systems. The latter make no more than a small contribution to the total density of galaxies, while galaxies belonging to any younger lattice may still be largely undeveloped. In this connection we note that our presence here on the Earth guarantees some such situation, since our presence demands a galaxy, stars, planetary formation, etc.

It has sometimes been objected to the steady-state theory that the mean age of all galaxies should be $\frac{1}{3}H^{-1}$, whereas in our locality observation suggests ages that are generally of order H^{-1}. We now see that our presence inside a fifth or sixth generation lattice unit would give systematic ages $\sim 1{\cdot}5 \times 10^{10}$ years for the developed galaxies around us.

In Fig. 1 we show the forms of lattices for the first and the fourth generations, the scale in the latter case being greater by e. The positions of the centres of the lattice units of any particular generation are probably *anticorrelated* with those of preceding and succeeding generations. This is because the formation of a primary condensation at a particular place probably inhibits the formation of a condensation at the same place in the succeeding generation. Since f is only $\sim\frac{1}{6}$ there is opportunity for the lattice units of any generation to form in the interstices of the lattice of the preceding generation.

5. *The general mathematical formulation.*—The line element of the steady-state theory is

$$ds^2 = c^2\,dt^2 - \exp(2Ht)[dr^2 + r^2(d\theta^2 + \sin^2\theta\,d\phi^2)], \tag{3}$$

where $r=0$ is the observer's position. Our discussion of the lattice distances, given in the preceding section, refers to a particular value of t, distances being given by $\exp(Ht)\int du$. The line integral with respect to u is here to be taken along a straight line in the Euclidean sub-space

$$du^2 = dr^2 + r^2(d\theta^2 + \sin^2\theta\,d\phi^2). \tag{4}$$

Indeed, if we choose the arbitrary zero of t to be the present, then the present lattice distances are simply coordinate distances.

The lattice points of any generation possess coordinates r, θ, ϕ independent of t. And once the lattice units reach the stage of uniform expansion, the clusters of galaxies that make up each lattice unit may also be taken as having constant coordinates, if we neglect the finite size of a cluster.

Taking $t=0$ as the present, we ask: what is the r-coordinate of a galaxy that we observe (at the present) to give a red-shift $\Delta\lambda/\lambda$? The answer in the steady-state theory is

$$r = cH^{-1}z, \tag{5}$$

where

$$z = \frac{\Delta\lambda}{\lambda}. \tag{6}$$

A galaxy of intrinsic bolometric luminosity L and red-shift z will be observed as having an apparent bolometric intensity P given by

$$P = \frac{LH^2}{4\pi c^2 z^2(1+z)^2} \tag{7}$$

where P is the energy flux normal to the direction θ, ϕ of the galaxy in question.

Suppose now that we wish to count the number of galaxies brighter than some specified P, on the basis that all galaxies possess the same intrinsic L. First we define a value of z, z_m say, by solving (7) for z, using the specified P. Our problem is to count the number of galaxies with $z<z_m$. We attempt this, first using the simple continuous steady-state theory. In this the number of galaxies per unit proper volume is a constant, independent of the epoch. We consider observations made at $t=0$. The proper volume in the coordinate range r to $r+dr$ is $4\pi r^2\,dr$ at $t=0$. The number of galaxies in this coordinate range is therefore

$$(\text{constant}) \times r^2\,dr.$$

By (5), the coordinate range r to $r+dr$ corresponds to a red-shift range z to $z+dz$, where z is given by (5), and $dz = c^{-1}H\,dr$. Thus the number of galaxies giving

red-shifts in the range z to $z+dz$ is of the form

$$(\text{constant}) \times z^2\, dz.$$

Hence, at first sight, the answer to our problem is given by integrating the latter expression from $z=0$ to $z=z_m$, viz. (constant) $\times z_m{}^3$. Since the constant is independent of the epoch, and also of P, a similar calculation for varying P gives the number count as a function of P. The count is not absolute, of course, since we have not specified any absolute proper density of galaxies.

This simple procedure overlooks, however, the point that some of the galaxies we have counted, and which now exist at $t=0$, did not exist at the time the radiation would need to have been emitted in order to reach us at the present day. For red-shift z the radiation would need to have been emitted a time $H^{-1}\ln(1+z)$ ago.

To cope with this complication we must introduce the age distribution of the galaxies. In the continuous steady-state theory the number of galaxies with present-day ages between τ and $\tau+d\tau$ is

$$(\text{constant}) \times \exp(-3H\tau)\, d\tau \text{ per unit proper volume.}$$

Thus if we are considering galaxies giving red-shifts between z and $z+dz$ we must restrict ourselves to those in the age distribution with $\tau \geqslant H^{-1}\ln(1+z)$. This number is

$$(\text{constant}) \times z^2\, dz \int_{H^{-1}\ln(1+z)} \exp(-3H\tau)\, d\tau, \tag{8}$$

where the upper limit of the integration with respect to τ remains to be stated.

The three-dimensional sphere at $t=0$ defined by a red-shift z, or by the corresponding $r=cH^{-1}z$, must now be compared with the lattice spacings of our model discussed in the previous section. If for generation n the lattice distance l_n exceeds $2r$ then certainly not more than one lattice unit of the nth generation can fall completely inside the sphere. The phenomenon is then essentially discrete. Continuous averages are no longer applicable.

The point of transition from the continuous picture to the discrete model is of necessity rather uncertain. We could, for instance, require that at least *two* adjacent lattice units of generation n should fall completely inside the sphere of radius r in order that the continuous picture be applicable up to the age implied by generation n. This requires $l_n < 6r/5$.

To deal with the slight measure of uncertainty involved in the transition to discreteness we apply the continuous picture up to a generation n defined by

$$l_n = kcH^{-1}z, \tag{9}$$

where k is a constant between 1 and 2. In a later section we shall show that the precise value of k is not important.

It remains to relate l_n to the lattice distance of the first generation. We have

$$l_n = l_1 \exp\frac{n-1}{3} = cH^{-1}z_1 \exp\frac{n-1}{3}.$$

With l_1 and z_1 specified for the first generation, the limit of applicability of the continuous theory occurs at generation n, determined by solving

$$kz \cong z_1 \exp\frac{n-1}{3}. \tag{10}$$

The age of the nth generation is $\frac{1}{3}nH^{-1}$. By (10) this is

$$H^{-1}\left(\tfrac{1}{3}+\ln\frac{kz}{z_1}\right).$$

However, this does not give the correct upper limit of the integral in (8), since the age of generation n has been reckoned from the time of formation of the primary condensations, whereas the zero of τ in (8) refers to *galaxies* of zero age. There is an interval of time, Δ say, between the formation of a primary condensation and the formation of galaxies within it. Above we took Δ to be $\sim\frac{2}{3}H^{-1}$. The correct upper limit is thus

$$H^{-1}\left(\tfrac{1}{3}+\ln\frac{kz}{z_1}\right)-\Delta,$$

which can be written as $H^{-1}\ln kz/z_1'$, where

$$z_1'=z_1\exp(H\Delta-\tfrac{1}{3}). \tag{11}$$

Thus the count for the range z to $z+dz$, given by the continuous picture, is

$$(\text{constant})\,z^2\,dz\int_{H^{-1}\ln(1+z)}^{H^{-1}\ln\frac{kz}{z_1'}}\exp(-3H\tau)\,d\tau. \tag{12}$$

The transformation $\chi=H\tau-\ln(1+z)$ reduces (12) to

$$(\text{constant})\cdot\frac{z^2\,dz}{(1+z)^3}\int_0^{\ln\frac{kz}{(1+z)z_1'}}\exp(-3\chi)\,d\chi. \tag{13}$$

To obtain the total count down to flux level P, i.e. for z up to z_m, we integrate (13) as follows

$$(\text{constant})\cdot\int_{\frac{z_1'}{k-z_1'}}^{z_m}\frac{z^2\,dz}{(1+z)^3}\int_0^{\ln\frac{kz}{(1+z)z_1'}}\exp(-3\chi)\,d\chi. \tag{14}$$

The integral is taken over an area in the (χ,z) plane enclosed by the z-axis, the line $z=z_m$, and the curve

$$\chi=\ln\frac{kz}{(1+z)z_1'}. \tag{15}$$

This gives the number of galaxies brighter than P, *in so far as this can be determined from the continuous theory*.

Over and above (14) there is the possibility that a further contribution arises from discrete effects. These do not have much importance, except in the case where a sphere of radius r, $r=cH^{-1}z$, $(z<z_m)$, is invaded by a lattice unit of a generation even older than the value of n corresponding to $z=z_m$ in (10). Such a case represents a genuine fluctuation that must be given special consideration. We shall return to this question at a later stage.

It is already a matter of interest that (15) vanishes for

$$z_m=\frac{z_1'}{k-z_1'}\cong\frac{z_1'}{k}\qquad(k\sim 1{\cdot}5\quad\text{and}\quad z_1{}^j\ll 1).$$

This implies that as z_m increases above $\sim z_1'/k$ the product $NP^{3/2}$ increases to a maximum value and thereafter declines. Hence we have a $\log N-\log P$ curve

that has a slope initially greater than $-1{\cdot}5$. This is not our answer to the criticism of Ryle, since the increased slope only applies for z_m somewhat greater than z_1'/k, which will turn out to be about $1/15$, whereas the observed slope maintains its steepness up to $z_m \cong 0{\cdot}3$ or $0{\cdot}4$. Ryle has argued that the slope is maintained up to $z_m = 1$ or more, but it seems to us that the evidence concerning angular diameters of radio sources scarcely supports this extreme view.

The simplest hypothesis capable of steepening the $\log N - \log P$ curve at a larger value of z_m is the following: only galaxies of age greater than T, say, become strong radio sources. We must then count the sub-class of galaxies with age greater than T. The number of these galaxies varies with z_m, and hence with P according to

$$(\text{constant}) \int^{z_m} \frac{z^2\,dz}{(1+z)^3} \int_{HT}^{\ln \frac{kz}{(1+z)z_1'}} \exp(-3\chi)\,d\chi. \tag{16}$$

In order that the integral with respect to χ shall yield a positive result it is necessary that

$$\frac{kz}{(1+z)z_1'} \geqslant \exp(HT). \tag{17}$$

For this to be certainly the case the lower limit of the integral with respect to z must be taken at the value of z given by considering the equality sign in (17). The count can only be applied for values of z_m greater than this particular value of z. Indeed, the count falls to zero at z_m equal to this z, and the $\log N - \log P$ curve is steeper than $-1{\cdot}5$ for z_m somewhat greater. That is to say, the slope exceeds $-1{\cdot}5$ for z_m somewhat greater than the value of z given by

$$\frac{kz}{(1+z)z_1'} = \exp(HT). \tag{18}$$

For T between $2H^{-1}$ and $3H^{-1}$ this yields a value of z of $\sim 0{\cdot}3$.

These considerations are a special case only, however, of the general situation that arises when the probability of a galaxy being a radio source is a function of the age of the galaxy. We consider the problem in the following terms.

(1) It may be that only galaxies with some special property become radio sources of the intense type that contributes appreciably to the $\log N - \log P$ curve. Examples of such properties might perhaps be those galaxies that are members of physically connected pairs, or perhaps E-type galaxies. So long as the property is not age-correlated, however, we simply choose out the sub-class of galaxies that possess the property, or properties, in question. This changes the counting scale but not the relative counts for variable P.

(2) The intrinsic radio luminosity will certainly not be the same for all radio sources. So long as the intrinsic luminosity is not age-correlated, however, it is possible to represent the luminosity function by a histogram, considering each section of the histogram in the manner described above, each section leading to an expression of the form (14), but each with a different z_m (for the same P). Varying P gives a $\log N - \log P$ curve for each section of the histogram. If none of these separate curves possesses slope greater than $-1{\cdot}5$, the combined curve cannot possess slope greater than $-1{\cdot}5$. The luminosity function can be represented to any required degree of accuracy by taking a sufficient number of sections in the histogram.

(3) The situation is changed only if either the probability of a galaxy being a radio source or the luminosity function is age-dependent (or of course both of these). The dependence of the probability on age we denote by $K(\tau)$. To deal with an age dependence of the luminosity function, we represent the luminosity function by a histogram at each value of τ, the histograms being chosen in the following related way. The luminosity function is first normalized to unit area for each τ, and the histograms are then made up of the same number of sections of the same areas. At different τ the sections of the histograms are related serially, the first to the first, the second to the second, and so on. In the following considerations we consider only one set of related sections of the histograms, and we denote the dependence of the intrinsic radio emission for this section by $L(\tau)$. The results for other sets are similar to those obtained below.

Consider galaxies with present ages between τ and $\tau+d\tau$ giving red-shifts between z and $z+dz$. The number of these galaxies that are radio sources is given by an expression of the form

$$(\text{constant})\, z^2\, dz K(\tau - H^{-1} \ln \overline{1+z}) \exp(-3H\tau)\, d\tau \qquad (19)$$

provided the values of z, τ can be related within the terms of the continuous theory. The relevant condition is that already discussed above, that

$$H\tau \leqslant \ln \frac{kz}{z_1'}. \qquad (20)$$

Introducing $\chi = H\tau - \ln(1+z)$ (19) and (20) can be written as

$$(\text{constant})\ \frac{z^2}{(1+z)^3} K(\chi) \exp(-3\chi)\, d\chi\, dz, \qquad (19')$$

$$\chi \leqslant \ln \frac{kz}{(1+z)z_1'}. \qquad (20')$$

A second condition is imposed by the requirement that the apparent bolometric flux be greater than P, viz.

$$P \leqslant \frac{H^2 L(\chi)}{4\pi c^2 z^2 (1+z)^2}. \qquad (21)$$

The radio astronomer does not of course measure the bolometric flux, but the flux per unit frequency range at some specified frequency. However, it can readily be shown that for sources with frequency spectra $d\nu/\nu$ the measurement of flux per unit frequency range yields the same relative counts of sources as does the total bolometric flux. Most radio sources possess spectra of about the form $d\nu/\nu^{0.8}$. This we regard as being sufficiently close to $d\nu/\nu$ for the difference to be neglected. The effect of $d\nu/\nu^{0.8}$, and of regarding P as the flux per unit frequency range, is to replace the factor $(1+z)^2$ in (21) by $(1+z)^{1.8}$. We have not troubled to take account of this slight modification.

To obtain the number of sources with flux greater than P, (19′) must be integrated over the portion of the χ, z plane defined by the conditions (20′) and (21). The (χ, z) plane is shown in Fig. 2. First, draw the curve

$$\chi = \ln kz/(1+z)z_1'.$$

Next draw the curve along which

$$z^2(1+z)^2 = \frac{H^2}{4\pi c^2 P} L(\chi). \qquad (22)$$

The relevant area is bounded by these two curves and by the z-axis, in the manner shown in Fig. 2.

It will be noticed that the age dependence of L does not affect the weighting function (19′), although it does affect the area of integration. The two functions $K(\chi)$, $L(\chi)$ do not therefore affect the counts in the same way. Indeed, it turns out that while $K(\chi)$ can have an extremely important effect on the $\log N - \log P$

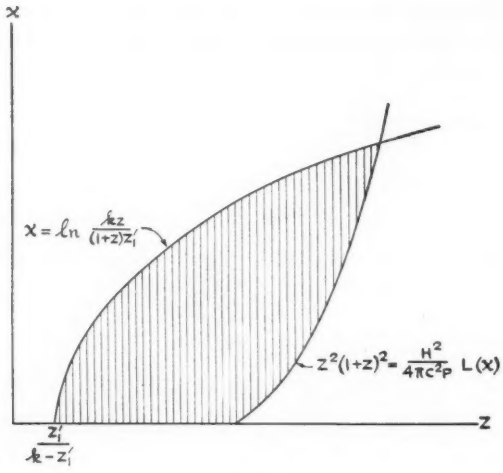

FIG. 2

curve, the dependence of the luminosity L on age is much less effective. This is demonstrated by an explicit example given in the Appendix. Since the form of $L(\chi)$ is comparatively unimportant, it will be sufficient in later work to take L independent of χ, keeping only the probability function $K(\chi)$. In this case the general integral reduces to a form very similar to (14), viz.

$$(\text{constant}) \int_{\frac{z_1'}{k-z_1'}}^{z_m} \frac{z^2\,dz}{(1+z)^3} \int_0^{\ln \frac{kz}{(1+z)z_1'}} K(\chi) \exp(-3\chi)\, d\chi. \tag{23}$$

Writing $q = \exp \chi$ gives the somewhat more convenient expression

$$(\text{constant}) \int_{\frac{z_1'}{k-z_1'}}^{z_m} \frac{z^2\,dz}{(1+z)^3} \int_1^{\frac{kz}{(1+z)z_1'}} K(q) \frac{dq}{q^4}. \tag{24}$$

6. *The basic $\log N - \log P$ distribution.*—In order that (24) give a result of an essentially new character, it is necessary that an appreciable contribution to the integral with respect to q shall come from the upper part of the range of q. This will be the case if $K(q)$ varies with q according to some power $\geqslant 3$. The simplest case is where $K \propto q^4$, when the integral is equally weighted over the whole range of q. We shall adopt this distribution throughout the following work, noting, however, that essentially similar results are obtained for any power law between

about 3 and 5. In this connection it may be noted that it is always possible, over a limited range of q, to represent any general function $K(q)$ by a power law. Thus $K \propto q^4$ simply means that over the range of q in question we regard K as being represented by this particular power law. It will turn out that the relevant range of q covers the generations of our lattice model from $n=5$ to $n=10$, and that values of z from about 0·1 to about 0·3 are mainly involved. The corresponding range of q is from 1 to about 3. Our dependence $K \propto q^4$ therefore implies that the probability of a galaxy (perhaps of a certain restricted type —e.g. members of pairs) being a radio source increases over the relevant generations by a factor $\sim 3^4$. A fuller discussion of these questions will be given at a later stage when numerical results have been derived, and when the various other physical factors of relevance have been discussed.

With $K \propto q^4$, (24) gives

$$\text{(constant)} \int_{\frac{z_1'}{k-z_1'}}^{z_m} \frac{z^2\,dz}{(1+z)^3}\left[\frac{kz}{(1+z)z_1'} - 1\right]. \tag{25}$$

An important point now emerges. We shall be concerned mainly with values of z_m in the range 0·15 to 0·3. Since the integrand of (25) is heavily weighted towards its upper limit, we can consider the factor

$$\frac{kz}{(1+z)z_1'} - 1$$

for values of z near z_m. It is seen then that $kz/(1+z)z_1'$ appreciably exceeds unity (k we expect to lie between 1 and 2, and k/z_1' will be found to be ~ 15). This means that, without severe approximation, we could neglect the -1 in this factor, in which case the uncertain factor k simply goes outside the integral and is absorbed into the multiplying constant. Hence we see that the choice of k does not affect the $\log N - \log P$ curve in any really important degree.

To obtain numerical values, k/z_1' must be specified. The value of z_1' is related to the first generation lattice by

$$z_1' = z_1 \exp(H\Delta - \tfrac{1}{3}),$$

where $z_1 = cH^{-1}l_1 \cong 0{\cdot}03$ for $l_1 \cong 90$ mpc ($H = 100\ \mathrm{km\,s^{-1}\,(mpc)^{-1}}$) and Δ is the time delay between the formation of a primary condensation and the development of the first radio sources within it (more precisely of the first radio sources that make an appreciable contribution to the count). The optical identifications available show a marked association of radio sources with galaxies of late colour index, the stars of which can scarcely have ages less than H^{-1}. Thus, allowing $\frac{2}{3}H^{-1}$ for galaxy formation, together with a further H^{-1} for the ageing of the stars we have $z_1' \cong z_1 \exp\frac{4}{3} = 0{\cdot}11$ for $z_1 = 0{\cdot}03$. The value given to k defines the cut-off from the continuous theory. We have seen that a value between 1 and 2 would seem appropriate. With $k \cong 1{\cdot}6$ $z_1' \cong 0{\cdot}11$, $k/z_1' \cong 15$. This will be the value used in succeeding work. As already emphasized, the results are not sensitive to this particular choice.

The integral (25) can be evaluated explicitly to give

$$\left[\left(1 - \frac{z_1}{k}\right)\log(1+z) + \frac{3z^2+2z}{2(1+z)^2}\cdot\frac{z_1'}{k} - \frac{11z^3+15z^2+6z}{6(1+z)^3}\right]_{\frac{z_1'}{k-z_1'}}^{z_m}. \tag{26}$$

Taking $k/z_1' = 15$ counts on an arbitrary scale can be worked out numerically as a function of z_m. Since $P \propto z_m^{-2}(1+z_m)^{-2}$ the corresponding energy fluxes can also be given on an arbitrary scale. (It will be recalled that so far we are only considering sources of a single fixed intrinsic luminosity.) Results are given in Table I. The associated value of $NP^{3/2}$, again on an arbitrary scale, are also given in Table I.

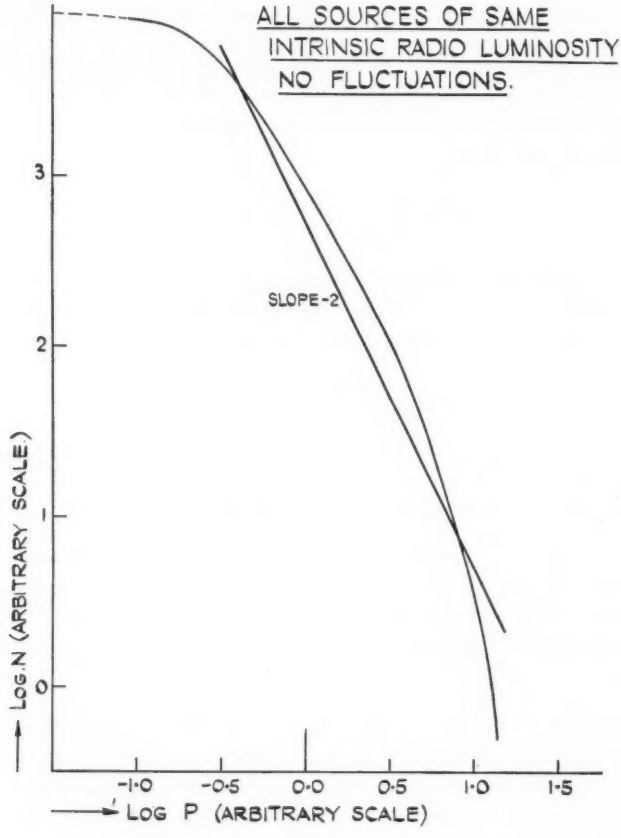

FIG. 3

The $\log N - \log P$ curve is plotted in Fig. 3. It is evidently steeper than $-1{\cdot}5$ over the range from $z = 0{\cdot}1$ to $z = 0{\cdot}3$. This range of z corresponds to a change by a factor 12·5 in P, as compared to about a factor 15 for the results upon which Ryle based his criticism of the steady-state theory. The slope of the $\log N - \log P$ curve is close to $-1{\cdot}8$ for z between 0·2 and 0·3, and the slope even exceeds -2 for z between 0·1 and 0·2.

To relate these results to observation it is necessary that the hitherto arbitrary scales of N and P be fixed so that N and P are in reasonable relationship to the values obtained in the observational surveys. To give a suitable association we take the unit of P to be 10^{-26} w.m^{-2} (c/s)$^{-1}$ and we regard N as the number of

TABLE I

z	·08	·09	·1	·11	·12	·13	·14	·15	·175	·2	·25	·3	·4	·5	·6
log P	1·61	1·50	1·40	1·31	1·23	1·15	1·08	1·01	·86	·72	·49	·30	$\bar{1}$·99	$\bar{1}$·73	$\bar{1}$·52
N	·15	·81	2·20	4·56	8·06	13·0	19·4	27·9	58·8	107	269	542	1356	2385	2498

TABLE II

I: 10^{26}w (c/s)$^{-1}$ at 160 Mc/s^{-1}. II: 3×10^{26}w (c/s)$^{-1}$. III: 10^{27}w (c/s)$^{-1}$. IV: 3×10^{27}w (c/s)$^{-1}$. V: 10^{28}w (c/s)$^{-1}$. VI: 3×10^{28}w (c/s)$^{-1}$
(P in 10^{-26}w.m^{-2}(c/s)$^{-1}$)

log P (10^{26}w.m^{-2}(c/s)$^{-1}$)	−·75	− ·5	−·25	0	·25	·5	·75	1	1·25	1·5	1·75	2
log $NP^{3/2}$ (Arbitrary scale for N)	·56	·76	·92	·99	1·04	1·03	1·01	·98	·93	·88	·83	·76
I	85	74[21]	59	48[19·75]	35	26[18·5]	17	14[17·25]	13	F[16]	F	F[14·75]
II	15	26[22·25]	7	43[21]	45	44[19·75]	38	30[18·5]	19	18[17·25]	16	F[16]
III			4	9[22·25]	8	25[21]	31	31[19·75]	28	24[18·5]	15	15[17·25]
IV					2	5[22·25]	11	16[21]	19	22[19·75]	19	20[18·5]
V							3	9[22·25]	20	32[21]	40	47[19·75]
VI									1	4[22·25]	10	18[21]

The values entered for the six luminosity classes give the percentage of each class at the various flux levels. F represents a fluctuation contribution. Estimated optical photographic magnitudes in brackets [ ], uncorrected for red-shift.

sources per steradian. This transfer to absolute scales yields information concerning absolute values of the probability function K and of the intrinsic emission L. We shall defer a discussion of the probability function until a later section.

The value of L can now be worked out from (7), by inserting $z=0{\cdot}3$, $P=2\times10^{-26}\,\mathrm{w.m^{-2}\,(c/s)^{-1}\,s^{-1}}$. The result is $L=3{\cdot}3\times10^{26}\,\mathrm{w\,(c/s)^{-1}}$, the values of P and L being taken at ~160 Mc/s. For a source with spectrum $dv/v^{0{\cdot}7}$ extending up to $v=3000$ Mc/s, the total energy emission would be $\sim4\times10^{42}\log\mathrm{s^{-1}}$, a value that falls within a factor of about 2 of the total emission of the source Hydra A. It is of course the case that a value must be ascribed to H in (7). In the present calculation $H=100\,\mathrm{km\,s^{-1}\,(mpc)^{-1}}$ was used.

7. *Fluctuations in the number count.*—Two quite different types of fluctuation enter the present theory: fluctuations in the number count due to the presence of the observer in or near one or more lattice units of the discrete model, and fluctuations from isotropy in the distribution of sources on the sky. The two types of fluctuation are affected by the discrete properties of the model in markedly different ways. The effect on the count is more extreme when the observer lies inside a lattice unit. This lifts the $\log N-\log P$ curve at large values of P, thereby reducing the overall slope of the curve to a greater degree than if the observer were to lie immediately outside a lattice unit—in the latter case the curve is unaffected at both large and small values of P, but receives a wiggle at intermediate values. Departures from isotropy only become an issue, on the other hand, when the discrete lattice units are projected on to small areas of the sky. Hence departures from isotropy must be considered for the case where the observer is distant from a lattice unit, not when he is inside it. The question of non-isotropy will be considered later in the paper. For the present, we are concerned with effects on the number count, particularly with placing the observer inside a lattice unit, or units.

First we note that an observer cannot lie in more than one lattice unit of a particular generation. If he lies in two lattice units of different generations, one of the units will have appreciably greater weight than the other. Thus if the two units belong to generations with ages great enough for them both to belong to the range of q in which $K(q)$ is rapidly increasing, but not so great that $K(q)$ has reached an ultimate saturation level, then the older of the two units contributes the greater weight. It follows that we need only consider the presence of the observer inside one lattice unit, the one giving the greatest weight.

The lattice units are never so large that the $1+z\cong1$ cannot be used as a tolerable approximation for the sources within the particular lattice unit in which the observer happens to be situated. These particular sources, taken by themselves, therefore follow a $\log N-\log P$ curve with slope close to $-1{\cdot}5$. The general effect is shown by Fig. 4, where $\log NP^{3/2}$ is plotted against $\log P$. Curve I is simply a plot of the values of Table I. At large P, the curve falls steeply away. Curve II of Fig. 4 shows the effect of a fluctuation. At large P the fluctuation dominates and $NP^{3/2}$ is effectively constant. Then as P decreases the curve first falls to a minimum, and thereafter rises steeply. The minimum is caused by reaching the limit of the local lattice unit at $\log P\simeq2{\cdot}0$, the contribution of the lattice unit ceasing at this value of P.

The reason why the fluctuation has been set at the level shown in Fig. 4 will now be explained. We have seen that the age of our own Galaxy suggests

that we are situated inside a lattice unit belonging to about the 6th generation. The 6th generation lattice has spacing $l_1 \exp 5/3$. The distance of an observer at the centre of a unit cube of this lattice from each of the nearest eight vertices is $(\sqrt{3}/2) l_1 \exp 5/3$. This distance corresponds to a red-shift $(\sqrt{3}/2) c^{-1} H l_1 \exp 5/3$. With $l_1 \cong 90$ mpc, $H = 100$ km sec^{-1} (mpc)$^{-1}$ (we have used these values throughout), the resulting value is 0·137. According to Table I the value of N at $z = 0{\cdot}137$ is ~ 17. If the whole of this count were contributed by the 6th generation alone then each of the eight lattice units of the unit cube would contribute ~ 2 to the count. This would ignore, however, the contribution of the 5th generation,

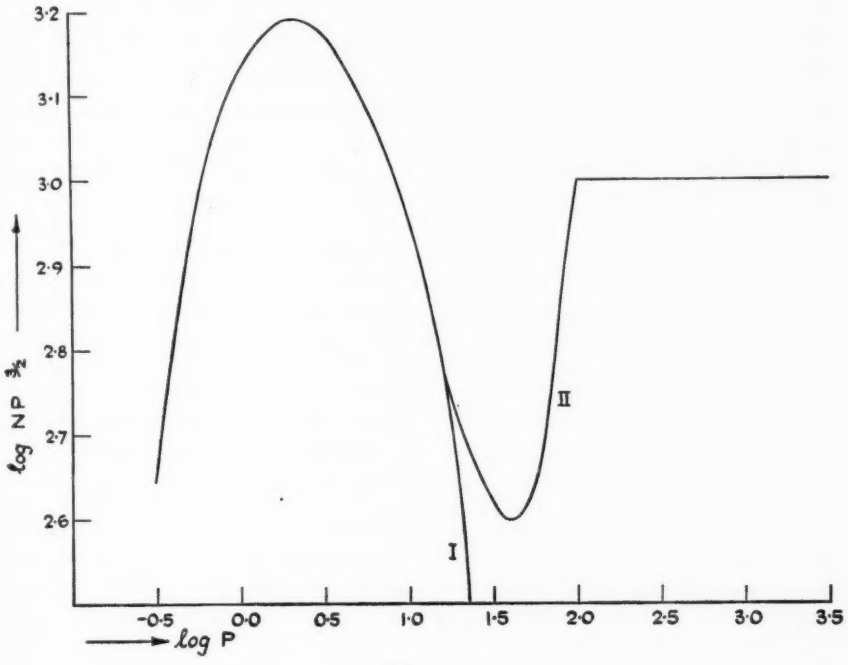

FIG. 4

and also the contribution from one or two lattice units of the 7th generation that may be observable at red-shifts $\leqslant 0{\cdot}137$. We have made allowance for this by taking half the count as coming from the 6th generation, in which case each of the eight lattice units of this generation contributes ~ 1 to N.

The radius of a 6th generation lattice unit $\sim \frac{1}{8} l_1 \exp 5/3$. A source at such a distance has red-shift $\sim \frac{1}{8} z_1 \exp 5/3$ ($z_1 = 0{\cdot}03$). Thus an observer situated at the centre of a 6th generation lattice unit will find that all the local sources coming from the unit in question give red-shifts $z \leqslant 0{\cdot}01 \exp 5/3 = 0{\cdot}053$. The value of $\log P$ at $z = 0{\cdot}053$, on the scale of Table I, is about 2·0. Thus with $N \cong 1$ at $\log P = 2{\cdot}0$, the constant level of $\log NP^{3/2}$ to be used for curve II of Fig. 4 is $\sim 3{\cdot}0$.

The precise depth of the minimum of curve II depends on the steepness in the region $\log P \cong 1{\cdot}5$ of the fluctuation-free curve. This is affected by our

choices for z_1, k, Δ. Since our choices are somewhat uncertain, the depth of the minimum, and its position with respect to P, is not well determined. All we can properly assert is that a minimum is to be expected in the region from $\log P \cong 1{\cdot}5$ to $\log P \cong 2{\cdot}0$.

If $10^{-26}\,\mathrm{w.m^{-2}\,(c/s)^{-1}}$ is the unit of P, then the values of N in Table I at $P \cong 10^{-25}\,\mathrm{w.m^{-2}\,(c/s)^{-1}}$ are approximately correct for the number of radio sources counted per steradian. On this basis $N \cong 1$ implies only about one source per steradian. It is clear, therefore, that although the fluctuation appears impressive when plotted in the form of Fig. 4, the actual number of sources introduced by the fluctuation is very small compared with the count at $P < 10^{-25}\,\mathrm{w.m^{-2}\,(c/s)^{-1}}$. The precise height of the fluctuation of curve II is not therefore a matter of great importance. Doubling the height (i.e. increasing $\log NP^{3/2}$ by $0{\cdot}3$) would only add about 1 source per steradian at flux levels $\geqslant 10^{-24}\,\mathrm{w.m^{-2}\,(c/s)^{-1}}$, and no profound attention would be paid to this. The existence of the minimum is of considerable theoretical interest, however, since it clears up an apparently puzzling point.

Consider a single object, with any probability function for being a radio source at rest in the usual cosmological frame of reference (r, θ, ϕ coordinates constant). Suppose that observations of the source are made by an ensemble of observers at rest with constant r, θ, ϕ coordinates. Imagine the observers collate their experiences and that they draw an average curve relating the probability of observing the radio source against flux P, the averaging being performed with equal weight per unit proper volume for observations made at the same value of t. Then the curve so obtained will be the same as the $\log N - \log P$ curve determined by a single observer in the case where an ensemble of objects, each exactly similar to the original object, is uniformly distributed throughout space. Hence an arbitrary set of objects distributed in space in any fashion will yield exactly the same result when averaged with respect to an ensemble of observers as will a grand ensemble of objects uniformly distributed in space. Now the continuous steady-state theory treats just the case of a grand ensemble—it treats a mixture of ages in the correct proportions. Taking account of the eventual saturation of any probability functions (so that divergences cannot occur) the smooth continuous theory yields the form of $\log N - \log P$ curve used by Ryle and his colleagues. Hence the latter curve must represent the average arrived at by the ensemble of observers. The discrete model of the present paper can lead to a particular observer obtaining a different $\log N - \log P$ curve, but it cannot prevent the average with respect to all observers from being of the usual form. The averaging of the observers must take place through a volume with dimensions greater than the lattice spacing of the oldest generation that makes an important contribution to the count. This is determined by the saturation of the probability function. The results derived above are unaffected by a saturation at the 10th generation. The relevant lattice spacing could therefore be $l_1 \exp 3 \cong 20 l_1 \cong 1800$ mpc. Averaging must therefore take place over the whole "observable" region of the Universe (this is defined as $cH^{-1} \cong 3000$ mpc, for $H = 100\,\mathrm{km\,s^{-1}\,(mpc)^{-1}}$). While it would be possible to raise logical objections to observers actually collating their experiences over regions as large as this, one can still carry through a mathematical average. The question arises as to how the results derived above could lead, when averaged for all observers, to the $\log N - \log P$ curve given by the usual continuous theory.

The answer lies in the minimum shown in curve II of Fig. 4. Some observers will be situated inside late generation lattice units, e.g. the 8th and 9th. The fluctuation level of $NP^{3/2}$ for an observer in such lattice units is not only lifted but the fluctuation extends to smaller values of P. The minimum of curve II of Fig. 4 is shifted left by $\sim 1{\cdot}0$ in $\log P$. The observer would find a $\log N - \log P$ curve with slope $-1{\cdot}5$ at high P, the slope would become somewhat less than $-1{\cdot}5$ as P decreased (due to the usual red-shift effect), but then for P around 10^{-25} w.m^{-2} (c/s)$^{-1}$ the slope would fall precipitately away to the minimum—the slope would be *markedly less* than that given by the completely continuous theory. Eventually at low values of P the slope might increase somewhat, but $NP^{3/2}$ would not rise back to its value at high P.

We expect observers of the sort described in the previous paragraph to have a large weight in determining the average for the whole ensemble of observers. This is because such observers add comparatively large numbers of sources at high values of P. The slope of a $\log N - \log P$ curve can be appreciably changed by adding only a moderate number of sources provided these are added at high and at medium P values. No great differences in the counts at low P values are needed. Indeed we expect all observers to obtain much the same counts at low flux values.

Can any explanation be given of why we do not ourselves lie inside a late generation lattice unit? On the basis of sheer probability the chance against lying inside a lattice unit of any particular generation is about 5/6 (cf. Section 4). The chance against lying inside lattice units belonging to the 7th, 8th and 9th generation would thus be $\sim (5/6)^3$, and this is not small. Moreover there could be biological and physical reasons of relevance, relating to our presence on the Earth. For life to be possible (in our particular form) rather stringent chemical conditions, as well as astronomical conditions, must very likely be satisfied. It is entirely possible that these conditions are only met with in galaxies of about the age $\frac{4}{3}H^{-1}$, in which case our presence inside a 6th generation lattice unit would not be an accident. And this could inhibit our chance of lying inside a 7th, or even an 8th, generation unit, since the lattice positions of succeeding generations are very likely anticorrelated. Nor is it an entirely unreasonable speculation that the degree of electromagnetic activity associated with 8th and 9th generation lattice units might be so great that biological development would be significantly affected by a very high cosmic ray background inside such units.

Quite apart from these points, however, it is important to notice that although a discrete model does not change the average of an ensemble of observers, *it does make each observation yield a $\log N - \log P$ curve that is different from the average curve.* The situation is not similar to the case of a Maxwellian distribution of particles, where most particles have energies close to the mean energy. A typical observer does not obtain a $\log N - \log P$ curve close to the average of the whole ensemble. Observers obtain widely differing curves depending on their individual relationships to the discrete structure of the condensations. Only after a very large-scale averaging process has been carried out does the mean $\log N - \log P$ curve appear.

Our answer to Ryle's criticism lies at exactly this point. Every observer taken individually obtains a $\log N - \log P$ curve differing from the mean curve. Hence every observer could interpret his result as disproving the steady-state theory, even though in the mean their results actually verified the theory. For

example, an observer situated inside a late generation lattice unit (8 or 9) could argue that as P decreased below 10^{-25} w.m^{-2} (c/s)$^{-1}$ the slope differed markedly from the continuous steady-state curve, but in just the opposite sense to that of the terrestrial observations. We are dealing with a property in which the fluctuations make an important contribution, particularly fluctuations arising from old lattice units. The property is due to the weighting effect of the probability function $K(\tau)$ which causes the mean situation to have no close resemblance to the situations in particular cases. Such an effect does not arise when K is independent of τ, as it is in the simple counting of galaxies.

8. *The effect of the luminosity function.*—In the previous sections we have shown how a $\log N - \log P$ curve appreciably steeper than $-1{\cdot}5$ can be obtained. In the present section we shall be concerned less with the precise value of the steepness of the $\log N - \log P$ curve than with the discussion of a realistic luminosity function, and with the relation of the luminosity function to an absolute scale for P. To obtain the best fit of the theory to known data concerning the luminosity function some sacrifice of steepness has to be made—the value obtained below for the slope resulting from the combination of a number of luminosity classes will turn out close to $-1{\cdot}6$.

We have seen in Section 6 that the unit of the $\log P$ scale in Table I and in Figs. 2, 3, 4 can be taken as 10^{-26} w.m^{-2} (c/s)$^{-1}$ if the intrinsic luminosity of the sources in question is $\sim 3 \times 10^{26}$ w. (c/s)$^{-1}$ at frequency 160 Mc s^{-1}. Such sources we refer to as of class II. We consider five other classes: I, $L = 10^{26}$ w. (c/s)$^{-1}$; III, $L = 10^{27}$ w. (c/s)$^{-1}$; IV, $L = 3 \times 10^{27}$ w. (c/s)$^{-1}$; V, $L = 10^{28}$ w. (c/s)$^{-1}$; VI, $L = 3 \times 10^{28}$ w. (c/s)$^{-1}$. Each class of source is taken as possessing a $\log (NP^{3/2}) - \log P$ curve of the form of curve II of Fig. 4, but with an appropriate displacement of the flux scale. Thus class I is displaced by $\sim 0{\cdot}5$ to the left (with respect to Fig. 4 for class II), class III by $\sim 0{\cdot}5$ to the right, class IV by $1{\cdot}0$ to the right, class V by $\sim 1{\cdot}5$ to the right, and class VI by $2{\cdot}0$ to the right. The maxima for I and II were taken as of equal height in the $\log NP^{3/2} - \log P$ plane, the maximum of III was reduced by $0{\cdot}2$ in the logarithm, that of IV by $0{\cdot}44$, that of V by $0{\cdot}24$, that of VI by $0{\cdot}64$. These choices were made in order to give what we feel to be reasonable agreement with all the available data, such as it is known to us. The result of combining the six classes is shown in Table II. The percentages of each class at the various five levels are given in the second part of the table.

The fluctuation introduced at high values of P brings in sources only at the places entered as F in Table II. The precise contribution of the fluctuation is uncertain within a factor 2. For curve II of Fig. 4, sources of class I would increase the total count at $\log P = 1{\cdot}5$, and at $\log P = 1{\cdot}75$ by about 30 per cent, while the count at $\log P = 2{\cdot}0$ would be approximately doubled.

Optical photographic magnitudes, uncorrected for spectrum red-shift effects, and making no allowance for galactic obscuration, are attached in brackets to the entries in the second part of Table II for the columns $\log P = -0{\cdot}5$, 0, $0{\cdot}5$, 1, $1{\cdot}5$, 2. Since optical and radio magnitudes vary with distance in the same way when spectrum red-shift effects are omitted (these are in any case small for the radio magnitudes) the optical magnitudes change by $1{\cdot}25$ when the $\log P$ changes by $0{\cdot}5$. And assuming that all radio sources are associated with galaxies of the same intrinsic optical luminosity, the optical magnitudes vary as $2{\cdot}5 \log L$ for the various radio classes. Since $\log L$ changes by $0{\cdot}5$ from one radio class

to the next, the optical magnitude therefore also changes by 1·25 as we pass from one radio class to the next at fixed P.

Remembering that Table I refers to class II sources (when the scale of P is 10^{-26} w.m^{-2} (c/s)$^{-1}$), we note that the red-shift for $\log P = 1$ is close to 0·15 for a class II source. At this red-shift, Humason, Mayall and Sandage give about +18·5 for the photographic magnitude of the brightest galaxy of the cluster 0025+2223. This value has been taken as the standard in Table II, other values being determined by differencing in the manner described in the previous paragraph.

The magnitudes in Table II are therefore chosen as bright as seems reasonably possible. They assume that all radio sources are associated with galaxies of abnormally great optical emissivity. While it is true that known optical identifications support this assumption, it is obvious that a selection effect exists in favour of making identifications with galaxies of abnormal luminosity. Also we may note that cluster 0025+2223 is at comparatively high galactic latitude $b = -40°$, where galactic absorption is only about 0·1 mag. In attempting identification with radio sources it will usually be necessary to work at lower galactic latitudes where absorption is greater. Hence it does not seem likely that we have set the optical magnitudes too faint in Table II.

The situation concerning the possibility of making optical identifications stands out clearly in the table. A satisfactory identification demands a highly accurate radio position, say ±0·5′ in both coordinates, and so far it has not been found possible to obtain such positions except for particularly bright sources. And the remarkable point emerges from Table II that the bright radio sources are just the ones that contain the highest proportion of classes IV, V and VI, all of which are distant objects associated with faint optical magnitudes.

A thoroughgoing attempt to secure optical identifications has recently been made by Bolton and Minkowski, who have considered about 100 bright sources with flux levels above about $\log P \cong 1{\cdot}5$ (160 Mc/s). The attempted identifications with galaxies brighter than +19·5 were successful in about 45 per cent of cases, which is about the percentage indicated by Table II, if the contribution F of class I is omitted. Table II suggests that some 35 per cent will be likely to fall between +17 and +19·5, as compared with the 30 per cent actually identified. The contribution F might have been expected also to yield some 30 per cent, whereas about 15 per cent were found at optical magnitudes bright enough to be associated with the nearby class I objects.

The values of Table II do not hold out much hope that many further optical identifications will be forthcoming, unless either it proves possible to work to magnitude +20 (or even +21 if spectrum red-shift effects become important) or accurate radio positions become available down to $\log P \cong 1$.

It is our impression that the following argument has surrounded the whole question of optical identifications. Taking the bright radio sources, roughly half of them cannot be identified with galaxies brighter than +19. Accordingly it seems fairly certain that these radio sources are distant objects. Then how much more distant must the faint radio sources be? Our table shows that the last step of this argument may well be quite erroneous. The effect of the red-shift (not in the spectrum now, but on the apparent bolometric magnitude) can produce a situation in which classes IV, V, VI dominate the count at high, and even medium, values of P, but in which the intrinsically faint classes I and II entirely

dominate the count at low flux values. This effect has already been noted by Mills (4).

It is of interest to consider the relation of our luminosity function to the recent work of Allen, Palmer and Rowson, on the surface temperatures of radio sources*. For the purpose of relating our results to the observations, we note that the L value for class VI is close to that of Cygnus A. Write T_{Cyg} for the measured surface temperature of Cygnus A Then if all radio sources possess the same physical size we expect the temperatures of our six classes to be given by

$$(\mathrm{I, II, III, IV, V, VI}) \cong (3.10^{-3}, 10^{-2}, 3.10^{-2}, 10^{-1}, 3.10^{-1}, 1) T_{\mathrm{Cyg}}. \quad (27)$$

Some uncertainty is attached to the appropriate value of T_{Cyg}. In the general surface temperature experiments, in which Cygnus A was treated in the same way as other sources, a value $T_{\mathrm{Cyg}} \cong 8 \times 10^8$ °K was found. Special information from the fuller analysis of Jennison *et al.* suggests a lower value of $T_{\mathrm{Cyg}} \cong 3 \times 10^8$ °K, however. A satisfactory compromise appears to be to accept the lower value of T_{Cyg}, but to continue to ignore the effect of the red-shift on the surface temperature, as we have already done in (27). The red-shift lowers the surface temperature by $(1+z)^{-4}$. If we restrict ourselves to sources that make the important contributions to Table II, the values of z are never greater than 0·3 to 0·4, so that the $(1+z)^{-4}$ factor is not larger than the measure of uncertainty in T_{Cyg}. For the Jodrell Bank experiments, $\log P$ is on the average near 1·2, and at this value of P the red-shift correction is small for sources of classes I, II and III, although it amounts to a factor $\sim 3^{-1}$ for class V.

We set the surface temperatures in relation to Cygnus A as follows

$$T_{\mathrm{I}} \cong 10^6,\ T_{\mathrm{II}} \cong 3 \times 10^6,\ T_{\mathrm{III}} \cong 10^7,\ T_{\mathrm{IV}} \cong 3 \times 10^7,\ T_{\mathrm{V}} \cong 10^8,\ T_{\mathrm{VI}} \cong 3 \times 10^8. \quad (28)$$

If the sources are not of the same physical size, if the intrinsically weaker sources are smaller in their dimensions, then the values of T for the lower classes have been set too low. Turning to the percentages given in Table II for $\log P = 1{\cdot}25$, we see that the most frequent source is of class III with surface temperature $\sim 10^7$ °K and that classes II and IV with temperatures $\sim 3 \times 10^6$ and 3×10^7 are symmetrically distributed about $\sim 10^7$ °K. This result is in close accord with the work of Allen, Palmer and Rowson, as also is the 20 per cent of sources at temperatures of order 10^8 °K.

These considerations, both of the optical identifications and of the surface temperatures of radio sources, show that we have been realistic in the absolute values of L that have been associated with the various classes, and hence that our taking 10^{-26} w.m^{-2} (c/s)$^{-1}$ as the unit of P is not an improper choice.

As we have already mentioned, the mixing of the various luminosity classes results in a reduced slope for the $\log NP^{3/2} - \log P$ curve. The values given in the first part of Table II are plotted in Fig. 5. The slope of the $\log N - \log P$ curve is now no greater than $-1{\cdot}6$ in the important range of P, although there is a steepening to $-1{\cdot}7$ at $\log P \cong 1{\cdot}5$. The effect of the fluctuation at $\log P > 1{\cdot}5$ has not been shown in Fig. 5. This would lift the curve in the region $1{\cdot}5 \leqslant \log P \leqslant 2$, probably yielding a sub-Euclidean slope in this range, exactly as in the case of curve II of Fig. 4.

* We are indebted to the Jodrell Bank workers for valuable discussions on their observations.

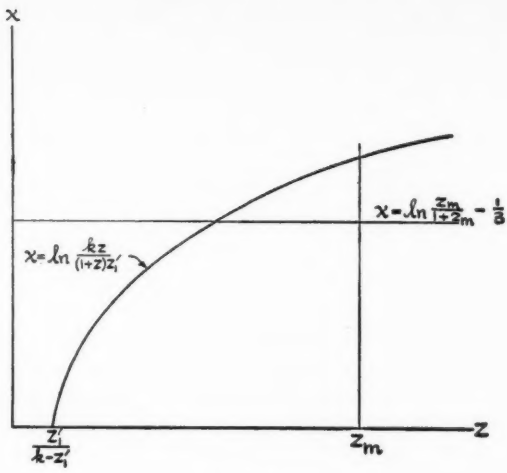

FIG. 5

The present results are of course related to our choice, $K(q) \propto q^4$, for the dependence of the probability function on age over the relevant generations (5th to 9th or 10th). A steeper rise of K would lead to a steeper $\log N - \log P$ curve. For this reason no particular significance we feel can be attached to an amount of the order of 0·1 or 0·2 in the slope. At the outset we noticed that whereas the latest Cambridge results yielded $-1{\cdot}8$, Mills has given reasons for believing that the slope should not exceed $-1{\cdot}5$. In these circumstances our value of $-1{\cdot}6$ does not seem unsatisfactory.

Although we have lost steepness in the slope for $0{\cdot}4 < \log P < 1$ we have gained in the behaviour of the $\log NP^{3/2} - \log P$ curve for $\log P < 0{\cdot}0$. This section is now very close to the ultimate slope suggested by Ryle to be the most probable interpretation of an analysis by Hewish (of deflections rather than source counts) using the method of Scheuer.

9. *The count from individual lattice units.*—We return to a consideration of the luminosity class II alone. The specification of a red-shift z defines a distance $cH^{-1}z$. Within this distance, if z is sufficiently large, there will be a particular generation n for which the volume of a unit cube, l_n^3, is comparable with $4\pi/3(cH^{-1}z)^3$. Observation to red-shift z is expected to include the eight lattice members (or part of them) belonging to such a unit cube. The question arises as to how many sources are to be associated with each of these eight members and how does this number vary with z, and hence with P. An answer to this question can be given to within an uncertainty of a factor of about 2. The uncertainty arises from connecting ideas that relate to the discrete model with values given by the continuous theory. To remove the uncertainty it would be necessary to work entirely in terms of an explicit discrete model. (Such a project is feasible if automatic computing were used. If the present theory turns out to survive any further immediate attacks we shall consider it worth while to abandon altogether the simple methods of the continuous theory and to go over entirely to a discrete situation.)

Referring back to (23), the number of sources counted to red-shift z_m is given by integrating the function

$$\frac{z^2}{(1+z)^3} K(\chi) \exp(-3\chi) \tag{29}$$

over the appropriate portion of the (χ, z) plane shown in Fig. 5. It will be recalled that χH^{-1} is the age of a source at the moment of emission or radiation, viz. $\chi = \tau H - \ln(1+z)$ where τ is the present age. The relevant area of the (χ, z) plane is that lying below the curve

$$\chi = \ln \frac{kz}{z_1'(1+z)}, \tag{30}$$

and enclosed by the z-axis, and by $z = z_m$.

It is easy to estimate what fraction of the total count to red-shift z_m is contributed by the "last generation", this being defined as the last range of $\frac{1}{3}$ in the interval of χ. The fraction is obtained by integrating the same function (29) over the portion of the (χ, z) plane enclosed by $\chi = \ln(z_m/1+z_m) - \frac{1}{3}$, by $z = z_m$, and by the curve (30). The fractional contribution is thus the ratio of the two integrals of (29) over the areas shown in Fig. 5. Introducing $q = \exp\chi$ again, we require the ratio of the following integrals

$$\int_{\exp\frac{1}{3}\cdot\frac{z}{1+z} = \frac{z_m}{1+z_m}}^{z_m} \frac{z^2\,dz}{(1+z)^3} \int_{-\frac{1}{3}+\frac{kz}{z_1'(1+z)}}^{\frac{kz}{z_1'(1+z)}} \frac{K(q)}{q^4}\,dq, \tag{31}$$

$$\int_{\frac{z}{1+z} = \frac{z_1'}{k}}^{z_m} \frac{z^2 dz}{(1+z)^3} \int_0^{\frac{kz}{z_1'(1+z)}} \frac{K(q)}{q^4}\,dq. \tag{32}$$

Computations for $0{\cdot}2 < z < 0{\cdot}4$ for $K(q) \propto q^4$ and for $k/z_1' = 15$, give ratios close to 2/9.

We turn now to the actual numbers N given in Table I. We have seen that if these numbers are interpreted per steradian they are in reasonable relation to the actual counts. Thus $\sim 4\pi N(z)$ is the order of the total count on the whole sky to red-shift z. We now see that $\sim 2/9$ of this must be attributed to the "last generation", viz. $\sim 3N(z)$.

The next step brings in the uncertainty of connection to the discrete model. We associate the "last generation", as defined above for the continuous picture, with the situation in the discrete model in which the observer sees the eight lattice units of generation n. Then each lattice unit of the "last generation", contributes a total of $\sim \frac{3}{8}N(z)$ sources. In view of the uncertainty of association we can simply say that the lattice units making the maximum contribution to the count to red-shift z contain of the order of $N(z)$ sources, where the functional dependence of N on z is given in Table I. (The present discussion essentially determines the order of the absolute value of the probability function K.)

Reference to Table II shows that we have made important use of class II sources down to about $\log P = -0{\cdot}5$. Table I shows that such a value of P corresponds to $z \cong 0{\cdot}6$, and at this red-shift $N(z) \cong 2500$ sources. It follows that the maximum population of the oldest lattice units (those of the $\sim$ 10th generation) is some 2500 sources of class II. The maximum populations required for the

other luminosity classes are easily estimated from Table II. For example, the relative proportions of classes I and II at $\log P = -0{\cdot}5$ is about 3/1. Our considerations down to this flux level therefore require the presence of some 7500 sources of class I. Results for the various classes are as follows:

Maximum number of sources required per lattice unit

Class I	7500
Class II	2500
Class III	250
Class IV	25
Class V	10
Class VI	< 1

Since the number of galaxies per lattice unit is $\sim 10^5$ it is clear that the maximum populations in the oldest lattice units only become at all comparable with the number of galaxies for the cases of classes I and II. Only these cases require further consideration.

Class II sources are comparable to the source Hydra A, for which Burbidge (**13**) has calculated a minimum total energy requirement of $\sim 10^{58}$ ergs. At an emission rate of 4×10^{42} erg sec^{-1} (the value arrived at in Section 6), such an energy reservoir would last for about $2{\cdot}5 \times 10^{15}$ sec. We require the main radio source activity throughout a lattice unit to last for an interval of time of the order of $\frac{1}{3}H^{-1}$. Thus if each of the $\sim 10^5$ galaxies were to become a radio source on one occasion during the relevant generation the number of sources existing at any particular moment would be of order $2{\cdot}5 \times 10^{15}/(\frac{1}{3}H^{-1}) \times 10^5$. H^{-1} must be expressed in seconds, viz. $H^{-1} \cong 3 \times 10^{17}$ sec. The number is thus very close to 2500.

A similar calculation for class I sources yields an equally satisfactory answer. Since the emission rate for class I is lower by a factor ~ 3 the time for which a given energy reservoir can maintain the radiation rate is increased by 3, and the number of sources existing at any moment of time is expressed by the same factor.

It is of course the case that we do not literally require every galaxy to become a radio source. It would be equally sufficient if a sub-class of galaxies became radio sources on an appropriate number of occasions, say 10 per cent of galaxies ten times more frequently. Energy requirements do not forbid such a situation. Thus the gravitational energy of a galaxy of mass M and radius r is of order GM^2/r; and for $M = 3 \times 10^{11} \odot$, $r = 15$ kpc, this is $\sim 5 \times 10^{59}$ erg. Hence an energy reservoir $\sim 10^{58}$ erg could be provided on a number of occasions.

It is entirely possible that the classes III–VI are simply cases where galaxies of abnormally large mass are involved. With M increased by ~ 10, gravitational energies are increased by $\sim 10^2$, which is of the order of difference between II and VI. The lower proportions required for the very strong radio sources could be simply a consequence of the small fraction of galaxies that possess masses of order $3 \times 10^{12} \odot$.

10. *The distribution of sources on the sky.*—The discrete model not only introduces fluctuations in the number counts, of the sort discussed in Section 7, but it also introduces fluctuations from strict isotropy in the distribution of sources on the sky. The discrete lattice units introduce patchiness. We have now to examine whether this patchy characteristic is consistent with the observations or not.

We note that MSH have drawn attention to a possible departure from isotropy, and that more recently Mills, Slee and Hill (**14**) report that between declinations $-20°$ and $-50°$ they find a marked deficiency of sources in R.A. 00^h to R.A. 02^h. (We have taken Mills' sources and have divided them into 12 groups. Each group covers 2^h in R.A. and the whole range of declination. We find only a negligible probability that the grouping is random. A test applied to the postulate that the source density varies in the ratio 4/3 from one area of sky of order 10^3 square degrees to another yielded a reasonable result.)

We proceed now to the theoretical discussion, and we do this, first, for a single luminosity class. When a limiting flux P is given, the generations of our model can be ordered in the following way. There will be a particular generation, $n(P)$ say, of which the observer will expect to see one complete unit cube with its associated 8 lattice units. For the $n(P)+s$ generation ($s=1, 0, -1, -2, \ldots$) the observer will expect to see $\sim 8\exp(-s)$ lattice units. The series of values of s must be taken only for $s \leqslant 1$, since for $s \geqslant 2$ the formula derived from the continuous theory ceases to have any relevance.

In the simple cubic model the 8 lattice units for $s=0$ present the smallest total solid angle to an observer at equal distances from each of them. With l as the lattice spacing, the observer's distance from the vertices is $(\sqrt{3}/2)l$. Since the radii of the units (in our model) is $\frac{1}{3}l$, the solid angle presented by each unit is 0·485 ster. The 8 units together therefore cover a fraction 0·31 of the whole sky.

For the generation $s=-1$, each lattice unit is smaller by $e^{-1/3}$. Thus a lattice unit of generation $s=-1$ at the same distance l subtends a solid angle smaller by $\sim e^{-2/3}$. There are, however, e times more units from generation $s=-1$ than from generation $s=0$. Generation $s=-1$ therefore subtends a total solid angle that is greater by at least $e^{1/3}$. (Not all the units of $s=-1$ are as far away as l, although the majority of them are at distances of this order.) Hence generation $s=-1$ covers at least a fraction $0{\cdot}31e^{1/3}=0{\cdot}43$ of the whole sky. In a similar way, one can easily see that generation $s=-2$ covers at least a fraction $0{\cdot}31e^{2/3}=0{\cdot}60$ of the whole sky.

The situation is somewhat more complicated for generation $s=1$. A lattice unit of this generation, if completely within range of observation, must subtend so large a solid angle that a simple inverse square law cannot be used. The most distant sources of the 8 lattice units of $s=0$, for an observer at the centre of a unit cube, demand observation not merely to $\sqrt{3}l/2$ but to $l(1/3+\sqrt{3}/2)$. If the sources of an $s=1$ lattice all lie within this distance, then the centre of the lattice unit cannot be further away from the observer than

$$l\left(\frac{1}{3}+\frac{\sqrt{3}}{2}\right)-\frac{1}{3}e^{1/3}$$

the radius of the unit being $\frac{1}{3}l\exp(\frac{1}{3})$. Hence the minimum solid angle subtended by such a unit must be 1·43 ster, *if the unit is to be completely observed.* Three such units would therefore cover at least a fraction 0·342 of the whole sky.

It is of course the case that the formula $8\exp(-s)$, derived from the continuous theory, does not require the value ~ 3, given by $s=1$, to be made up of three complete lattice units of generation $s=1$. The three could be made up by partial contributions from more than three lattice units. Indeed a system of partial contributions is certainly much more probable. Such a system would have a smaller departure from isotropy, since there would be more than three

patches on the sky, and each patch would contribute fewer sources. We shall keep, however, to the worst case in which the observer sees three complete lattice units of generation $s=1$. Summarizing we have:

Generation s	Number of lattice units	Solid angle subtended by each lattice unit (ster.)	Minimum fraction of the sky covered
1	3	1·43	0·34
0	8	0·48	0·31
−1	22	0·25	0·43
−2	60	0·13	0·60

It is useful to consider departures from isotropy by dividing these four generations into two pairs $s=-1, -2$; $s=1, 0$. The first of these pairs has so many lattice units that it is essentially free from ambiguities; and the sum of the fractions of the sky covered adds almost exactly to unity, which is a convenient simplification. Since successive generations are expected to be anticorrelated we consider the patches of $s=-1$ to interlace those of $s=-2$.

Write X for the total number of sources contributed by $s=-1, -2, -3, \ldots$. The work of the previous section suggested that $\sim 2/9\ X$ are contributed by $s=-1$, about $\frac{2}{9}.\frac{7}{9}$ by $s=-2$, etc. So many lattice units are contained in $s=-3, -4$, that we regard their contribution as being isotropic. That is to say, $49X/81$ sources are distributed isotropically. It is easily seen that the average source density per unit area for a patch from $s=-1$ to that for a patch from $s=-2$ is

$$\left[0{\cdot}604+\frac{2}{9}(0{\cdot}43)^{-1}\right]\Big/\left[0{\cdot}604+\frac{14}{81}(0{\cdot}57)^{-1}\right]\cong\frac{5}{4}, \qquad (33)$$

where, for simplicity, we have slightly reduced the fraction of the sky covered by the $s=-2$ patches from 0·60 to 0·57.

To test the effect of such a patchiness we took 27 squares arranged in three rows of 9. The squares were of two categories A and B. Equal probabilities were attached to each individual square being of type A or of type B. Decisions were made using random number tables: it turned out that 11 squares were assigned to type A and 16 to type B. The next step was to divide each such square into 100 sub-squares. A probability $\frac{4}{3}p$ was attached to there being a source in each sub-square belonging to type A, and p was attached to there being a source in each sub-square belonging to B. The value of p was chosen so that a total number of sources closely equal to the $3C$ catalogue was obtained, and the probabilities were again controlled by random number tables. As a final detail, when a source happened to fall in a sub-square, its position in that sub-square was also randomized. The result is shown in the second section of Fig. 6, the first part being a plot of the $3C$ sources.

Since the ratio 4/3 used in this test represented a greater measure of anisotropy than was estimated above in (33), it seems unlikely that the anisotropy arising from generations $s=-1, -2$ can bring us into a conflict with observation. It is of course true that statistical effects would be weakened if the total count X were increased—the "signal" carried by the probability ratio would stand out more in relation to the statistical "noise" as X increased, the signal-to-noise ratio improving essentially as $X^{1/2}$. According to the recent Cambridge results,

about 8000 sources would be counted on the whole sky in a survey down to $P \cong 2 \times 10^{-26}$ w.m^{-2}(c/s)$^{-1}$. Of these, about 4000 would belong to the pair $s = 0, 1$ which has still to be considered. The appropriate value of X for the pair $s = -1, -2$ would thus be about 4000 in such a survey, as compared with about 1000 used in Fig. 6. Hence an improvement in "signal-to-noise ratio" by ~ 2 would be expected in such a survey, *if all sources belonged to a single luminosity class.* The mixing of sources of different luminosity classes reduces the signal-to-noise ratio, however, first by reducing the value of X appropriate for each class, and second by increasing the "noise". The "noise" is increased because the different luminosity classes give different values of $n(P)$. The distribution of patches is accordingly different for the different classes (the flux level P being specified).

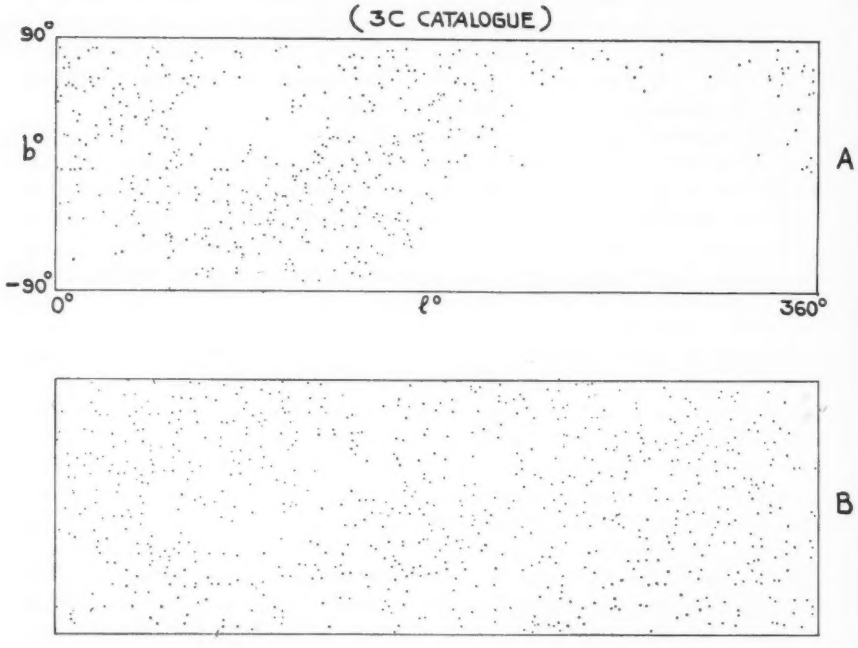

FIG. 6

We turn to the pair $s = 1, 0$. Write Y for the total number of sources from the whole series $s = 1, 0, -1, \ldots$. Then about 2/9 Y come from $s = 1$, about 14/81 Y from $s = 0$, and 49/81 Y from $s = 1, -2, \ldots$ (i.e. $X \cong 0{\cdot}6\ Y$). Roughly half of the sources therefore arise in the pair $s = 1, 0$.

Since the number of patches from both $s = 1$ and $s = 0$ together is only of order 10, it is very reasonable to regard the positions on the sky of the patches as being anticorrelated to those of the $s = 0$ patches. If the two generations together are regarded *as covering the whole sky* then no crucial issue arises. The two generations cover approximately equal fractions of the sky, while they contribute numbers of sources in the ratio 9/7.

This ratio may somewhat underestimate the anisotropy, since a corresponding calculation using the discrete model gives a rather greater anisotropy. The above ratio 9/7 is derived from the value 2/9 Y for $s=1$, 14/81 Y for $s=0$, obtained in Section 9 from the continuous picture. Instead, we can argue, perhaps more simply, that each lattice unit of $s=1$ contributes $e^{4/3}$ times more sources than each lattice unit of $s=0$. With three of the former and eight of the latter, the ratio is $3e^{4/3}/8=1{\cdot}43/1$. But even with a ratio as great as 3/2 the fluctuation of source area density would merge with the smaller anisotropy of the generations $s=-1, -2$. A combination of the pairs $s=-1, -2$; $s=1, 0$ could hardly yield a patch ratio significantly worse than 4/3 even if the two pairs were not anticorrelated.

The serious question is whether the generations $s=1, 0$ really do cover the sky, and it appears to turn very largely on this issue as to whether a detectable anisotropy can be expected to arise or not. According to the above estimates, generations $s=1, 0$ cover 2/3 of the sky, but this estimate was very definitely a minimum value. The following argument is of interest in showing how far the fraction 0·31 for $s=0$ is a minimum.

It will be recalled that the value 0·31 was obtained for an observer at equal distances from all eight lattice units of generation $s=0$. A change of the observer to other positions increases the total solid angle subtended by these units. A calculation based upon a cubic lattice, of the effect of placing the observer in other positions, would attach too great an importance to the precise structure of the cubic lattice however. As stated in Section 4, one must take care not to use the cubic lattice model in such a way as to obtain results that are peculiar to this particular lattice, since in actuality the lattice may be expected to have no particular regularity. We therefore consider the following argument from which all lattice regularity is removed.

Write ν for the number of condensation centres per unit volume in generation $s=0$. To obtain eight such centres we require a sphere of radius a where

$$\frac{4\pi a^3\nu}{3} \cong 8.$$

Suppose a lattice unit at distance a subtends a solid angle Ω_a, and approximate by taking the solid angle at distance r $(<a)$ as $\Omega_a(a/r)^2$—once again this can only underestimate the solid angle. Then, on the average, the total solid angle subtended by the eight lattice units inside the sphere of radius a is

$$4\pi\nu\Omega_a a^2\int_0^a dr = 4\pi a^3\nu\Omega_a \cong 2 \times \Omega_a$$

which is three times the value given by placing the whole eight units at equal distances a from the observer.

This argument must not be given too great weight, however, since it considers no correlation at all in the positioning of the centres of the lattice units, but it does show how far varying the observer's position, and varying the regularity of the lattice structure, could increase the total solid angle. To lift our 0·31 of Table IX to ~0·5 we need a much smaller increase than the factor 3 given by this argument.

Turning now to $s=1$, we need to increase the 0·34 of Table IX also to $\sim 0{\cdot}5$. This could be achieved in two ways: by viewing more than three lattice units in a partial way—the advantages of this from the point of view of diminishing the anisotropy have already been mentioned—or by slightly decreasing the distance of the observer from the centres of each lattice unit. The estimate 0·34 was based on a maximum distance consistent with complete visibility of all the sources of the three lattice units of $s=1$. The solid angle is very sensitive to the precise distance of the observer, a slight decrease of distance producing a large increase of solid angle. To increase the fraction of the sky covered by the three lattice units from 0·34 to $\sim 0{\cdot}5$ it is only necessary to decrease the distance of the observer from their centres by some 20 per cent.

We may sum up the above discussion as follows: dividing the generations contributing to the counts in the manner described, the generations $s=-3, -4, \ldots$ are sensibly isotropic. It is unlikely that any anisotropy in the pair $s=-1, -2$ can readily be detected. And if the pair $s=0, 1$ fill the whole sky, it is also unlikely that anisotropy in $s=0, 1$ can be at all easily detected. If, however, there is a failure to fill the sky, a fluctuation of the source density over large areas of the sky might well be expected. The relevant areas are of order 1 steradian. In this connection it is of interest that the fluctuation reported by Mills is over an area of this order. It is possible that Mills' result arises from some systematic error, but if so the error would illustrate the experimental difficulty of giving a decisive answer to whether such large-scale fluctuations exist or not.

APPENDIX

It might appear at first sight that results of the previous section can be reproduced by introducing an age–luminosity function $L(\tau)$ instead of the age–probability function $K(\tau)$. As mentioned earlier, the two cases are not equivalent. While $K(\tau)$ affects the integrand in (19) the function $L(\tau)$ affects the limits. It is proposed to give an example where we take $K(\tau)=$ const. and introduce $L(\tau)$. We will consider the $\log N - \log P$ curve on the hypothesis that $L(\tau) \propto \exp(3H\tau)$ on analogy with the form chosen for $K(\tau)$.

The count to power level P is given by

$$N(P) = \int\int \frac{z^2}{(1+z)^3} \exp(-3H\chi)\, d\chi\, dz \tag{34}$$

where the area of integration is specified in Fig. 7 by the shaded region. The upper curve α is given by

$$\chi = \ln \frac{kz}{(1+z)z_1}, \tag{35}$$

and the lower one β by

$$\chi = \tfrac{1}{3} \ln [Pz^2(1+z)^2], \tag{36}$$

where χ is measured in units of H^{-1}.

Let (z_2, χ_2), (z_3, χ_3) denote the intersections of α and β; $z_2 > z_3$. If P is large enough, $\chi_3 < 0$, and we have to integrate from z_3 to z_2. If P is small, so that $\chi_3 > 0$, we have to integrate from $z_1/k - z_1$ to z_4, and from z_4 to z_2, where z_4 is the point where the curve β intersects OZ, as shown in Fig. 7. In the absence of a power–age correlation, the curve β would simply be a straight line parallel to the χ-axis.

It is best to express N, P as functions of the parameter z_2 and to obtain their values for different values of z_2. From the figure it can be seen that P has a maximum value P_0, when the curves α, β touch one another. This happens when $z_2 = z_3 = 0{\cdot}25$. For $P > P_0$, $N = 0$. Here again we encounter the effect of discreteness on the $N-P$ curve.

The double integral can be evaluated for various values of z_2. Some values are given in the following table, with $z_1'/k = 1/15$ as before.

z_2	z_3	z_4	N	P	$NP^{3/2}$
0·25	0·25	—	0	·081	0
0·5	0·11	—	0·26	·0658	4·38
1·0	—	·086	2·618	·03125	14·46
1·5	—	·123	6·526	·0154	12·47
2·0	—	·163	15·203	·0082	11·29

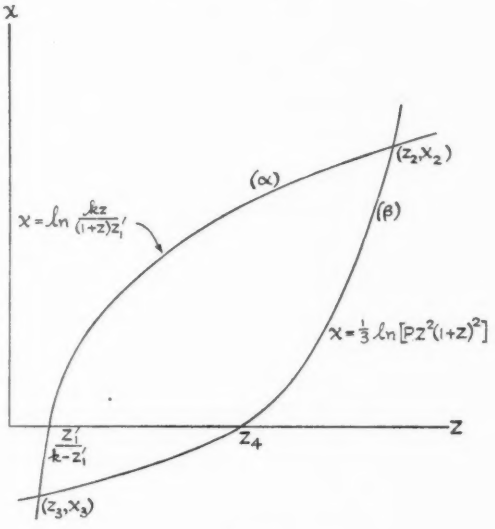

FIG. 7

Here also $NP^{3/2}$ increases initially as P decreases. But the increase is very rapid and is maintained only over a small range in P (a range ~ 2), while the decrease is gradual. It therefore does not reproduce the observed results. An exponential $L \propto \exp(4H\tau)$ would give similar behaviour, the case $L \propto \exp(3H\tau)$ was adopted because of the resulting simplicity of the integrals involved.

Thus though the amount of radiation contributed by a cluster of age τ is the same when $L(\tau) = f(\tau)$, $K(\tau) = \text{const.}$ as when $K(\tau) = f(\tau)$, $L(\tau) = \text{const.}$ the two cases are not equivalent as far as the $N-P$ curve is concerned.

This discussion, however, does not rule out the possibility of a combination of a power–age correlation with an age-dependent probability.

St John's College, Cambridge:
1961 *June.*

Fitzwilliam House, Cambridge:

References

(1) J. R. Shakeshaft, M. Ryle, J. E. Baldwin, B. Elsmore, and J. H. Thomson, *Mem. R.A.S.* **67,** 97, 1955; D. O. Edge, J. R. Shakeshaft, W. B. McAdam, J. E. Baldwin, and S. Archer, *Mem. R.A.S.*, **68,** 37, 1959; P. F. Scott, M. Ryle, and A. Hewish, *M.N.*, **122,** 95, 1961.
(2) B. Y. Mills, O. B. Slee, and E. R. Hill, *Aust. J. Phys.*, **11,** 360, 1958.
(3) K. I. Kellermann and D. E. Harris, *Observations of the California Institute of Technology Radio Observatory*, 1960.
(4) B. Y. Mills, *Aust. J. Phys.*, **13,** 550, 1960.
(5) F. Hoyle, 11th Solvay Conference, p. 53.
(6) F. Hoyle, *I.A.U. Symposium on Radio Astronomy, Paris* 1958, (Stanford), p. 529.
(7) M. Harwit, *M.N.*, **122,** 47, 1961.
(8) E. Lifshitz, *Journ. of Phys. U.S.S.R.*, **10,** 116, 1946.
(9) T. Gold and F. Hoyle, *I.A.U. Symposium, Paris* 1958, p. 583.
(10) C. D. Shane and C. A. Wirtanen, *A.J.*, **59,** 285, 1954; C. D. Shane, *A.J.*, **61,** 292, 1956.
(11) G. O. Abell, *Ap. J. Supp.*, **3,** 211, 1958.
(12) J. Crampin and F. Hoyle, *M.N.*, **122,** 27, 1961.
(13) G. Burbidge, *I.A.U. Symposium, Paris* 1958, p. 541.
(14) B. Y. Mills, O. B. Slee, and E. R. Hill, *Austr. J. Phys.*, **13,** 676, 1960.
(15) M. Ryle and R. W. Clark, *M.N.*, **122,** 349, 1961.
(16) M. Ryle, *Observatory*, **75,** 137, 1955.

EXTRAPOLATION OF THE NUMBER-FLUX DENSITY RELATION OF RADIO STARS BY SCHEUER'S STATISTICAL METHOD

A. Hewish

(Received 1961 June 14)

Summary

An attempt is made to assess the usefulness of Scheuer's statistical method of analysing the records derived from a phase-switching receiver. A Monte Carlo technique is described which enables the probability distribution of the recorded deflections to be computed rapidly in EDSAC for any assumed distribution of radio sources. Some typical models are considered and it is concluded that, subject to a small enough receiver noise, the statistical method gives information about the source distribution at flux densities considerably lower than those at which the sources may be counted individually. The method is applied to some observations at 178 Mc/s using the method of aperture synthesis. It is shown that the log N − log S relation cannot have a uniform slope of $-1{\cdot}5$. A slope of $-1{\cdot}8$ yields good agreement provided that the source density is suitably truncated at small flux densities.

1. *Introduction*

Records obtained during a survey of radio stars may be analysed in two different ways. The usual method is to extract the positions and flux densities of individual sources; in this case the limiting flux density reached in the survey is determined either by the sensitivity of the receiver or by confusion errors arising from the presence of more than one source in the reception pattern simultaneously. To reduce confusion errors to an acceptable level, several authors have suggested that it is necessary to limit the number of sources extracted to about one source in 20 beam areas.

A different analysis of the data may also be carried out in which no attempt is made to isolate individual sources, but which gives statistical information concerning their number and flux density. In this method the record is sampled at equal intervals of time without regard to the occurrence of particular sources. For the case of an interferometer the deflection D at a given instant is defined as the modulus of the quasi-periodic record, while for a total power system it is simply the total deflection as shown in Fig. 1. When a sufficient number of samples has been obtained, the result may be presented as the distribution function $P(D)$ where $P(D)\,dD$ is the probability of a deflection lying in the range D to $D+dD$. The shape of $P(D)$ depends, of course, on whether an interferometer or a total power system is used and in this paper only interferometric systems are considered.

The quantity D has the dimensions of flux density S, and the physical meaning of $P(D)$ is clarified by considering the ideal case of an aerial which receives with uniform sensitivity over a prescribed beam area. In this case, for sufficiently large values of D corresponding to sources of high flux density which are clearly resolved, we have $P(D)\equiv P(S)$ where $P(S)$ is the chance that a source of flux density S to $S+dS$ lies within one beam area; for smaller values of D this equivalence no longer holds, since there is then a finite chance of several sources lying in the beam area at once, and $P(D)\to 0$ as $D\to 0$ while $P(S)$ may increase without limit. When the reception pattern has an arbitrary

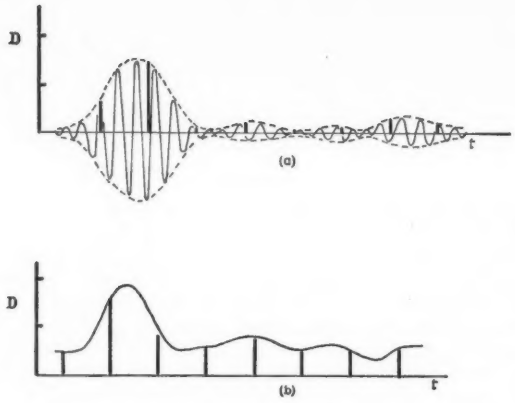

FIG. 1.—*Values of D derived by sampling the output of (a) a phase-switching receiver and (b) a total power receiver.*

profile $P(D)$ and $P(S)$ are similarly related but a constant of proportionality is involved.

The precise relation between $P(D)$ and $P(S)$ has been fully discussed by Scheuer (1957). He showed that it was not possible to derive $P(S)$ uniquely from $P(D)$: what may be done, however, is to assume some relation for $P(S)$ which enables $P(D)$ to be calculated theoretically and then compared with the observed curve. If the experimental $P(D)$ curve agrees with the theoretical one, then the assumed $P(S)$ is consistent with the data. A population of radio sources is usually defined by $N(S)$ where $N(S)$ is the total number of sources per steradian having flux densities greater than S; but

$$N(S) \propto \int_S^\infty P(S)\, dS$$

so that assumed models of $N(S)$ may be directly related to $P(S)$. By this process it is possible, in principle, to extrapolate the observed $N(S)$ relation towards low flux densities where the sources can no longer be counted with accuracy owing to confusion errors. The utility of the statistical method in any practical application will, however, depend on the sensitivity of $P(D)$ to variations in the assumed values of $N(S)$.

In this paper an attempt is made to assess the usefulness of the statistical method. Analytical methods which allow $P(D)$ to be computed when $N(S)$ is given have been described by Scheuer (1957). The computations are laborious, however, and do not lend themselves readily to rapid comparison of different $N(S)$ models. A method has therefore been adopted in which $P(D)$ is computed by a Monte Carlo technique using the electronic computer EDSAC II. The basis of the method is to consider a typical beam area and to populate it, with appropriate statistical fluctuations, according to some assumed $N(S)$ model. The different contributions to the total deflection are then combined with random phase and the computation is repeated until $P(D)$ may be determined with sufficiently small statistical uncertainty. Using pseudo-random numbers generated in the computer it is possible to derive

$P(D)$ for a given model in a matter of minutes. The computational method is given in Section 2, and in Section 3 the general utility of the statistical method is discussed in the practical case where receiver noise must be taken into account.

Finally, in Section 4, the method is applied to results obtained at 178 Mc/s in a survey using the principle of aperture synthesis. The radio observations have been fully described in another paper (Scott, Ryle and Hewish 1961) where it was explained how the observed $P(D)$ relation was automatically derived from the computer as part of the routine synthesis programme. A summary of the available data concerning the observed $N(S)$ relation obtained during this and other surveys has also been given (Scott and Ryle 1961) and it has been shown that effects due to the angular diameter and clustering of sources can only be relevant to a small fraction of the total number (Leslie 1961). In the present paper the statistical method is used to extrapolate the observed $N(S)$ relation to smaller flux densities. It is shown that the shape of the observed $P(D)$ relation cannot be explained by any $N(S)$ model such that $N(S) \propto S^{-1.5}$ for all values of S. Models with $N(S) \propto S^{-1.8}$ are in good agreement with the observations, provided that the source density is appropriately truncated at small flux densities.

2. *Computation of P(D) by a Monte Carlo method*

For a phase-switching interferometer the value of D at any given sampling instant is the resultant of a large number of contributions of different amplitude and phase arising from the sources lying within the beam area at that moment. The essence of the Monte Carlo method is to consider a typical beam area, to populate it randomly with sources whose mean distribution is defined by some $N(S)$ model and to sum the different contributions with random phase. The computation is repeated for a large number of hypothetical beam areas, the population being varied randomly from sample to sample, until the theoretical $P(D)$ may be derived with a reasonable statistical certainty. About 3000 samples were usually taken which gave statistical errors comparable to those of the observations. The computation will now be discussed in detail.

(i) *The correction for the experimental reception pattern.*—The basic computation was carried out for an assumed ideal reception pattern having uniform sensitivity over the entire beam area. With a realistic reception pattern a source of given flux density may give rise to a variety of deflections according to its position in the beam. This effect could have been introduced into the computation without difficulty by means of another parameter subject to random variations, but it involved less computing time to adopt an alternative procedure in which the $N(S)$ model was suitably modified as a preliminary step. Since the sources lying within each interval of flux density S to $S+dS$ will give deflections of different magnitudes appropriate to a random sampling of the reception pattern, the result obtained when using a graduated reception pattern is exactly simulated by smoothing the $N(S)$ model. The smoothing process is an exact convolution if the reception pattern is formulated as the probability of obtaining a given deflection when a constant source is randomly positioned within it. The essential randomness is then introduced in calculating the random population of the beam area as discussed below. When calculating in this way it is assumed that both the phase and amplitude of the quasi-periodic record may be considered as independent random variables. This assumption

is justified if, as in the present case, the interference pattern contains many cycles.

The equivalent areas of the experimental 178 Mc/s reception pattern, considered constant over small intervals of relative sensitivity, are shown in Fig. 2; these values were derived from the published reception pattern (Scott, Ryle and Hewish 1961) and include the effect of side lobes. The logarithmic intervals adopted are the same as those employed in the main computation discussed below.

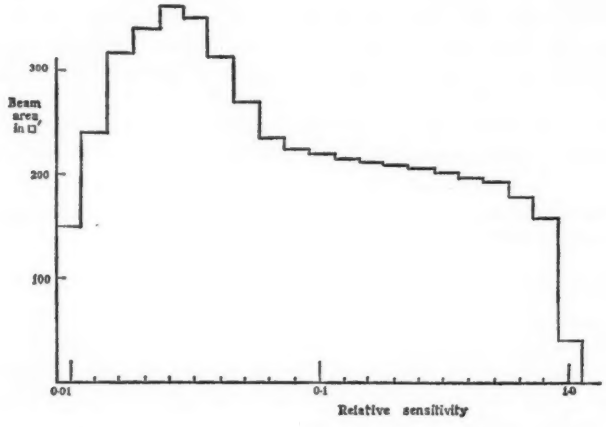

FIG. 2.—*The experimental 178 Mc/s reception pattern expressed as increments of beam area for equal logarithmic intervals of relative sensitivity.*

The result of convolving $N(S)$ with the probability distribution of the reception pattern may be denoted by $N(D)$ where $N(D)$ is the total number of deflections $> D$ which combine to give the net deflection appropriate to each beam area. It should be noticed that whereas $N(S)$ is expressed as the number of sources per steradian, $N(D)$ is the number of deflections per beam area. When $N(S)$ obeys a simple power law, e.g. $N(S) \propto S^{-1.5}$, $N(S)$ and $N(D)$ are related by a simple scale factor; but when $N(S)$ is terminated, or suffers a change of slope, the corresponding change in $N(D)$ will be smoothed by the convolution process. An example of this is shown in Fig. 3 where $N(D)$ is given for an abruptly terminated $N(S)$ model.

(ii) *Populating the sample beam area.*—For simplicity the full range of D was partitioned into discrete intervals ΔD such that $\log_{10} \Delta D/D = 1/10$. Within a given partition the ΔN deflections were all assumed to have the same magnitude. The first stage of the main computation was to populate the partitions randomly according to an average distribution defined by some particular model $N(D)$. This process is equivalent to constructing a typical beam area containing a random distribution of sources of different flux density. The manner in which the required population was computed depended upon the value of ΔN and four different methods were employed.

(*a*) $\Delta N \ll 1$. This case corresponds to the small chance of obtaining a large deflection in one beam area. Here it was sufficient to generate a random number

in the range 0–1000 and to add a deflection if the random number fell inside a given range of $1000 \times \Delta N$ integers. Different selections of integers were chosen to represent the different partitions and one trial was allowed for each partition. This method will lead to errors, however, if there is a finite chance of obtaining more than one deflection in a given partition during a run of, say, 3000 sample beam areas, that is, when $3000\,\Delta N^2 \sim 1$ or $\Delta N \sim 1{\cdot}8 \times 10^{-2}$.

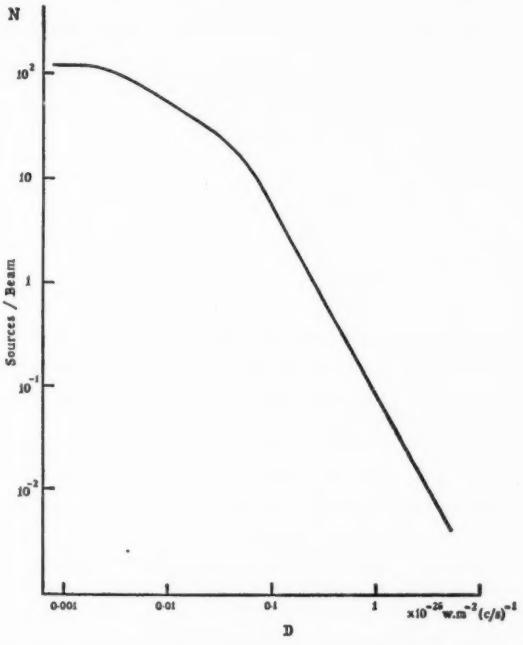

FIG. 3.—*N(D) derived by convolving the N(S) model (c) depicted in Fig. 5 (b) with the reception pattern as expressed in Fig. 2.*

(*b*) $10^{-2} < \Delta N < 5$. To achieve the correct population when a given partition may contain zero, or more than one deflection, a range of partitions was considered such that $\overline{\Sigma \Delta N} \sim 10$. In a true random population ΔN will vary, from sample to sample, by an amount δN such that $\overline{\delta N^2} \sim \overline{\Sigma \Delta N}$ where δN is approximately normally distributed. For each sample beam area a deviation δN was generated by taking a random number and using it to choose one term in a table of random deviates. This determined the value $\Sigma \Delta N' = \overline{\Sigma \Delta N} + \delta N$ for the sample and a further $\Sigma \Delta N'$ random numbers were then generated and used to distribute the $\Sigma \Delta N'$ deflections amongst the different partitions with a probability proportional to ΔN.

(*c*) $5 < \Delta N < 50$. For small enough values of D there is a negligible chance of obtaining zero deflections within any partition. In this case it was sufficient to compute a series of values $\Delta N' = \Delta N \pm \delta N$ in order to specify the random

population. One random number was therefore generated for each partition and used to assign a random deviation as in case (*b*).

(*d*) $\Delta N > 50$. When the number of deflections in any partition is sufficiently large, corresponding to many weak sources in the beam area simultaneously, there is no longer any necessity to compute the random walk summation by Monte Carlo methods. The contribution from any one partition will be a vector of random phase whose amplitude is governed, from sample to sample, by the well-known Rayleigh distribution function. For many of the $N(D)$ models a simple power law was adopted in the region of small D and in this case the contribution due to the Rayleigh component was easily calculated. If $N(D) = AD^n$, where A is constant, the mean square deflection $d(\overline{D^2})$ due to components in the range D to $D+dD$ is given by

$$d(\overline{D^2}) = nAD^{n+1}\, dD$$

so that

$$\overline{D^2} = \int_{D_0}^{\infty} nAD^{n+1}\, dD$$

giving

$$D_{\mathrm{RMS}} = \left(-\frac{nN_0}{n+2}\right)^{1/2} D_0.$$

To compute the precise value of the deflection in each sample beam area a random number was generated and used to assign a deviation drawn at random from a table of deviations appropriate to a Rayleigh distribution having a standard deviation given by $D_{\mathrm{RMS}}/\sqrt{2}$.

For some of the models N tended to a constant value for small values of D and D_{RMS} had to be derived by numerical integration.

(iii) *The random walk summation.*—Having populated a sample beam area it remains to add the component deflections with random phase. For each component a random phase angle was generated by choosing a unit vector from a table of vectors tabulated at 3° intervals in the range 0–2π, the choice being determined by a random number. Throughout the computation random numbers were generated as required by the multiplicative process $M_{n+1} = M \,.\, M_n$ (modulo 2^{39}) with $M = 5^{13}$ and $M_0 = 1$. Pseudo-random series of this nature are non-repetitive within a period of 2^{37} (Moshman 1954) and an initial test was carried out to check the randomness in a run of the required length. As an additional safeguard an arrangement was made whereby the calculation was halted if $M_n = M$; no such event occurred.

The resultant of the random walk summation for each sample beam area was accumulated as a histogram, together with the total population of each partition.

(iv) *Receiver noise.*—In any practical determination of $P(D)$, deflections arising from noise in the receiving system will be present in addition to those due to signals from the aerials. In the method of aperture synthesis the output of the receiver is recorded on punched tape, and the final integration, normally performed by the output filter of a receiver, is carried out by a convolution process in the computer itself. The equivalent filter is arranged to have a narrow frequency response centred on the mean frequency of the quasi-periodic signal and this ensures that noise fluctuations alone will produce a quasi-periodic output whose modulus is specified by a Rayleigh distribution. The deflection

due to receiver noise has a character which is thus exactly equivalent to case (ii(d)) and it may be treated in precisely the same manner. Putting $D_{\mathrm{RMS}}=(D^2+D_N{}^2)^{1/2}$, where $D_N{}^2$ is the mean square deflection due to noise alone, makes allowance for both quantities simultaneously.

(v) *The validity of the Monte Carlo method.*—Because a number of approximations have been used in the computation it is desirable to test the validity of the method by using it to reproduce well-known results before proceeding to unknown cases. Two such tests were applied. In the first a model was taken such that $N(D)\propto D^{-1\cdot5}$ and the random population was assigned as described above. In the random walk summation, however, the individual deflections in all the partitions were given equal magnitudes. In this case $P(D)$ is the well-known Rayleigh distribution and it is seen from Fig. 4 (a) that the Monte Carlo result is in very good agreement.

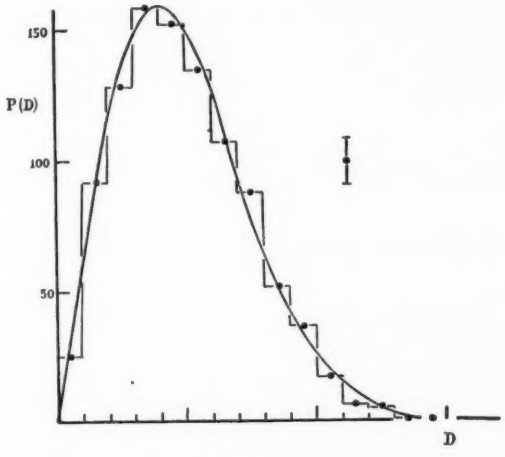

FIG. 4 (a).—*The continuous curve shows a Rayleigh distribution. The histogram indicates the same result obtained by the Monte Carlo method.*

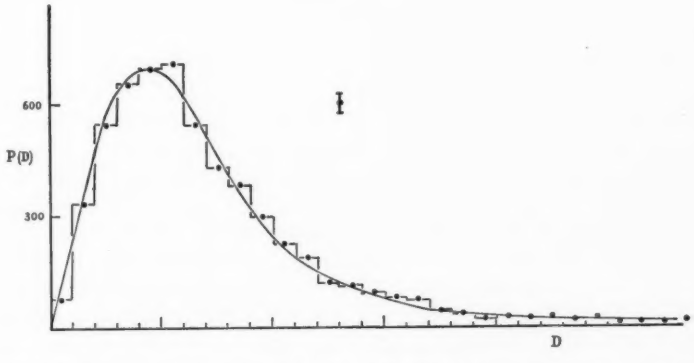

FIG. 4 (b).—*$P(D)$ derived analytically by Scheuer for $N(S)\propto S^{-1\cdot5}$ (continuous curve) compared with the histogram given by the Monte Carlo method.*

As a second test the same model was taken and the computation carried out in the normal way. For this model, corresponding to a uniform spatial distribution of radio sources, $P(D)$ has been computed analytically by Scheuer (1957) and both results are shown in Fig. 4 (*b*); the agreement is again seen to be close. It should be noted that " curve fitting " plays no part in the Monte Carlo method. A given model of $N(S)$, and hence of $N(D)$, defines the scale of D absolutely.

3. *The value of the statistical method*

To estimate the usefulness of the statistical method it is necessary to investigate the sensitivity of $P(D)$ to changes in $N(D)$. Only when such changes are greater than the statistical uncertainty inherent in a practical determination of $P(D)$ can the method be usefully applied. Initially it is assumed that the receiver is ideal, so that noise components do not contribute to $P(D)$. Two types of model have been considered, as shown in Figs. 5 (*a*) and 5 (*b*), such that $N(S) \propto S^{-1.5}$ and $N(S) \propto S^{-1.8}$; the latter model is more relevant to the actual distribution of

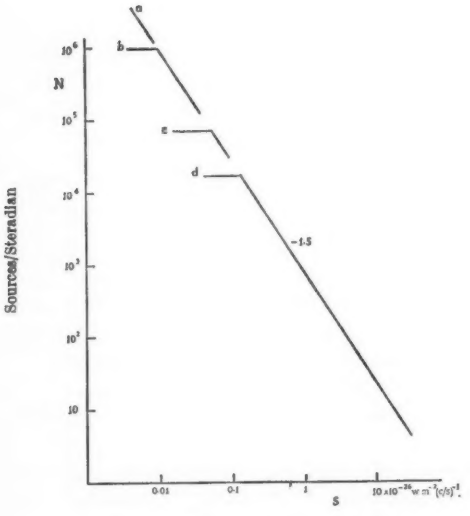

FIG. 5 (*a*).—*Models in which* $N(S) \propto S^{-1.5}$.

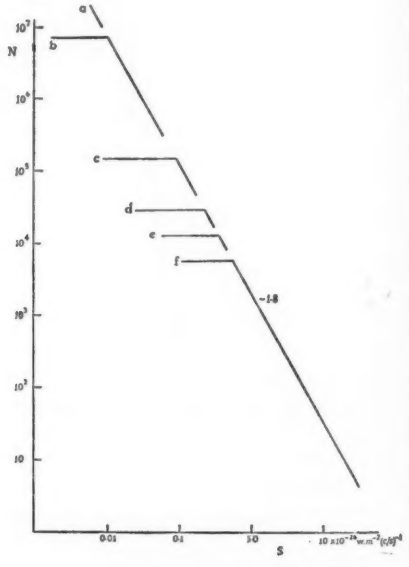

FIG. 5 (*b*).—*Models in which* $N(S) \propto S^{-1.8}$.

sources. In both cases the effect of arbitrarily terminating $N(S)$ at various values of S was investigated. $P(D)$ corresponding to the different cases is plotted in Figs. 6 (*a*) and 6 (*b*); for slope $-1{\cdot}5$ a significant change in $P(D)$ can be detected when $N(S)$ is terminated at $S = 0{\cdot}01$, corresponding to the level at which there are 50 sources per beam area. For slope $-1{\cdot}8$ there is a more pronounced change in $P(D)$ when $N(S)$ is terminated at $S = 0{\cdot}01$, where there are 250 sources per beam area.

It is therefore clear that, in the absence of receiver noise, the statistical method gives information about $N(S)$ at flux densities considerably lower

than those at which the sources may be counted individually. To investigate the effect of receiver noise the model shown in Fig. 5 (*b*) was taken and $P(D)$ computed for two different RMS noise levels. The results are shown in Figs. 7 (*a*) and 7 (*b*). While $P(D)$ is modified, as would be expected for sufficiently large noise levels, it is seen that the sensitivity of $P(D)$ to changes in $N(S)$ is not appreciably diminished provided that the maximum of $P(D)$,

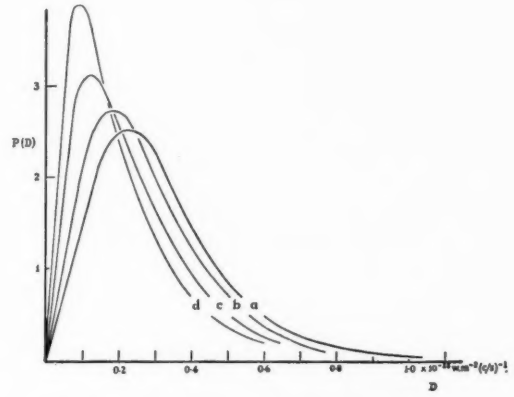

FIG. 6 (*a*).—*P(D) derived from the N(S) models illustrated in Fig.* 5 (*a*).

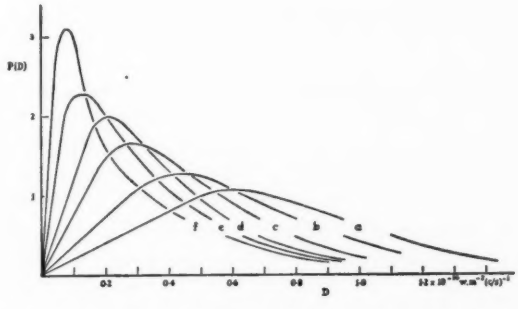

FIG. 6 (*b*).—*P(D) derived from the N(S) models illustrated in Fig.* 5 (*b*).

in the absence of receiver noise, occurs at a flux density somewhat higher than the RMS noise level. This result is to be expected in view of the Rayleigh-like character of $P(D)$. When the noise level is high enough to cause a significant displacement of the maximum of $P(D)$, but not so high that the shape of $P(D)$ is dominated by it, the receiver noise must necessarily be accurately known if the statistical method is to be applied without loss of precision.

The discussion of the preceding sections has been confined to interferometric systems. For a total power recording the situation is similar but the maximum of $P(D)$ is then located at a flux density near the mean d.c. level of the receiver output. While it is simple to compute $P(D)$ for a given $N(S)$ model by the

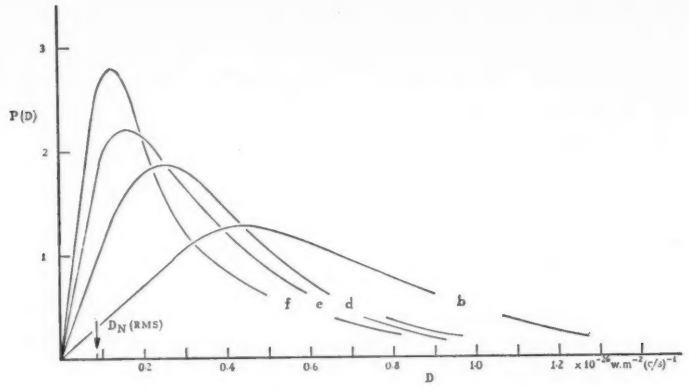

FIG. 7 (*a*).—*P*(*D*) *derived from the N*(*S*) *models shown in Fig.* 5 (*b*) *with an assumed RMS receiver noise* D_N *of* $0{\cdot}085 \times 10^{-26}$ *w.m*$^{-2}$ (*c*/*s*)$^{-1}$.

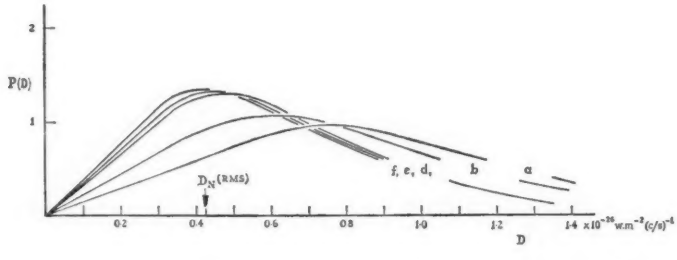

FIG. 7 (*b*).—*The corresponding P*(*D*) *curves with a receiver noise of* $0{\cdot}42 \times 10^{-26}$ *w.m*$^{-2}$ (*c*/*s*)$^{-1}$.

method described in Section 2, except that the contributions to D are added directly and not with random phases, it is difficult in practice to define a flux density corresponding to the mean receiver output. The comparison of theoretical and observational $P(D)$ relations must then rely on the shape of the curves and the position of the maximum cannot be used as a criterion of agreement.

4. *Application of the method to observations at* 178 *Mc*/*s*

As described in detail in another paper (Scott, Ryle and Hewish 1961) the reduction of the observations made at 178 Mc/s using the method of aperture synthesis included the automatic computation of $P(D)$. In Fig. 8 is shown the experimental curve derived from a survey of 0·3 steradians ($\alpha = 20^h\,40^m - 19^h\,15^m$, $\delta = 40° - 44°$); the RMS noise level was determined in a separate experiment and found to be $0{\cdot}085 \times 10^{-26}$ w.m^{-2} (c/s)$^{-1}$. Counts of individual sources derived from this survey, and from "whole sky" surveys using different arrangements of the 178 Mc/s interferometer, gave the relation $N(S) \propto S^{-1{\cdot}8}$ for sources having flux densities greater than 2×10^{-26} w.m^{-2} (c/s)$^{-1}$ (Ryle and Clarke 1961).

In attempts to account for the observed $P(D)$ curve in terms of appropriate models, attention was concentrated in the region of the maximum of $P(D)$, and models were sought which fitted this portion of the curve most closely.

For larger values of D the statistical uncertainty is relatively greater since $P(D)$ is small; moreover, we have

$$\int P(D)\, dD \propto N(S)$$

(cf. Section 1) for large D so that no information is gained by studying $P(D)$ in this region, where $N(S)$ is already known from the observed source counts.

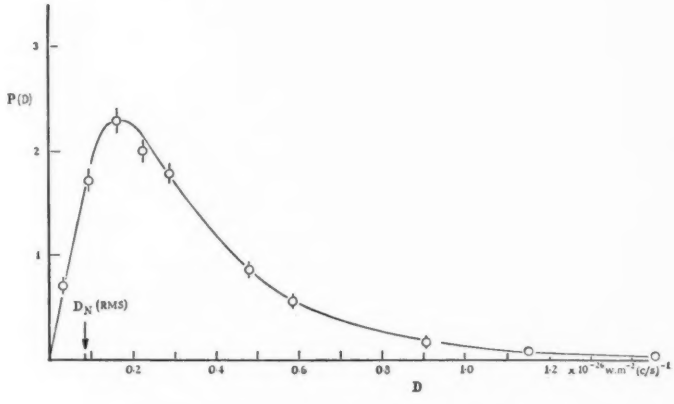

FIG. 8.—*P(D) derived from observations at 178 Mc/s.*

As a first attempt to account for the observations, models were taken such that $N(S) \propto S^{-1.5}$. The three models are illustrated in Fig. 9 (*a*) and the corresponding $P(D)$ curves are given in Fig. 9 (*b*). It is immediately clear that none of the models is satisfactory. From the trend of the curves it can be seen that the maxima are either too high (model (*c*)) or occur at too large a flux density (models (*b*) and (*a*)). Even without evidence provided by individual source counts it may be concluded that no model having $N(S) \propto S^{-1.5}$ can give a satisfactory explanation of the observed $N(S)$ relation.

In a second attempt to find a suitable model the observed $N(S)$ relation was extrapolated at constant slope ($-1{\cdot}8$) and successively truncated at a series of flux densities. These models were discussed in a different context in the previous section and are shown in Fig. 5 (*b*). The corresponding $P(D)$ curves are shown in Fig. 7 (*a*) and it was found that model (*e*) fitted the observed $P(D)$ within the statistical error. For this model the truncation occurs at a flux density of $0{\cdot}35 \times 10^{-26}$ w.m^{-2} (c/s)$^{-1}$ corresponding to the level at which one source occurs, on the average, in two beam areas.

It was also possible to account for the observations by extrapolating from a flux density near the limit of the observed number counts with a slope of $-1{\cdot}5$ and truncating at a flux density of $0{\cdot}18 \times 10^{-26}$ w.m^{-2} (c/s)$^{-1}$. Models of this type and the corresponding $P(D)$ curves are indicated in Figs. 10 (*a*) and 10 (*b*).

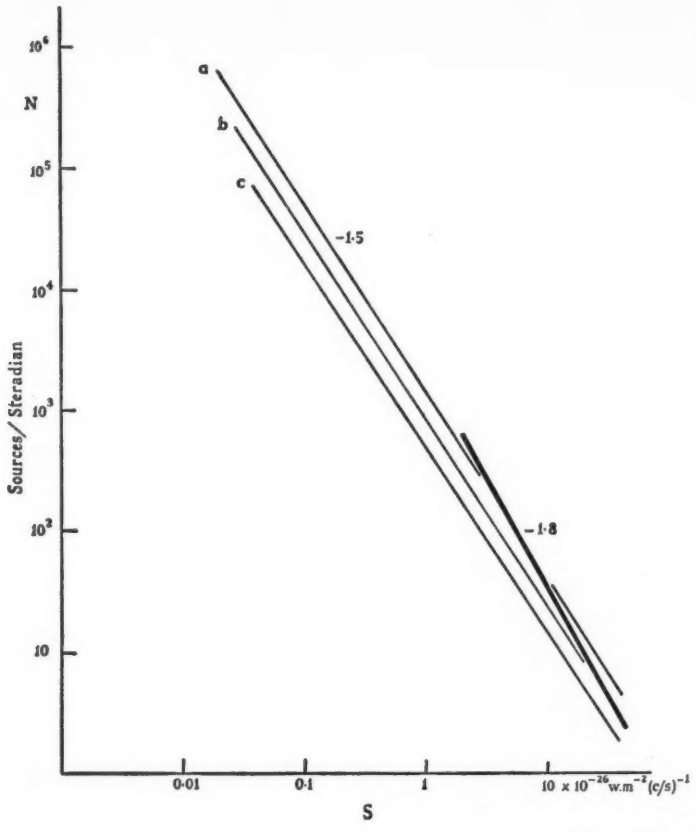

FIG. 9 (*a*).—*Three models such that* $N(S) \propto S^{-1.5}$ *used in an attempt to explain the observed* $P(D)$. $N(S)$ *obtained directly from source counts at* 178 *Mc/s is denoted by the thick line.*

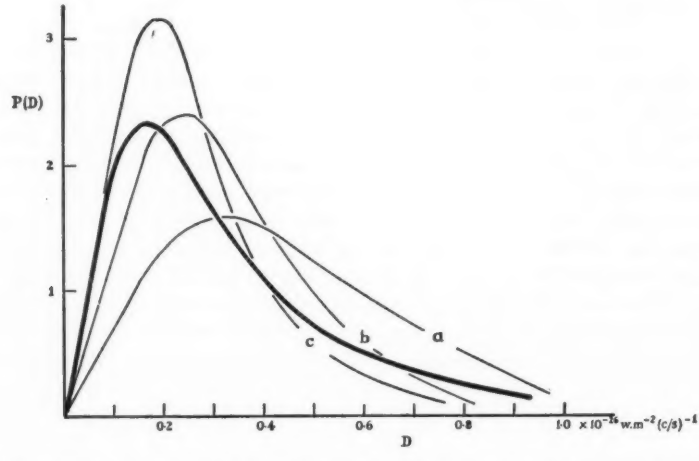

FIG. 9 (*b*).—$P(D)$ *computed from the models shown in Fig.* 9 (*a*). *The observed* $P(D)$ *is also shown (thick line).*

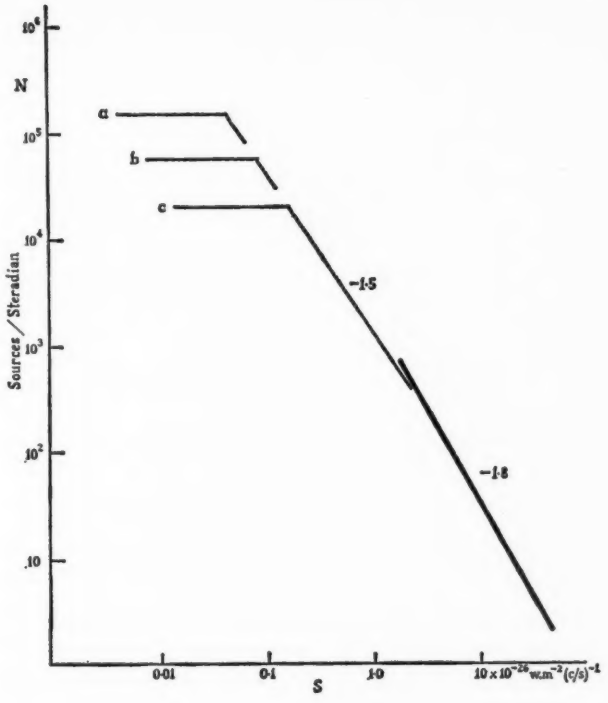

FIG. 10 (*a*).—*N*(*S*) *models in which the observed source counts are extrapolated with a slope of* −1·5.

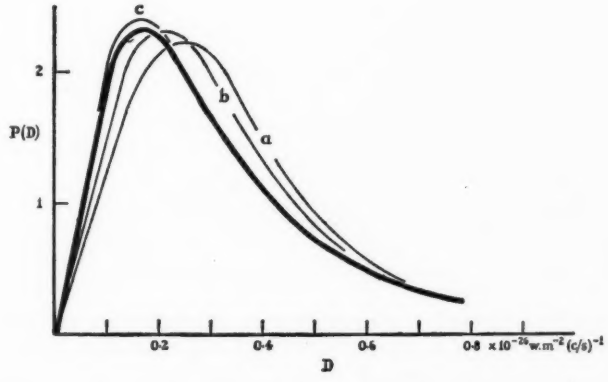

FIG. 10 (*b*).—*P*(*D*) *computed for the models shown in Fig.* 10 (*a*). *The observed P*(*D*) *is shown* (*thick line*).

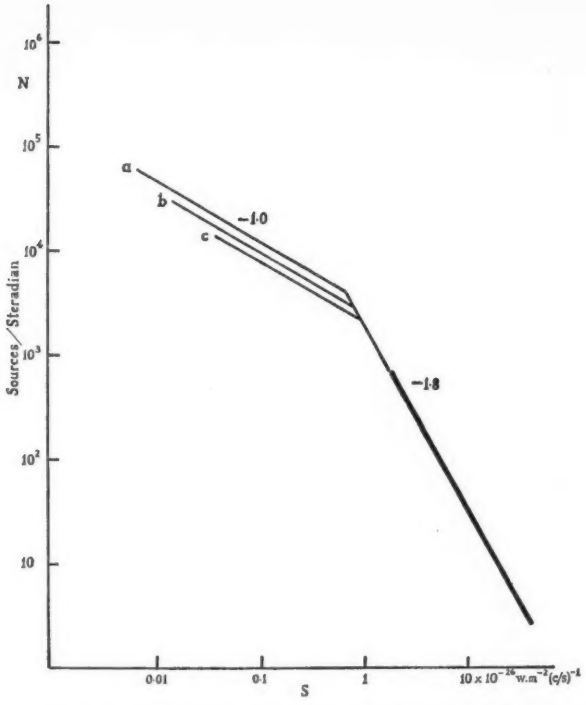

FIG. 11 (*a*).—*Models in which the observed source counts are extrapolated with a slope of* −1·0.

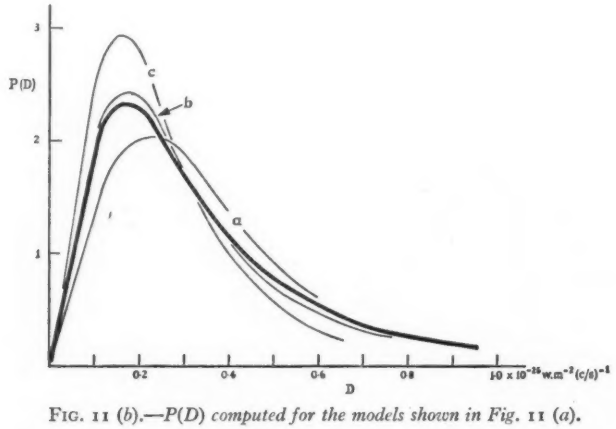

FIG. 11 (*b*).—*P*(*D*) *computed for the models shown in Fig.* 11 (*a*).

Since a sudden truncation corresponds to an unrealistic physical situation another series of models was taken in which the $N(S)$ relation was extrapolated to zero flux density with a slope of −1·0. This series is shown in Figs. 11 (*a*) and 11 (*b*) and it was again possible to derive a curve in reasonable agreement with the observations.

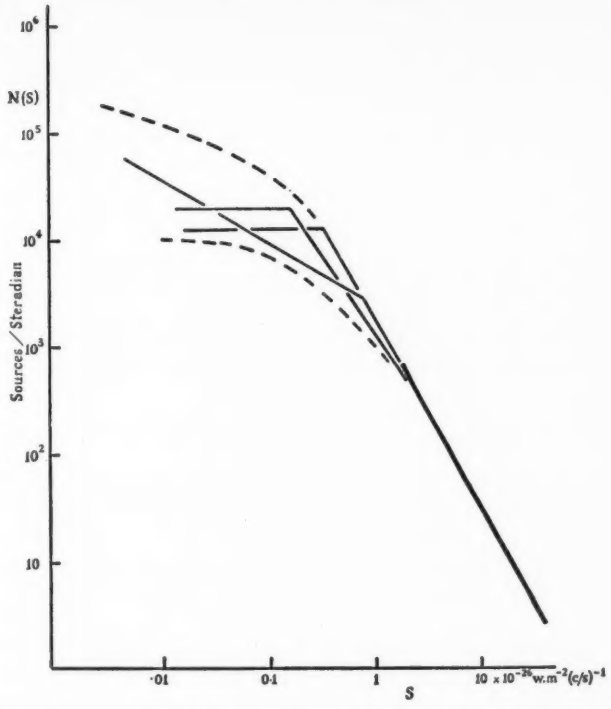

FIG. 12.—*Extrapolations of the observed source counts which are consistent with the observed P(D) relation.*

The three models which fitted the observations most closely are shown together in Fig. 12 and it appears that any satisfactory model must lie within the boundaries indicated. It is interesting to notice that the number of sources begins to depart appreciably from the expectations of a linear extrapolation of the observed source count at a flux density in the range 0·1 to $1{\cdot}0 \times 10^{-26}$ w.m^{-2} (c/s)$^{-1}$. In view of the strong evidence favouring an extragalactic origin of the radio sources (Ryle and Clarke 1961) this decrease is presumably a cosmological effect. The discontinuities in the curves will, of course, be smoothed by any spread in absolute luminosity. The magnitude of this effect may be estimated with reference to the smoothing action of the reception pattern already discussed in Section 2(i). Fig. 3 indicates the rounding-off which would occur for a sudden cut-off in the source distribution if the spread in absolute luminosity were of the order of 100 : 1.

Mullard Radio Astronomy Observatory,
Cavendish Laboratory,
Cambridge:
1961 *May.*

References

Leslie, P. R. R., 1961, *M.N.*, **122**, 51.
Moshman, J., 1954, *J. Assoc. Comp. Mach.*, **1**, 88.
Ryle, M., and Clarke, R. W., 1961, *M.N.*, **122**, 349.
Scott, P. F., and Ryle, M., 1961, *M.N.*, **122**, 389.
Scheuer, P. A. G., 1957, *Proc. Camb. Phil. Soc.*, **53**, 764.
Scott, P. F., Ryle, M., and Hewish, A., 1961, *M.N.*, **122**, 95.

THREE SOUTHERN SPECTROSCOPIC BINARIES

William Buscombe and Pamela M. Morris

(Received 1961 June 19)

Summary

Radial velocities from 51 spectra, obtained in 1955–60, are presented for three single-lined binaries, HD 184035, 114911 (η Mus) and 217792 (π PsA). HD 184035 is a newly discovered binary. For the other stars early observations at the Lick Chile Station and at the Cape have been included in the determination of the orbital elements, which for all three stars are listed in Table VI.

Introduction.—A programme is under way at Mt Stromlo to determine the radial velocities of certain bright stars in the fundamental catalogue N30 (**1**), for which reliable values were not available. In addition to the intrinsic interest in solving the orbits of binary stars, there is the hope that ephemerides of their velocity variation may be useful for standardizing measures from future objective-prism surveys.

Most of the observations on this programme were made with the 3-prism spectrograph at the Cassegrain focus of the 30-inch reflector. For a few of the spectrograms we are especially indebted to other observers, who have observed the stars at our request during particular phases, as indicated in Tables III and V below. A few plates were also taken with the 2-prism spectrograph at the Newtonian focus of the 74-inch reflector. For convenience, details of the various instruments from which observations have been included in this discussion are listed in Table I. The three stars are named in Table II, of which the final column indicates the spectrographs from which observations are available.

TABLE I

Instruments

Observatory	Telescope	Spectrograph dispersion at Hγ	
Royal Cape, South Africa	24-inch refractor	4-prism	19 A/mm
Lick, Santiago, Chile	36-inch Cassegrain	2-prism	20
		1-prism	37
Mt Stromlo, Australia	30-inch Cassegrain	3-prism	36
	74-inch Newtonian	2-prism	90

TABLE II

The binary stars

HD	Star	Mag.	Spectrum	R.A. (1950)	Dec.	Obs.
114911	η Mus	4·79	B8 V	$13^h11^m.8$	$-67°37'$	L1, St2, St3
184035	201G Sgr	5·90	A3 III	19 30 ·7	−40 09	St2, St3
217792	π PsA	5·13	Fo IV	23 00 ·7	−35 01	C4, L2, St3

In an earlier communication to the Society (**2**), the authors have reported on the progress of the general programme, with special reference to experience in measuring the spectra of standard-velocity stars and in the selection of wavelengths for the absorption lines. Further details are now in the press, including some results of the extension of this work to the Newtonian spectrograph.

Since the number of observations of each star is not large, or uniformly distributed through the different phases, the method outlined by Irwin (**3**) was followed. After the period is found, points on the assumed velocity curve are read at certain fractions of the amplitude K. Using these values in various combinations, auxiliary diagrams are drawn to determine the most probable values of e and ω by the use of Irwin's tables. Under the circumstances, the computation of adjustments to the preliminary orbital parameters seems unwarranted.

HD 114911.—From the very approximate value of its radial velocity as determined at the former Lick Southern Station (**4**), some authors have considered HD 114911 as a possible member of the Scorpio-Centaurus Association. However, the luminosity class indicates that it is a foreground object. The extrema in velocity observed in 1924 and in 1960 establish the orbital period, but the number of measures secured may be regarded as the fewest possible for computing a reliable orbit.

TABLE III

Observations of HD 114911

JD	Phase	V_0	O–C	Notes
243....		km/sec		
6979·221	0·412	− 3·5	+3·3	Underexposed
6982·228	·562	+30·7	−0·3	Newtonian spectrogram
7002·179	·560	+30·3	+0·4	Overexposed
7064·995	·700	+44·8	−0·2	
7076·992	·299	−44·0	−4·4	
7082·936	·597	+28·6	−7·7	Weak comparison
7098·903	·395	−17·1	−5·2	
7108·934	·896	+ 0·2	−4·7	Observer: A. Przybylski
7111·929	·046	−53·7	+1·7	Observer: H. Gollnow
7111·937	·046	−45·8	+9·8	Underexposed
7130·871	0·993	−39·5	−2·7	

The velocities measured at Mt Stromlo are listed in Table III, with the values of the residuals from the spectrographic orbit. The computed velocity curve is shown in Fig. 1. The parameters derived are shown in Table VI. The absorption lines are rather broad, and Huang (**5**) has estimated the rotational velocity component in the line of sight as 240 km/sec.

HD 184035.—The spectrum of HD 184035 shows unusually sharp lines for an A-type star, from which the velocity measures are remarkably consistent. As exposures of more than one hour became necessary with the Cassegrain spectrograph on the photographic emulsion 103aO available in 1960, the last three observations were obtained with the 74-inch reflector and the Newtonian spectrograph.

Since few cycles of the velocity variation have been observed, the period cannot be determined with high accuracy. However, Fig. 2 shows that the observations listed in Table IV are well represented by the velocity curve computed from the orbital parameters given in Table VI.

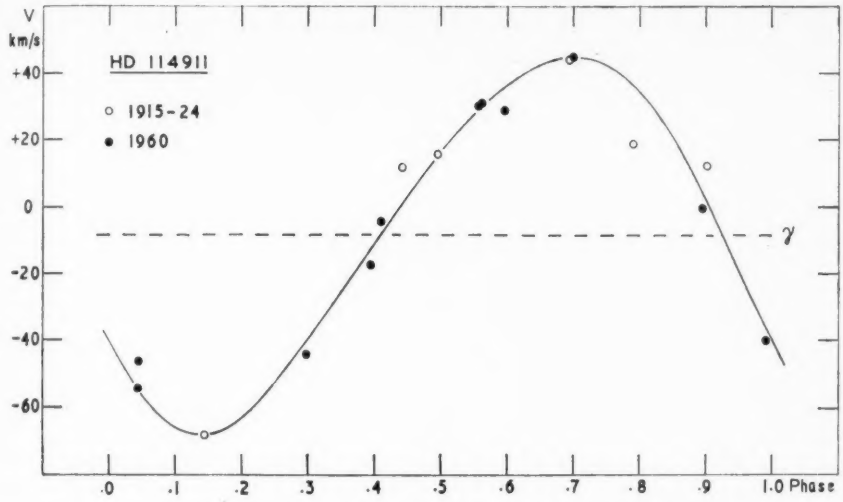

FIG. 1.—*The radial velocity curve of η Mus. Open circles represent Lick observations, filled circles Mt Stromlo.*

TABLE IV

Observations of HD 184035

JD 243....	Phase	V_0 km/sec	O–C	Notes
6739·165	0·942	+56·5	+15·1	
6778·065	·353	+21·1	+ 5·5	
7065·284	·454	−22·4	− 1·4	
7077·245	·040	+72·3	− 8·6	
7099·197	·787	−30·8	+ 1·2	
7115·147	·235	+57·0	− 6·0	
7122·138	·747	−44·7	− 0·9	
7172·988	·742	−43·0	+ 2·1	
7174·964	·169	+86·1	+ 4·0	Underexposed
7177·947	·810	−24·2	− 0·7	
7182·940	·893	+14·7	− 1·3	
7210·915	·942	+43·6	+ 2·2	
7216·899	·236	+68·0	+ 5·1	
7237·917	·780	−31·8	+ 2·4	Newtonian spectrogram
7242·905	·859	− 3·6	− 2·1	Newtonian spectrogram
7245·892	0·505	−36·2	− 0·2	Newtonian spectrogram

HD 217792.—Before we made our observations it was informally suggested to the authors that this star might be a cepheid. In view of the long period, the low luminosity and the shape of the velocity curve, this seems most unlikely. It is noteworthy that several of the earlier measures, especially from the Cape Observatory (**6**), deviate systematically from the adopted curve for our recent observations. If a secular change in the orbital elements has occurred, larger values of both e and ω would satisfy the early data somewhat better than the

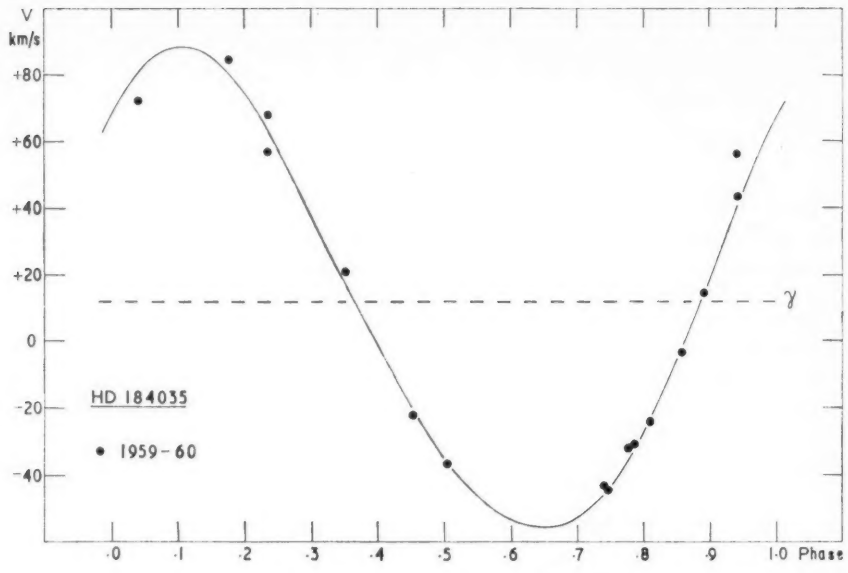

FIG. 2.—*The radial velocity curve of HD 184035.*

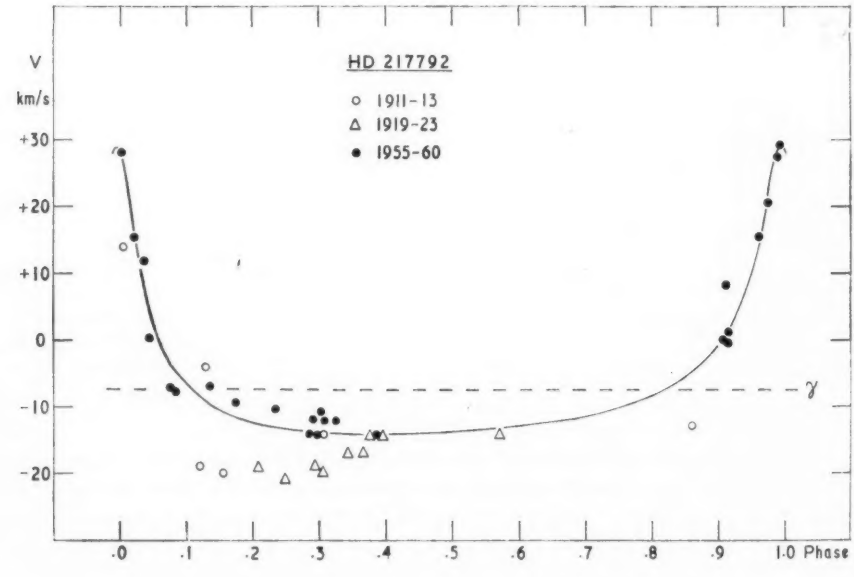

FIG. 3.—*The radial velocity curve of π PsA. Open circles, Lick; triangles, Cape; filled circles, Mt Stromlo.*

TABLE V

Observations of HD 217792

JD	Phase	V_0	O–C	Notes
243		km/sec		
5293·272	0·911	+ 8·4	+7·4	
5386·026	·172	− 9·2	+2·3	Observer: G. Hagemann
6035·214	·992	+27·5	−1·1	Observer: S. Gaposchkin
6036·214	·995	+29·6	+0·7	
6038·217	·001	+28·2	−0·3	
6067·144	·082	− 7·8	−3·2	
6143·926	·297	−14·1	−0·4	
6175·945	·387	−14·1	−0·1	Underexposed
6410·188	·044	+ 0·1	−4·9	
6478·010	·234	−10·1	+2·9	Observer: A. Przybylski
6501·954	·301	−10·6	+3·1	Observer: H. Gollnow
6503·935	·307	−12·0	+1·8	
6509·922	·324	−12·0	+1·9	Observer: H. Gollnow
6718·243	·908	0·0	−0·5	
6720·317	·914	− 0·5	−1·9	
6737·310	·961	+15·5	+0·9	
6778·196	·076	− 7·1	−3·4	
6799·150	·135	− 6·9	+2·9	
6851·990	·283	−13·9	−0·3	
7077·333	·915	+ 1·1	−0·5	
7099·325	·977	+20·7	−1·3	
7115·280	·021	+15·4	−1·6	
7121·254	·038	+12·0	+4·5	
7210·989	0·290	−11·8	+1·8	

TABLE VI

Orbital parameters

HD	114911	184035	217792
P, days	20·0052	4·625	356·567
γ, km/sec	−8·1	+11·9	−7·3
K, km/sec	56·5	72·5	21·5
e	0·12	0·09	0·70
ω	120°	315°	10°
T − JD 240 0000	20606·722	36702·433	34968·266
$10^{-6}\, a \sin i$, km	15·4	4·6	75·3
$f(m)$, solar masses	0·36	0·18	0·13

present ones. The early observations from the Mills Expedition of Lick Observatory (**4**), especially those near the sharp velocity maximum, were useful in establishing the period. The Stromlo velocities are listed in Table V, and all the available data are shown in Fig. 3. A few spectrograms of this star have been re-measured, for confirmation, by Mr John Graham and by Miss Willy van Pelt. The orbital elements are listed in Table VI.

Mount Stromlo Observatory,
Canberra, A.C.T.,
Australia:
1961 *June.*

References

(1) H. R. Morgan, *Astr. Papers Am. Eph. Naut. Almanac*, Washington **13**, (3), 1952.
(2) W. Buscombe and P. M. Morris, *M.N.*, **118**, 609, 1958.
(3) J. B. Irwin, *Ap. J.*, **116**, 218, 1952.
(4) W. W. Campbell *et al.*, *Lick Obs. Publ.*, **16**, 195, 1928.
(5) S. S. Huang, *Ap. J.*, **118**, 285, 1953.
(6) H. Spencer Jones, *Cape Annals*, **10**, (8), 244, 1928.

Summary of Edinburgh paper

SPECTROPHOTOMETRIC MEASUREMENTS OF EARLY-TYPE STARS*

VII. Results and Discussion for 10 Stars of MK Type B5 and 7 Stars of Miscellaneous Types

H. E. Butler and G. I. Thompson

Summary

This paper concludes the spectrophotometric programme on early-type stars. It is in two parts:

Section 1

Equivalent widths are given for 56 absorption lines in the spectra of 10 stars of MK type B5. The data are strictly comparable with those of previous papers of this series. Comparing their behaviour with that of the B3 stars, no unexpected trends have shown up except that He I 6678 and 5675 have become appreciably luminosity sensitive. Al III has disappeared while S II and Fe II are perceptible.

There is a suggestion of an emission band in the supergiants centred on 4745A. This is tentatively identified as C II. There is also a broad but unidentified absorption in 67 Oph at 4272-80A.

Unusually sharp emission wings are visible in the profiles of Hα and Hβ in the supergiant 5 Per. An appreciable change in the absorption component of Hα has also been observed.

Section 2

This section deals with stars that did not fit into the previous parts, or whose spectra have changed.

One A0 supergiant and one A0 dwarf have been reduced in a manner comparable with the rest of the programme.

Three Be stars, previously described and showing Hα in emission, were later re-observed and showed Hα in a changed form. New reductions show that the changes were, in fact, confined to the hydrogen lines and to the D-lines of sodium. This latter observation suggests that the D lines are largely circumstellar rather than interstellar.

Further plates of ω Ori (B3 IIIe) confirm the existence of an unexplained depression centred at 4348 in the red wing of Hγ.

The unusual and nearly featureless spectrum of the star 59 Cyg is studied and its relation to abnormal stars such as ϕ Per and ψ Per commented on.

*The full text of this paper appears in *Publications of the Royal Observatory, Edinburgh*, **2**, No. 6, 1961.